Biochemical study of the interactions between cohesin and DNA

James Edward Collier

Corpus Christi College

University of Oxford



A thesis submitted for the degree of

Doctor of Philosophy

Trinity 2020

Abstract

Cohesin is a ring like SMC-kleisin complex (S-K ring) that mediates DNA interactions between chromosomes. It is responsible for the phenomenon of sister chromatid cohesion (SCC) and ensures the faithful segregation of chromosomes during mitosis. Cohesin also mediates interactions within chromosomes by organising DNA into loops in both interphase and mitosis. SCC is thought to be mediated by co-entrapment of sister DNAs within a single cohesin S-K ring. Cohesin will also entrap individual chromosomes within its S-K ring during G1, and it is thought this activity is a pre-requisite to cohesion establishment during S phase. To improve our understanding of the mechanism of the entrapment of DNA by S-K rings, I developed a protocol to measure this activity in vitro. By using a cysteine-cysteine crosslinking protocol, I was able to covalently circularise the cohesin ring on DNA and through this create protein-DNA catenations that can resist protein denaturation. This revealed that S-K entrapment was dependent on Scc3 and ATP binding, and was stimulated by Scc2 and ATP hydrolysis. I found both Scc2 and Scc3 are DNA binding proteins and discover that this DNA binding activity is essential for cohesin's ability to entrap DNA within its S-K ring. I then set out to identify where within the cohesin ring DNA was entrapped, and through this managed to identify a novel mode of DNA interaction, whereby DNA becomes entrapped within two compartments created through cohesin binding to ATP. Entrapment within these two compartments was not associated with passage of DNA into S-K rings, and I propose entrapment of this nature may represent the first step in cohesin's topological association with DNA.

Acknowledgements

I would like to thank Kim Nasmyth for mentoring me over the course of this work. For all the advice, encouragement, and criticism he has given me during my time in his lab. Through this, I have learnt a great deal about science, and more importantly, what it takes to discover some small truth about this world.

I would like to thank all the members of the Nasmyth group, both past and present. In particular Thomas Gligoris, for being there to initially instruct me in the art of biochemistry. Also to Byung-Gil Lee and Jan Lowe, I have enjoyed working with you both and hope our collaboration continues into the future.

I would like to thank Isobel Johns, without your support I would have wasted away long ago. Finally, to all my family, thank you. This would not have been possible without you.

Contributions

Some aspects of this work were carried out in collaboration. Calibrated ChIP sequencing was performed by N. J. Petela. Scc3 EMSA experiments were carried out by M. B. Roig. The Scc3 mutations that abolished DNA binding were first identified by S. Yatskevich.

Abstract i
Acknowledgements ii
Contributions iii
Table of contents iv
Abbreviations vi

Chapter 1 - Introduction 1
- The Cell Cycle 2
- Mitosis 3
- Chromosome Segregation 3
- Chromosome Condensation 5
- SMC Complexes 6
- The Mechanism of Cohesion 10
- Entrapment of Individual DNA Molecules 13
- The Entry Gate 15
- The Mechanism of Loop Extrusion 17
- DNA Binding to SMC Complexes 19
- Dissociation from DNA 21
- Topology: Even or Odd Number of DNA Passages 22
- Thesis Objectives 24

Chapter 2 - Measuring Topological Entrapment of DNA by Cohesin in vitro 25
- Introduction 26
- Expression and purification of the cohesin complex 26
- An assay to measure S-K entrapment of DNA by cohesin 29
- S-K entrapment is dependent on Scc3 and ATP binding, and stimulated by Scc2 and ATP hydrolysis 30
- DNA binding to Scc3 facilitates entrapment by S-K rings 32
- DNA binding to Scc2 facilitates entrapment by S-K rings 33

Chapter 3 - Does DNA reside in the S or K compartments? 35
- Introduction 36

- DNA is never entrapped in J-S compartments and only rarely in J-K compartments. 36
- The rapid entrapment of DNA in E-S and E-K compartments 37

Chapter 4 - How does DNA become entrapped in the E-S and E-K compartments? 41
- Introduction 42
- E-S entrapment disrupts coiled coil interactions proximal to the heads 42
- Scc2 and DNA disrupt the J-state in the absence of ATP 43
- Rapamycin induced head dimerization does not prevent chromosome association 44

Chapter 5 – Discussion 46

Chapter 6 - Bibliography 61

Chapter 7 - Materials and methods 71

AEC	anion exchange chromatography
APC/C	anaphase promoting complex
bacmid	bacterial artificial chromosome
BMOE	bis-maleimidoethane
bp	base pair
CEN	centromere
CDs	catenated dimers
CMs	catenated monomers
cryo-EM	cryo-electron microscopy
dsDNA	double-stranded DNA
E	engaged
E-K	engaged heads-kleisin
E-S	engaged heads-SMC
EMSA	electromobility shift assay
EtBr	ethidium bromide
G1	gap 1 phase
G2	gap 2 phase
HAWK	HEAT proteins associated with kleisins
HEAT	Huntington/EF3/PP2A/Tor1
J	juxtaposed
J-K	juxtaposed heads-kleisin
J-S	juxtaposed heads-SMC
LDS	lithium dodecyl sulphate
rpm	rotations per minute
S	synthesis
SAC	spindle assembly checkpoint
SDS	sodium dodecyl sulphate
SDS-PAGE	sodium dodecyl sulphate-polyacrylamide gel electrophoresis
SCC	sister chromatid cohesion
SEC	size exclusion chromatography
SMC	structural maintenance of chromosome
S-K	SMC-kleisin
TADs	Topologically associated domains

Chapter 1 – Introduction

The Cell Cycle

All cellular life stores genetic information in chromosomes, encoded in double-stranded DNA (dsDNA) molecules. These DNA molecules are huge, and even bacterial chromosomes range in size of between 100 kbp to 10 Mbp. Bacterial chromosomes contain either a single dsDNA molecule, or a small handful of distinct molecules, that can each be either linear or circular in form. Eukaryotic cells on the other hand have multiple linear chromosomes with a combined length varying between 12 Mbp in *Saccharomyces cerevisiae* to a staggering 130 Gbp in some plants. These molecules must be copied, condensed into a state amenable to spatial manipulation, and finally segregated so that following cell division each daughter cell inherits an entire copy of the genome.

To achieve this, cells execute a highly choreographed series of events collectively known as the cell cycle (Figure 1-1), and in eukaryotes this can be broadly divided into two phases: interphase and mitosis. Interphase can be further divided into three phases: an initial gap phase (G1), a synthesis phase (S), followed by a second gap phase (G2). Both G1 and G2 are growth phases during which the cell will synthesis all the necessary components required to progress into S phase and mitosis, respectively. During S phase the cell copies their genome, doubling the chromosome content of the cell. Once copied, the cell will divide chromosomes equally into two territories, a process known as mitosis, following which the cell cleaves in two, permanently separating each copy of the genome and leaving two genetically identical daughter cells in its wake.

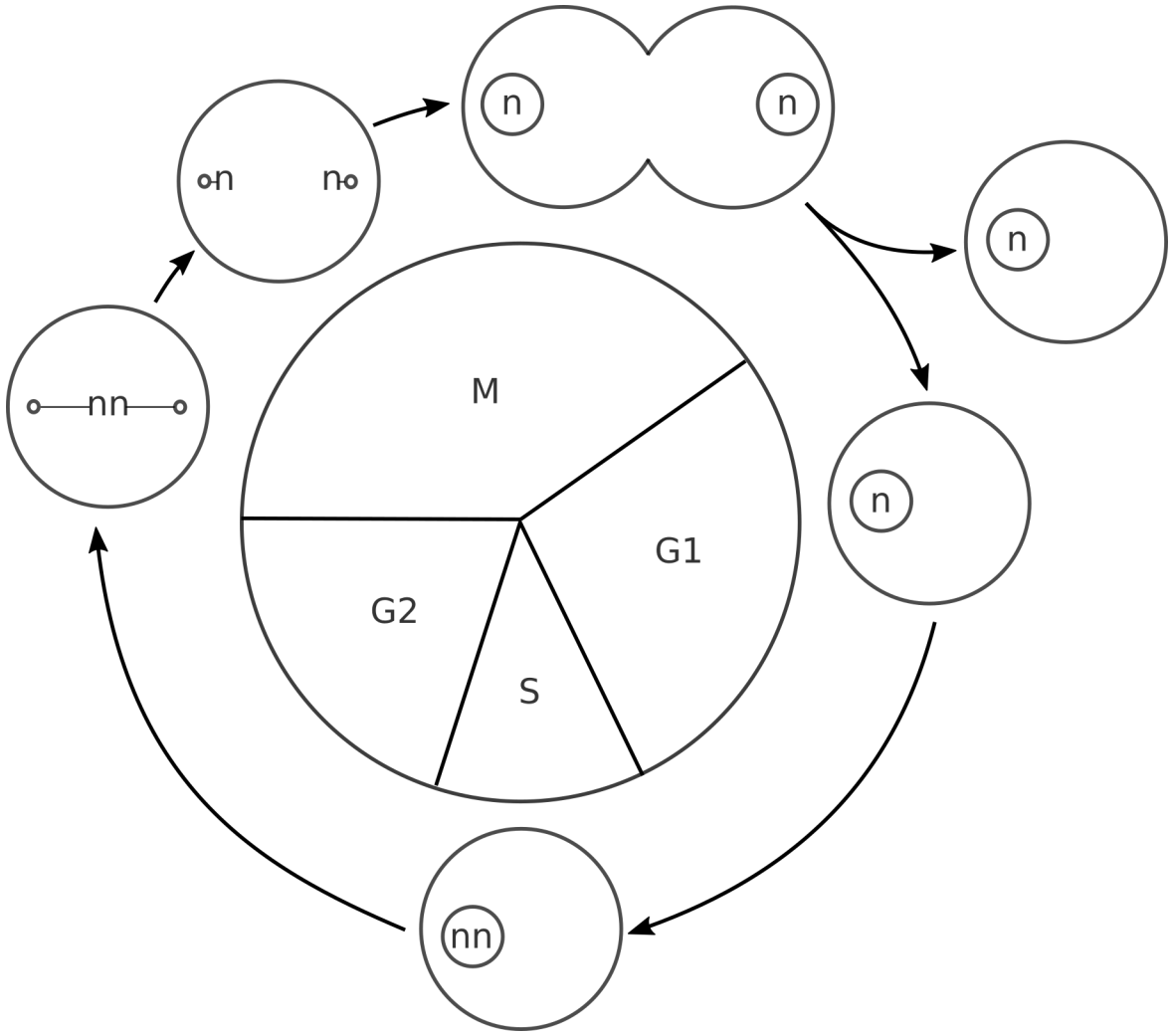


Figure 1-1. The cell cycle.

A typical eukaryotic cell cycle. During G1, cells prepare themselves to copy their genome, which then takes place during S phase (n to nn). Following this, cells then enter G2, where they begin preparations for dividing chromosomes equally into two. When these preparations are complete, cells then enter mitosis and chromosomes align along the cell equator, before one of each copy is pulled to opposite cell poles. Cytokinesis then takes place producing two daughter cells. The cycle then continues ad infinitum. Relative duration of each stage varies from organism to organism and the figure has not been drawn to scale.

Mitosis

Chromosome replication during S phase produces genetically identical DNA molecules called sister chromatids and doubles the DNA content of the cell. The doubling of DNA content is crucial to the propagation of the cell, as each nascent cell must inherit an entire copy of the genome following mitosis. Missegregation of chromatids during mitosis produces daughter cells with an unequal number of chromosomes, known as aneuploidy, which has disastrous consequences for the cell, usually resulting in death. There are four distinct stages of mitosis, characterised by the morphology and position of the chromosomes: prophase, metaphase, anaphase, and telophase, and it is during mitosis that two of the most striking events in all of cell biology occur; chromosome condensation and segregation.

As cells enter prophase, chromosomes begin to condense into thread-like structures. The transition from a diffuse, highly amorphic structure, into well-defined entities acts to individualise chromosomes and is essential for their segregation. During metaphase, chromosomes then align along the metaphase plate. Once aligned, cells progress into anaphase and chromosomes are pulled to opposite cell poles through a shortening of the microtubules. Chromosome condensation has continued up until this point, and by anaphase chromosomes are at their most compact. Chromosomes then begin to decondense during telophase. This marks the completion of mitosis, following which cytokinesis occurs and the cell divides into two daughter cells.

Chromosome Segregation

Eukaryotic genomes can sometimes consist of hundreds of individual chromosomes and ensuring their faithful segregation is a significant logistical challenge. The cell

must inherit exactly one chromatid of each chromosome. If left to random segregation alone, aneuploidy would be rife. Instead, the cell has evolved an elegant solution to this problem. Rather than allowing sister chromatids to randomly separate after S phase, they instead remain physically associated with one another; a phenomenon known as sister chromatid cohesion (SCC). As cells progress into mitosis, filamentous microtubules are polymerised which explore the cellular space and will attach to chromosomes at their kinetochores (reviewed in Tanaka, 2010). Once attached, these microtubules will pull the chromosomes towards their respective pole. If sister kinetochores are bound by microtubules that originate from opposite poles, a process known as biorientation, each sister chromatid will be pulled in opposite directions. SCC resists the opposing pulling forces of the spindle and this creates tension across the spindle-chromosome structure. This also causes chromosomes to align between the two spindle poles, explaining the observation of chromosome alignment during metaphase.

In the absence of tension, spindle attachments are destabilised by aurora B kinase (Shimogawa et al., 2009; Tanaka et al., 2002). Tension has been suggested to stabilise spindle kinetochore attachments by causing the spatial separation of aurora B kinase from its substrates. In the absence of biorientation, the cell is prevented from entering anaphase by the mitotic checkpoint (reviewed in Musacchio & Salmon, 2007), which forms the mitotic checkpoint complex (MCC) on unbound kinetochores. The MCC prevents the onset of anaphase by inhibiting the anaphase-promoting complex (APC/C; Figure 1-2). Successful biorientation of each chromosome relieves this inhibition and the APC/C targets securin and cyclin B for degradation (reviewed in Zachariae and Nasmyth, 1999). Securin acts as a stoichiometric inhibitor of separase, a protease required for the destruction of SCC at the onset of anaphase

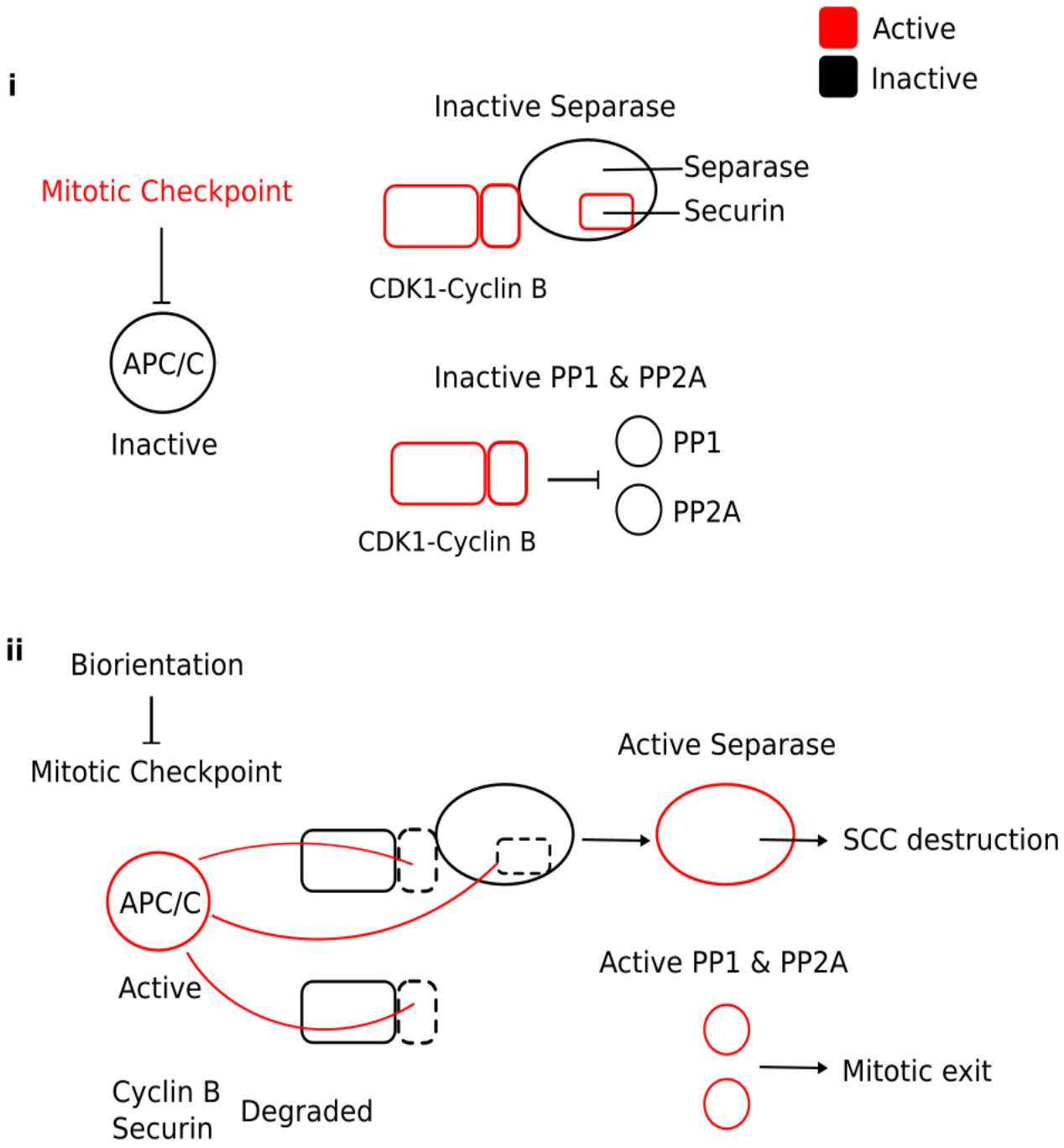


Figure 1-2. Chromosome biorientation leads to anaphase onset and the destruction of sister chromatid cohesion

i) In the absence of chromosome biorientation, the mitotic checkpoint inhibits the activity of the APC/C. Securin binds to and inhibits the activity of separase, and CDK1-cyclin B inhibits both separase and the mitotic exit phosphatases PP1 and PP2A through phosporylation. **ii**) In the presence of complete chromosome biorientation the mitotic checkpoint is inactivated, and the APC/C becomes active. The APC/C then targets cyclin B and securin for degradation. This alleviates the inhibition of separase, which goes on to destroy SCC, and the destruction of cyclin B activates PP1 and PP2A.

(Ciosk et al., 1998; Oliveira et al., 2010; Uhlmann et al., 1999, 2000). Cyclin B forms part of the cyclin-B dependent kinase (CDK1-cyclin B) complex, which further inhibits separase through phosphorylation (Gorr et al., 2005; Stemmann et al., 2001), as well as inhibits the mitotic progression phosphatases which in humans are PP1 and PP2A (Dohadwala et al., 1994; Yamano et al., 1994; Castilho et al, 2009; Cundell et al, 2016). Activation of the APC/C targets both securin and cyclin B for degradation which alleviates inhibition of separase, causing the destruction of SCC and enables segregation of sister chromatids. Cyclin B destruction also activates PP1 and PP2A which go on to dephosphorylate and activate a cornucopia of downstream targets whose activity is necessary for mitotic exit and cytokinesis.

Chromosome Condensation

As well as the establishment of cohesion between sister chromatids, chromosome segregation also depends on the ability to individualise chromosomes during mitosis. Fully stretched out, a genome of 130 Gbp would be roughly 44 m long yet possess a diameter of only 2 nm; a length to width ratio of 22 billion. As anyone who has ever reached into a drawer full of cables is likely all too familiar with, such structures are prone to tangling, which would significantly hinder any attempt to separate them. It is therefore vital that prior to their segregation chromosomes are first built into discrete, easily manipulatable units. This is achieved through organising metaphase chromosomes into a series of loops (Earnshaw and Laemmli, 1983), which acts to condense and individualise chromosomes. Loops are thought to be built processively, through a process of loop extrusion (LE) (Nasmyth, 2001). In principle, this ensures that during DNA condensation, loop extruders keep track of the molecule of DNA they are working on and do not grab different molecules of DNA

and tangle the two, a feature that would be necessary for chromosome individualisation.

A similar organisational process has been shown to be at play during interphase, and mammalian interphase chromosomes have been found to be organised into megabase sized domains (Dixon et al., 2012; Nora et al., 2012). Within these domains, sequences interact with themselves much more frequently than with sequences outside, and as such have been termed topologically associated domains (TADs). These TADs are thought to be DNA loops, and LE has also been proposed as the mechanism through which these are built (Fudenberg et al., 2016; Sanborn et al., 2015). An alternative model for loop generation has been proposed based on Brownian motion and loop capture (Cheng et al., 2015), and it has been suggested that both LE and loop capture models would be sufficient to build mitotic chromosomes and account for interphase contacts (Gerguri et al., 2020).

SMC Complexes

We now know that organising chromosomes into loops and ensuring the faithful segregation of chromosomes are carried out by a class of highly conserved proteins known as structural maintenance of chromosome (SMC) proteins. These form large ring like protein complexes that are thought interact with DNA through topological mechanisms (reviewed in Yatskevich et al., 2019). All SMC complexes contain a pair of SMC proteins; large rod-shaped proteins composed of an ABC-like ATPase head domain at one end and a dimerization domain at the other, known as the hinge, separated by a ~50 nm intramolecular antiparallel coiled coil (Haering et al., 2002). Each SMC hinge forms a half-torus which come together and interact at two interfaces (Griese et al., 2010; Kurze et al., 2011), known as the north and south

interfaces (Figure 1-3i). Hinge dimerization causes the formation of V-shaped SMC structures (Anderson et al., 2002; Haering et al., 2002); an SMC heterodimer in eukaryotes but a homodimer in prokaryotes. The SMC dimer is bridged by a kleisin protein, whose N-terminal binds to the neck of one SMC and C-terminal to the base of the ATPase of the other (Gligoris et al., 2014; Haering et al., 2004), giving SMC complexes a ring-like architecture (Bürmann et al., 2013; Gruber et al., 2003; Haering et al., 2002; Onn et al., 2007), that can be referred to as an SMC-kleisin (S-K) ring (Figure 1-3i).

In the absence of ATP, SMC complexes adopt a rod-like conformation (Bürmann et al., 2019; Chapard et al., 2019; Diebold-Durand et al., 2017; Soh et al., 2015), with the SMC coiled coils closely juxtaposed along the length of the proteins, from the heads to the hinge (Figure 1-3ii). Recent structural analyses have also revealed the SMC rod to be folded roughly halfway along their length (Collier et al., 2020; Higashi et al., 2020; Lee et al., 2020), at a region known as the elbow, bringing their hinge domain within close proximity to the heads, at least for cohesin and condensin (Figure 1-4). The functional significance of this folding is not understood. When not bound to ATP, the SMC head domains are not stably associated, and insertion of TEV sites in the coiled coils just above one of the heads and subsequent exposure to TEV protease causes dissociation of the head domain (Gruber et al., 2003; Haering et al., 2002). Despite this, the heads are in close enough proximity to be efficiently crosslinked in vivo and are thought to be closely juxtaposed and said to be in the juxtaposed state (J state) (Chapard et al., 2019; Vazquez Nunez et al., 2019). When in the J-state, due to the association of the heads, SMC complexes can be thought to be divided internally into two regions (or compartments): one above the juxtaposed heads and between the hinge, known as the juxtaposed-heads SMC (J-

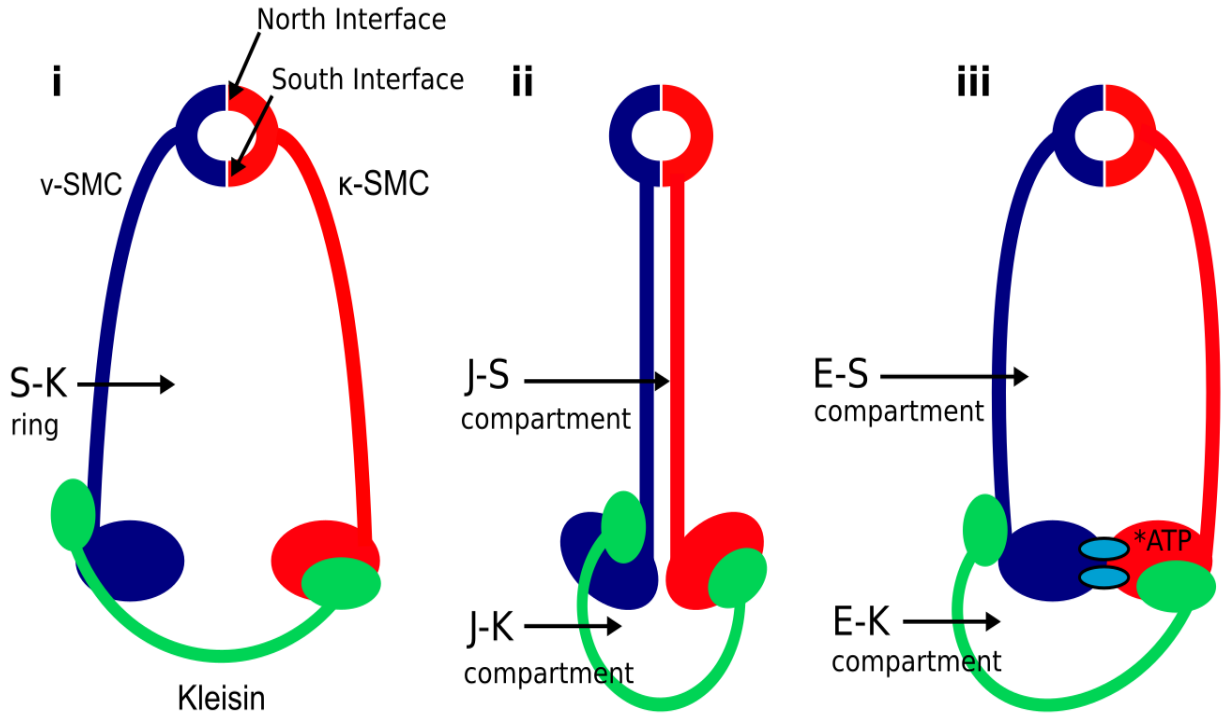


Figure 1-3. SMC-kleisin complexes.

i) Schematic of the SMC-kleisin (S-K) ring with an open ring like conformation, **ii)** with heads together in a juxtaposed (J) state showing the positions of J-S and J-K compartments, **iii)** with heads associated in the presence of ATP in the engaged (E) state, showing the E-S and E-K compartment.

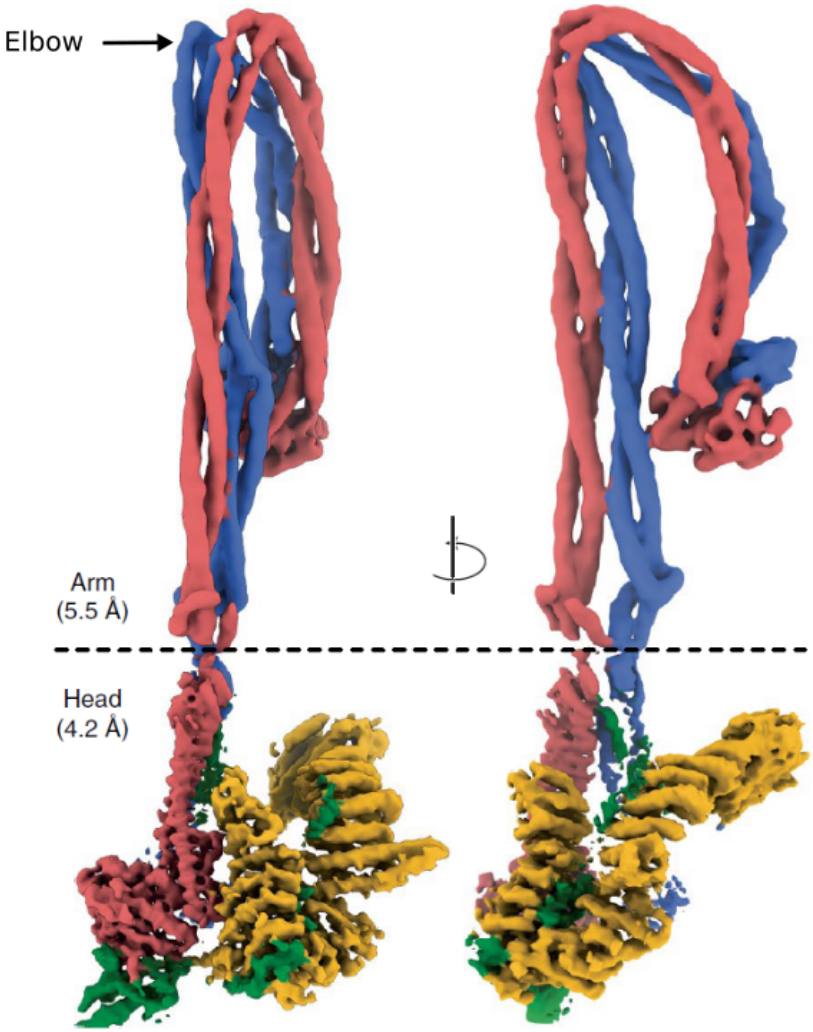


Figure 1-4. SMC complexes are folded at the elbow.
Cryo-EM structure of *S. cerevisiae* condensin folded at the elbow (Lee et al., 2020). Showing Smc2 (red), Smc4 (blue), Brn1 (green), and Ycs4 (Yellow).

S) compartment, and one below the heads and between the N- and C-terminal kleisin-SMC binding interfaces, known as the juxtaposed-heads kleisin (J-K) compartment. However, as the SMC coiled coils are thought to be associated along their length in the J-state (Diebold-Durand et al., 2017) the J-S compartment may be entirely inaccessible.

The SMC head domains undergo dimerization upon the binding of ATP (Arumugam et al., 2003; Lammens et al., 2004; Marcos-Alcalde et al., 2017; Onn et al., 2007), with each head forming one half of a functional ABC-like ATPase. The active site of each head domain is comprised of Walker A and Walker B sites, as well a Signature motif (Figure 1-5) (Arumugam et al., 2003; Holland and A. Blight, 1999). ATP binds to each head through interactions with the Walker A site, which correctly positions the α- and β-phosphates. ATP bound to the Walker A site of one head has its γ-phosphate bound to the signature motif of the other. ATP binding thus causes engagement of the SMC head domains and sandwiches two molecules of ATP between them. Head engagement is a pre-requisite to ATP hydrolysis, and is required to expose the bridging ATP γ-phosphate bonds to hydrophilic attack from a participating water molecule that is coordinated by an invariant glutamate of the Walker B site and an Mg^{2+} cofactor (Oldham and Chen, 2011). Hydrolysis of both γ-phosphate bonds causes the formation of 2ADP + Pi, along with head dissociation. ADP and Pi are then released, and ATP binds again. ATP hydrolysis by cohesin also depends on the presence of Scc2 (Petela et al., 2018), as well as either DNA or Scc3, although the reason for this is not fully understood.

The ATP-engaged state (E-state) of the heads is distinct from the J-state (Chapard et al., 2019; Vazquez Nunez et al., 2019) and also partitions the SMC ring into two

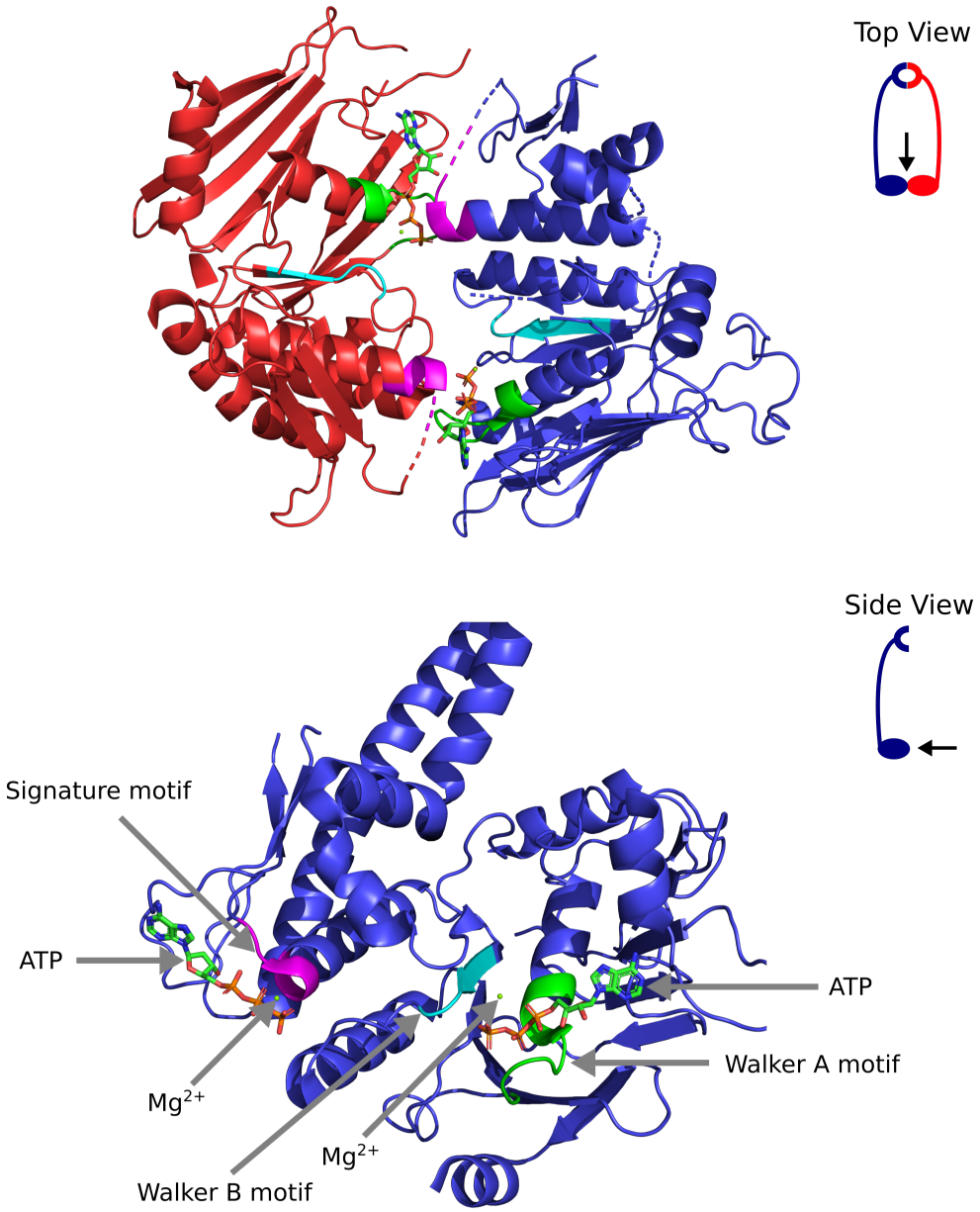


Figure 1-5. The ATPase head domains.

The SMC ABC-like ATPase domains. Top panel – Smc1 (Red) and Smc3 (Blue) head domains engaged in the presence of ATP. Viewed from "above" the SMC heads looking down. Bottom panel – The Smc3 head domain viewed from the side. Labelled are the two ATP molecules as well as their coordinated Mg^{2+} ions. The Walker A motif (green), Walker B motif (cyan) and signature motif (purple) are labelled.

compartments (Figure 1-3iii), one above the engaged-heads and below the hinge, known as the engaged-heads SMC (E-S) compartment, and one below the heads and between the N- and C-terminal kleisin SMC binding interfaces, known as the engaged-heads kleisin (E-K) compartment. The ability of SMC complexes to bind and hydrolyse ATP are crucial for their function in vivo, with mutants unable to bind or hydrolyse ATP unable to support viability (Arumugam et al., 2003; Weitzer et al., 2003). In vivo, hydrolysis activity appears to be crucial for cohesin to stably associate with chromosomes (Arumugam et al., 2003; Hu et al., 2011), however, a precise biochemical description of the consequences of the ATP hydrolysis cycle of SMC complexes remains to be elucidated.

In eukaryotes, the SMC complexes responsible for the formation of cohesion between sister chromatids during S phase and the condensation of chromosomes during mitosis were identified through genetics screens (Guacci et al., 1997; Hirano and Mitchison, 1994; Larionov et al., 1985; Michaelis et al., 1997; Strunnikov et al., 1993). Cohesin was found to establish SCC during S phase (Uhlmann and Nasmyth, 1998) and condensin the condensation of chromosomes during mitosis (Hirano and Mitchison, 1994; Hirano et al., 1997). Cohesin has since also been found responsible for the formation of TADs during interphase (Rao et al., 2017), and in fact the stabilisation of cohesin on DNA during interphase leads to the formation of metaphase like chromosome structures (Wutz et al., 2017). Eukaryotic SMC complexes associate with large, hook-shaped, HEAT (Huntington/EF3/PP2A/Tor1) repeat containing proteins that are recruited to the complex via their kleisin subunit, known as HEAT proteins associated with kleisins (HAWKs; Wells et al., 2017). Cohesin has three HAWKs (Figure 1-6): Scc2, Scc3, and Pds5; although it is thought that only two HAWKs associate with Scc1 at any one time (Petela et al., 2018)

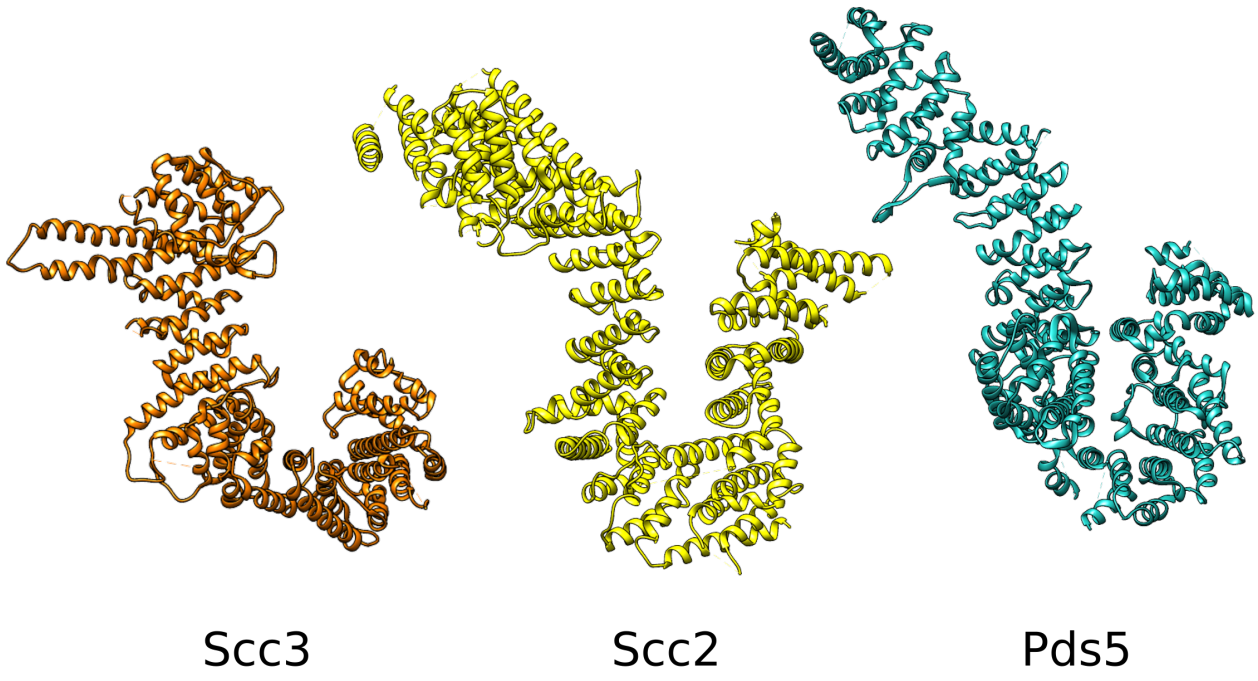


Figure 1-6. The HAWKs.

Eukaryotic SMC complexes are associated with large hook-shaped HEAT- repeat proteins known as HAWK proteins. Cohesin has three HAWKs: Scc3 (orange - PDB 6H8Q), Scc2 (yellow - PDB 6ZZ6), and Pds5 (cyan - PDB 5ME3).

The Mechanism of Cohesion

The destruction of cohesion at the onset on anaphase was found to coincide with cleavage of cohesin's Scc1 subunit by the cysteine protease separase (Uhlmann et al., 1999, 2000). This, coupled with the discovery that cohesin possessed a ring like architecture suggested that SMC proteins may interact with DNA through a topological principle (Gruber et al., 2003; Haering et al., 2002). A simple hypothesis was proposed to explain how cohesin might establish cohesion between chromosomes during S phase, namely through the co-entrapment of sister chromatids within a single cohesin ring (Figure 1-7i). If this were the case, then cohesion dissolution at anaphase could be achieved through cleavage of either Smc1, Smc3, or Scc1, or similarly through opening of their respective interfaces. This would explain the observation that anaphase onset was initiated by cleavage of Scc1 (Uhlmann et al., 1999) and even artificially inducible through TEV cleavage of Scc1 (Uhlmann et al., 2000). Similar TEV cleavage experiments have shown that cleavage of Smc3 coiled coils also leads to loss of cohesion (Gruber et al., 2003) further demonstrating that the integrity of the cohesin ring is required for cohesion.

More direct evidence for the entrapment of sister DNAs inside cohesin rings has emerged from in vivo minichromosome entrapment studies, whereby through insertion of cysteine pairs into each of the S-K ring's three protein interfaces, namely the hinge, and between the N- and C-terminus of Scc1 with Smc3 and Smc1 respectively (Gligoris et al., 2014), cohesin has been shown to be able to topologically catenate replicated sister minichromosomes, known as catenated dimers (CDs). Importantly, CD formation was not due to cohesin's association with catenated DNA (Haering et al., 2008; Srinivasan et al., 2018), produced as a

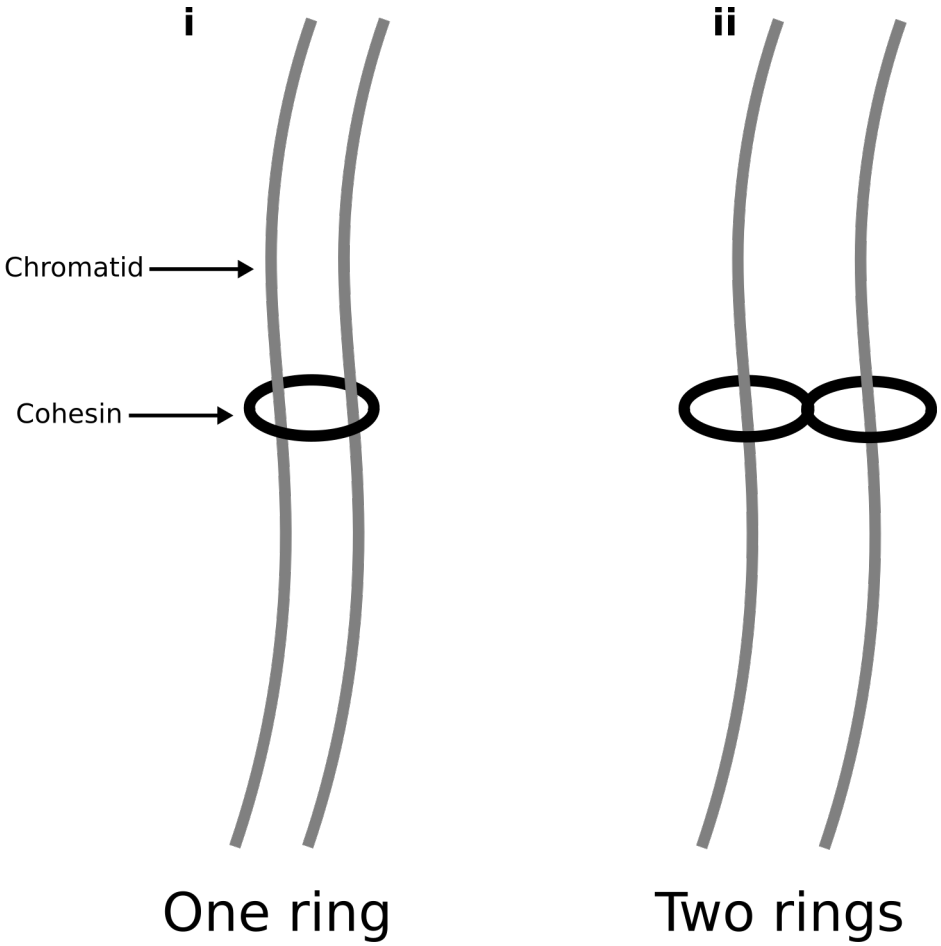


Figure 1-7. One ring or two ring models for cohesion.

i) Cohesin may mediate cohesion through co-entrapment of DNA within a single cohesin ring, or **ii)** through cohesin entrapping individual chromosomes and associating together.

consequence of the replication of circular templates, and was instead shown to be DNA-cohesin-DNA catenations, held together by topological co-entrapment of two DNA molecules within a single S-K ring. A subsequent study found that CDs may in fact be entrapped within the J-K compartment of the S-K ring (Chapard et al., 2019). Whether or not all CDs are entrapped within the J-K compartment, or whether this represents just one population of cohesive cohesin, will require a more detailed understanding of the dynamics of the head domains when cohesin entraps DNA. Alternative models suggest cohesion is mediated through the interaction of multiple cohesin rings (Figure 1-7ii), with each sister chromatid associated a separate cohesin ring and an interaction between the two, with many variations on this theme (Huang et al., 2005; Nasmyth, 2005; Zhang et al., 2008). Cohesin has also been shown to be able to entrap individual minichromosomes (Gligoris et al., 2014; Haering et al., 2008) and so stable interaction between cohesin rings embracing separate sister chromatids is a possible mechanism for cohesion.

Cohesion establishment at S phase is associated with acetylation of Smc3 at two highly conserved lysine residues, Smc3K112 K113 in *S. cerevisiae,* by the acetyltransferase Eco1 (Ivanov et al., 2002; Rolef Ben-Shahar et al., 2008; Unal et al., 2008). The consequence of this acetylation is not well understood, however appears to be involved in stabilising cohesin's association with DNA (Collier et al., 2020; Murayama and Uhlmann, 2015), an obvious pre-requisite for stable SCC. Pds5 has been shown to promote this acetylation, as well as prevent its deacetylation during G2 (Chan et al., 2013). More recently, it has been reported that one consequence of acetylation of Smc3 during S phase is to promote cohesin dimerization (Shi et al., 2020a), suggesting a role for interaction between multiple cohesin rings during cohesion establishment. If cohesion were mediated by interaction between multiple

cohesin rings, then it may be possible to isolate mutations that abolish cohesin-cohesin interactions but otherwise do not affect DNA association or other cohesin activities. However, genetic screens looking for suppressors of inactivation of separase, to allow progression through mitosis in the absence of Scc1 cleavage, failed to find evidence for interaction between multiple cohesin rings, instead finding only suppressor mutations in the three canonical S-K ring interfaces (Xu et al., 2018). These data imply that weakening either the hinge, or either Scc1 SMC interface, is sufficient to allow for the destruction of cohesion in the absence of separase activity, in agreement with the single ring hypothesis. While direct interaction between cohesin subunits from different complexes has been reported (Shi et al., 2020a; Zhang et al., 2008) the functional significance of these interactions remain unknown. That the screen for separase suppressors failed to identify any interactions between different cohesin rings (Xu et al., 2018), coupled to the observation the that cohesin is able to hold replicated minichromosomes together with an apparent stoichiometry consistent with a single cohesin ring (Haering et al., 2008) casts doubt on the tenability of the multi-ring hypothesis.

Cohesion establishment is tightly coupled to DNA replication, and many of the replication fork associated proteins, including Ctf4, Chl1, Csm3/Tof1, Mrc1, and Ctf18-RFC were found to cause cohesion defects with apparent little effect on replication (Hanna et al., 2001; Mayer et al., 2001, 2004; Petronczki et al., 2004; Xu et al., 2004). These proteins were found to act in two redundant cohesion establishment pathways (Srinivasan et al., 2020; Xu et al., 2007) one involving conversion of cohesin associated with DNA during G1 into CDs, and another involving de novo loading of cohesin at the replication fork. De novo establishment of cohesion at S phase is Scc2 dependent, while the conversion pathway is Scc2

independent, at least at S phase. However, as Scc2 is required for cohesin's association with DNA in the first place, strictly speaking, even the conversion pathway has a requirement for Scc2. As such, it is possible that cohesion established by both pathways are produced through identical mechanisms; with the de novo pathway having to execute the entire cohesion establishment pathway rapidly at the replication fork, whereas the conversion pathway may have the early, Scc2 dependent steps already completed.

Evidence for what the mechanism for cohesion establishment might be has come from in vitro studies (Murayama et al., 2018) which found that cohesin stably associated with dsDNA is able to subsequently associate with a second DNA molecule, but only if this is single stranded DNA (ssDNA). Furthermore, this ssDNA can then be converted to dsDNA and remain stably associated. With the presence of both dsDNA and ssDNA at the replication fork, the notion that cohesin first entraps dsDNA, then subsequently entraps ssDNA produced during replication, that is then subsequently converted to dsDNA producing co-entrapped sister DNAs, is an attractive idea.

Entrapment of Individual DNA Molecules

In budding yeast, cohesin associates with DNA during late G1, when Scc1 is first synthesised (Guacci et al., 1997; Michaelis et al., 1997), and will entrap individual minichromosomes inside S-K rings (Srinivasan et al., 2018) known as catenated monomers (CMs). CM formation is dependent on Scc2, as well as the binding and hydrolysis of ATP by Smc3. Further lines of evidence for entrapment of individual DNAs have come from in vitro studies using *Schizosaccharomyces pombe, S. cerevisiae,* and human cohesin (Davidson et al., 2016; Minamino et al., 2018;

Murayama and Uhlmann, 2014). Stable association between cohesin and DNA was dependent on Scc3, Scc2/4, and ATP binding. While it is unclear precisely what is being measured by these in vitro experiments, that stable association is destroyed upon cleavage of Scc1 or linearization of the DNA template suggests a topological mechanism is at play. Whether this mechanism is one of entrapment within S-K rings is however uncertain. Cohesin containing mutations in its hinge which are unable to form CMs, but nonetheless associate with the genome normally, as measured by ChIP (Srinivasan et al., 2018), are also removed from chromosomes when Scc1 is cleaved during S phase, demonstrating that Scc1 cleavage may generally destabilise cohesin's association with DNA. Interestingly, Scc4 was dispensable for stable association in vitro (Chao et al., 2015; Minamino et al., 2018), demonstrating that this activity is mediated primarily by Scc2 and the Scc4 binding domain can be completely deleted with no apparent loss of function. Similarly, Scc4 has been shown to be entirely dispensable for activation of cohesin's ATPase activity in vitro (Murayama and Uhlmann, 2014; Petela et al., 2018).

Currently, it is not well understood the functional significance of CM formation. One possibility is that CD formation is dependent on the preformation of CMs, and that CMs are actively converted to CDs upon S phase, possibly through the replication machinery passing through the cohesin ring (or through a topologically equivalent mechanism). It appears that at least one way CDs are formed is through this conversion mechanism (Srinivasan et al., 2020). A recent cytological study found that cohesin association can indeed persist through replication fork passage (Rhodes et al., 2017), but whether this was a result of replication fork passing through the ring, the ring opening but nonetheless remaining associated with DNA, or whether cohesin dissociated and re-associated in the immediate vicinity, is not known.

The Entry Gate

Biochemical and structural studies suggest that cohesin exists primarily as a stable ring (Collier et al., 2020; Gligoris et al., 2014; Gruber et al., 2003; Shi et al., 2020b), and the route that DNA takes during the process of S-K ring entrapment is an unresolved question. For DNA to enter the ring it must pass through either the hinge, the Smc3-Scc1, or the Smc1-Scc1 interface. In vitro studies have suggested that DNA can enter the ring via passage through the Smc3-Scc1 interface (Murayama and Uhlmann, 2015) based on the observation that under certain conditions Pds5/Wpl1 can promote stable association between DNA and cohesin in vitro. As Pds5/Wpl1 are thought to promote release of cohesin already bound to DNA through passage through the Smc3-Scc1 interface in vivo (Beckouët et al., 2016; Chan et al., 2012), entrapment through this mechanism has been suggested to be a reverse release reaction. However, in vivo studies have shown that fusing Scc1's N-terminus to Smc3, or Scc1's C-terminus to Smc1 is viable, and still facilitates entrapment by S-K rings (Gruber et al., 2006; Srinivasan et al., 2018).

One possibility is that entry into S-K rings is not through just one Scc1 interface, but through either: a "bicycle lock" mechanism. In this model, fusing only one of the two Scc1 interfaces may indeed be inconsequential. Only through preventing both interfaces opening would S-K ring entrapment be abolished. This model was tested by combining the Smc3-Scc1 protein fusion with Frb and Fkbp12 domains fused to the C-terminus of Scc1 and Smc1, respectively (Gruber et al., 2006). The Frb and Fkbp12 domains dimerize upon addition of rapamycin, offering a method to close the Scc1-Smc1 interface orthogonal to the Smc3-Scc1 interface. The authors were unable to create a direct Smc3-Scc1-Smc1 protein fusion due to protein instability. The addition of rapamycin did not result in lethality, however, caused a significant

growth defect in these cells; a defect only observed in the presence of rapamycin, suggesting this to be specific to co-closure of both interfaces and not a result of the protein fusions themselves. As only one interface was covalently shut, namely that of Scc1-Smc3, it is, strictly speaking, possible that dimerization of Scc1-Frb Smc1-Fkbp12 is leaky and allows enough DNA passage for viability. A method to covalently close both interfaces in vivo is required to eliminate this possibility.

If neither Scc1-SMC interface acts as the entry gate, then DNA must enter through the hinge. Attempts to seal this interface have involved the same rapamycin induced Frb Fkbp12 dimerization, with these domains introduced into flexible loops in the Smc3 and Smc1 hinge domains, respectively (Gruber et al., 2006). Addition of rapamycin caused lethality in these cells, suggesting that opening of this interface is necessary for cohesin's function and is thus the best candidate for the DNA entry gate. Indeed, that structures of open SMC hinges have been reported (Griese et al., 2010; Haering et al., 2002), one even bound to a small stretch of ssDNA (Shi et al., 2020b), support this claim. However, it is possible that inviability stems from reasons besides the inability to open this interface. Recent cryo-electron microscopy (cryo-EM) structures show that cohesin adopts a folded rod conformation (Collier et al., 2020; Higashi et al., 2020; Shi et al., 2020b), with the coiled coils folded about halfway along their length. This brings the hinge into close proximity to the head domains, and it appears the hinge may interact with the coiled coils around this region. The functional significance of this folding, or the interactions between the hinge and the rest of the complex are not well understood, however, it is possible that inviability may instead stem from disruption of some of these interactions.

Alternatively, despite the strong suggestion the cohesion is mediated by co-entrapment of DNA in S-K rings (Haering et al., 2008; Srinivasan et al., 2018), it has not really been demonstrated that S-K entrapment is an essential function of the cohesin complex, in which case, viability may be an entirely inappropriate measurement for loss of S-K ring entrapment. For example, it is possible the mechanism that leads to S-K entrapment during G1 may be distinct from that which leads to sister DNA entrapment during S phase. Only through identifying the exact mechanism through which DNA enters the S-K ring during G1, and specifically preventing this activity, will we discover the functional significance of S-K entrapment.

The Mechanism of Loop Extrusion

The LE model proposes that SMC complexes binds to DNA and translocates along it, progressively growing a DNA loop in their wake (Nasmyth, 2001). Recent in vitro studies have managed to produce an activity resembling LE for both *S. cerevisiae* condensin and human cohesin (Davidson et al., 2019; Ganji et al., 2018; Kim et al., 2019). For cohesin, this activity was dependent on the presence of ATP and its ability to be hydrolysed, as well as both Scc2 and Scc3. Interestingly, this activity could occur entirely independently from entrapment of DNA within the S-K ring, as it was demonstrated to still occur in complexes that were covalently circularised, by fusion of Scc1 N- and C-terminal domains with Smc3 and Scc1 respectively, combined with covalent crosslinking of the hinge domain (Davidson et al., 2019). This is consistent with the notion that cohesin possessing mutations in its hinge (Smc3 R665A K668A R669A Smc1 K554D K661D), which is unable to entrap DNA in S-K rings, can nonetheless condense *S. cerevisiae* rDNA into threads (Srinivasan et al., 2018). This mutant was found to associate normally across the genome, despite being lethal,

showing no CD formation, and very little CM formation. This implies that the vast majority of cohesin that is associated with chromosomes may be associated in a manner distinct from that of S-K ring entrapment. More importantly, if this is indeed the case, it suggests that the bulk of cohesin is engaged in activities separate to those that require entrapment within S-K rings, most likely corresponding to its activities in organising the genome via LE.

An important mechanistic consideration for LE is whether the activity is mediated by one or more SMC rings (Figure 1-8). In vitro studies suggests that loop extrusion by condensin is mediated by single condensin rings (Ganji et al., 2018). The stoichiometry of cohesin engaged in LE is less clear, and studies have suggested both individual rings (Davidson et al., 2019), and a pair of rings as being responsible for this activity (Kim et al., 2019). A further consideration is whether LE proceeds in a symmetrical (by growing the loop on both sides) or an asymmetrical (only growing the loop on one side) manner. Evidence here suggests cohesin extrudes loop symmetrically (Davidson et al., 2019; Kim et al., 2019) and condensin asymmetric (Ganji et al., 2018). Theoretical models have however claimed that the observed ~ 1000-fold compaction of DNA observed during metazoan mitosis (Earnshaw and Laemmli, 1983) cannot be adequately explained by asymmetric LE (Banigan and Mirny, 2020a), unless asymmetric extrusion were in fact two-sided extrusion with one side far more processive than the other (Banigan and Mirny, 2020b).

Two models have been proposed that attempt to bridge the divide between SMC structure and function in regard to LE. ATP hydrolysis has been shown to be essential for this process in vitro (Davidson et al., 2019; Ganji et al., 2018; Kim et al., 2019) and so both models are linked intimately to the ATP hydrolysis cycle. One

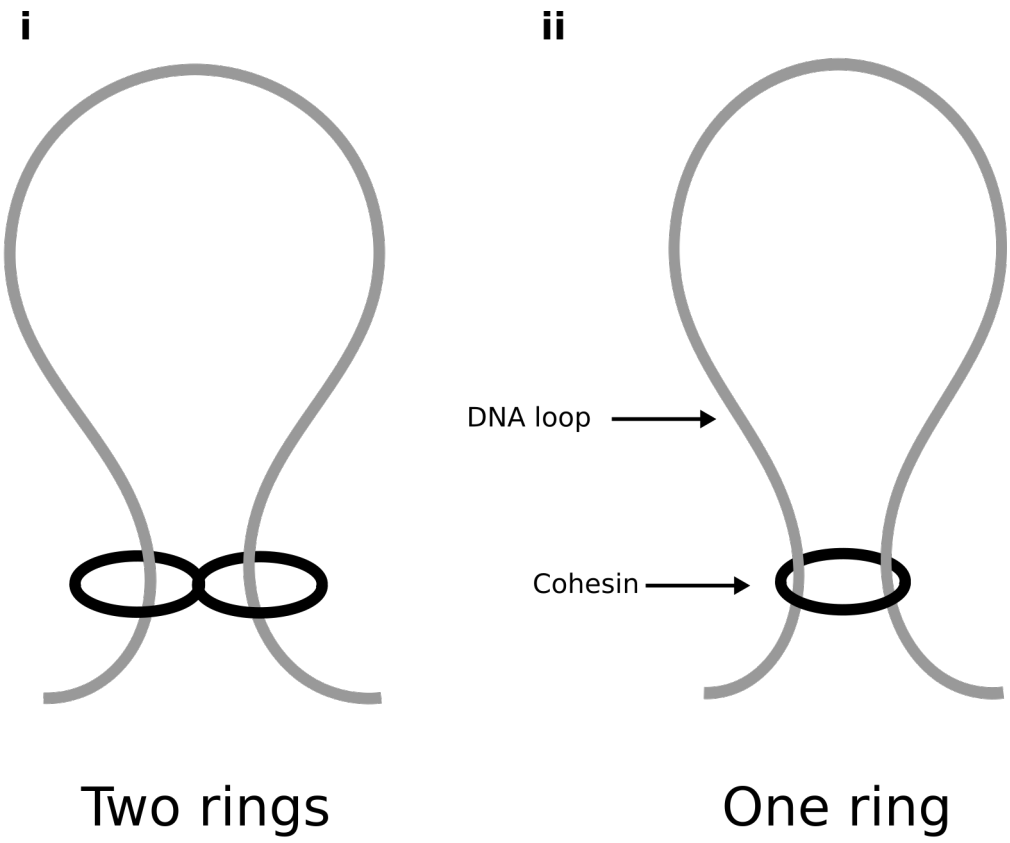


Figure 1-8. One ring or two ring models for loop extrusion.

i) SMC complexes may extrude DNA loops through the activity of a single ring, or **ii)** two rings. One section of the loop remaining stationary while the other is extruded would result in asymmetric loop extrusion, whereas both sections of the loop being extruded simultaneously would cause symmetric loop extrusion.

model has proposed that cycles of ATP driven head engagement, and hydrolysis driven disengagement, is coupled to the folding and unfolding of the coiled coils at the elbow (Bürmann et al., 2019). This might cause transition from a folded rod to that of extended rod conformation, and back again, and if coupled to DNA binding at the hinge is one mechanism which could drive this process. The second suggests that loop extrusion is driven through a pumping mechanism, whereby small loops of DNA are captured within the S-compartment and "pumped" into the K-compartment below (Diebold-Durand et al., 2017), driven by cycles of coiled coil association and dissociation.

DNA Binding to SMC Complexes

To understand the mechanism through which cohesin and other SMCs can organise DNA by LE, and how cohesin entraps DNA within its S-K ring, requires a precise understanding of the interactions between these complexes and DNA. SMC complexes and their subunits are known to make a number of electrostatic interactions with DNA. Cohesin's Scc2/4 complex (Chao et al., 2015; Murayama and Uhlmann, 2014), Scc3 subunit (Murayama and Uhlmann, 2015), and the Ycg1 subunit of condensin (Kschonsak et al., 2017) have been shown to bind dsDNA, and these interactions could contribute to the recruitment of SMC complexes to chromosomes or to stabilise their association when bound. For example, the kleisin of condensin, Brn1, has been shown to wrap around DNA that is bound to Ycg1, and this interaction has been suggested to anchor condensin onto DNA during LE (Kschonsak et al., 2017).

Purified cohesin hinge domains have also been shown to possess both dsDNA and ssDNA binding activity (Chiu et al., 2004), which may be a hint towards a

mechanistic route to capturing a second DNA molecule during cohesion establishment as has been suggested (Murayama et al., 2018). DNA binding to the hinge has also been reported for *Bacillus subtilus* SMC (Vazquez Nunez et al., 2019) and condensin hinge domains (Griese et al., 2010). However, bacterial SMC defective in DNA binding to the hinge associates with chromosomes like WT complexes (Vazquez Nunez et al., 2019), with apparently no effect on cell viability or SMC function, and so the role of DNA binding to the hinge, if any, is unclear.

The SMC DNA damage repair protein, Rad50, has also been shown to bind DNA when its head domains are engaged in the presence of nucleotide (Liu et al., 2016), along a positive groove on top of the heads that is created as a consequence of head engagement. This same DNA binding has been demonstrated in *B. subtilus* SMC (Vazquez Nunez et al., 2019), and eukaryotic cohesin (Collier et al., 2020; Higashi et al., 2020; Shi et al., 2020b), and it is likely a feature of all SMC proteins. Unlike DNA binding to the hinge, which appears dispensable for normal *B. subtilus* SMC function, mutation of the head DNA binding site caused lethality (Vazquez Nunez et al., 2019). Such complexes also appeared unable to translocate far from sites of DNA recruitment, which may hint towards defects in LE activity. Whether or not mutation of this interface affects cohesin function, and whether this interface is accessible without passing through any of S-K interface (such as by passing "up" through disengaged heads) will be important questions for the future.

Cohesin has been shown to associate with chromosomes through mechanisms independent to those yielding entrapment within S-K rings. Mutation of Smc3's Walker B site (Smc3E1155Q) in budding yeast causes lethality and abolishes S-K entrapment (Arumugam et al., 2003; Srinivasan et al., 2018). However, despite

chromosome association being lost throughout the majority of the genome in this mutant, there is significant enrichment at the centromere (*CEN)* (Hu et al., 2011; Petela et al., 2018). This is in contrast to what is observed when Smc3's Walker A site is mutated (Smc3K38I), which causes a complete loss of cohesin across the genome. It is possible *CEN* enrichment in this Walker B mutant is due to the recruitment of cohesin to the *CEN* through the interaction between Scc4 and the *CEN* associated protein Ctf19 (Chao et al., 2015; Hinshaw et al., 2017), but this raises the question as to why a similar enrichment is not observed with cohesin containing Walker A mutants, which can presumably still bind Ctf19 through Scc4. Interestingly, head engagement, stabilised by the addition the nucleotide analogue ADP-BeFx, has been shown to stabilise the interaction between Scc2 and cohesin (Çamdere et al., 2018). It is possible that Smc3E1155Q may similarly stabilise head engagement by allowing ATP binding but not its hydrolysis, and through stabilising head engagement also stabilise Scc2's interaction with cohesin. Increased Scc2-cohesin interaction, coupled with Scc4's recruitment to the *CEN* through interaction with Ctf19, could explain this *CEN* specific enrichment in cohesin complexes deficient in ATP hydrolysis.

Dissociation from DNA

Cohesin can dissociate from DNA through at least two pathways. The first, involves proteolytic cleavage of Scc1 by separase at the onset of anaphase (Uhlmann et al., 1999, 2000). This acts to destroy SCC by releasing DNA trapped inside S-K rings and enables chromosomes to segregate. The second path to cohesin removal does not involve proteolytic cleavage. In metazoan cells, the bulk of cohesin associated with the genome is dissociated during prophase (Sumara et al., 2000), known as the prophase pathway. The bulk removal of the majority of cohesin at prophase does not

occur in yeast, although it turns out the same mechanism of release is active throughout interphase (Chan et al., 2012; Gerlich et al., 2006) and is responsible for cohesin turnover (although it is not hyperactive in yeast and metazoan interphase like it is during prophase in metazoan cells). This pathway is separase independent, and instead relies on the regulatory subunit Wpl1 which binds to Pds5 (Gandhi et al., 2006; Kueng et al., 2006). Evidence suggests that this is achieved through opening of the N-terminal-Scc1 Smc3 interface (Beckouët et al., 2016). A function of acetylation of Smc3 by Eco1 during S phase may be to stabilise this interface and thus prevent Wpl1 mediated dissociation (Chan et al., 2012). It turns out that release of DNA through this interface may also be a more general mechanism to remove cohesin from DNA, as dissociation of cohesin from DNA occurs even in the absence of Wpl1 and is blocked by covalently fusing the Smc3-Scc1 interface (Srinivasan et al., 2019). In the absence of the Smc3-Scc1 fusion, Scc2 is required to counteract this release pathway, suggesting that Scc2 may play a role in keeping this interface closed and that one function of Wpl1 may be to dissociate Scc2 from cohesin.

Topology: Even or Odd Number of DNA Passages

The precise topological nature of the interaction between cohesin and DNA will be discussed in this work, and so it is important to summarise the different forms this may take. When considering topology, the cohesin ring can be considered a simple ring, and DNA as an extended line. If a line passes through the inner cavity of the ring only once, we can consider this as a one-strand passage mode of topological association (Figure 1-9i left panel). If the line itself has a closed topology with no end (such as with a circular piece of DNA), the only way to enter into this topology is for one of the rings to break and pass the other through (and subsequently seal the break). Interestingly, to pass a line through a circle any odd number of times (1, 3, 5,

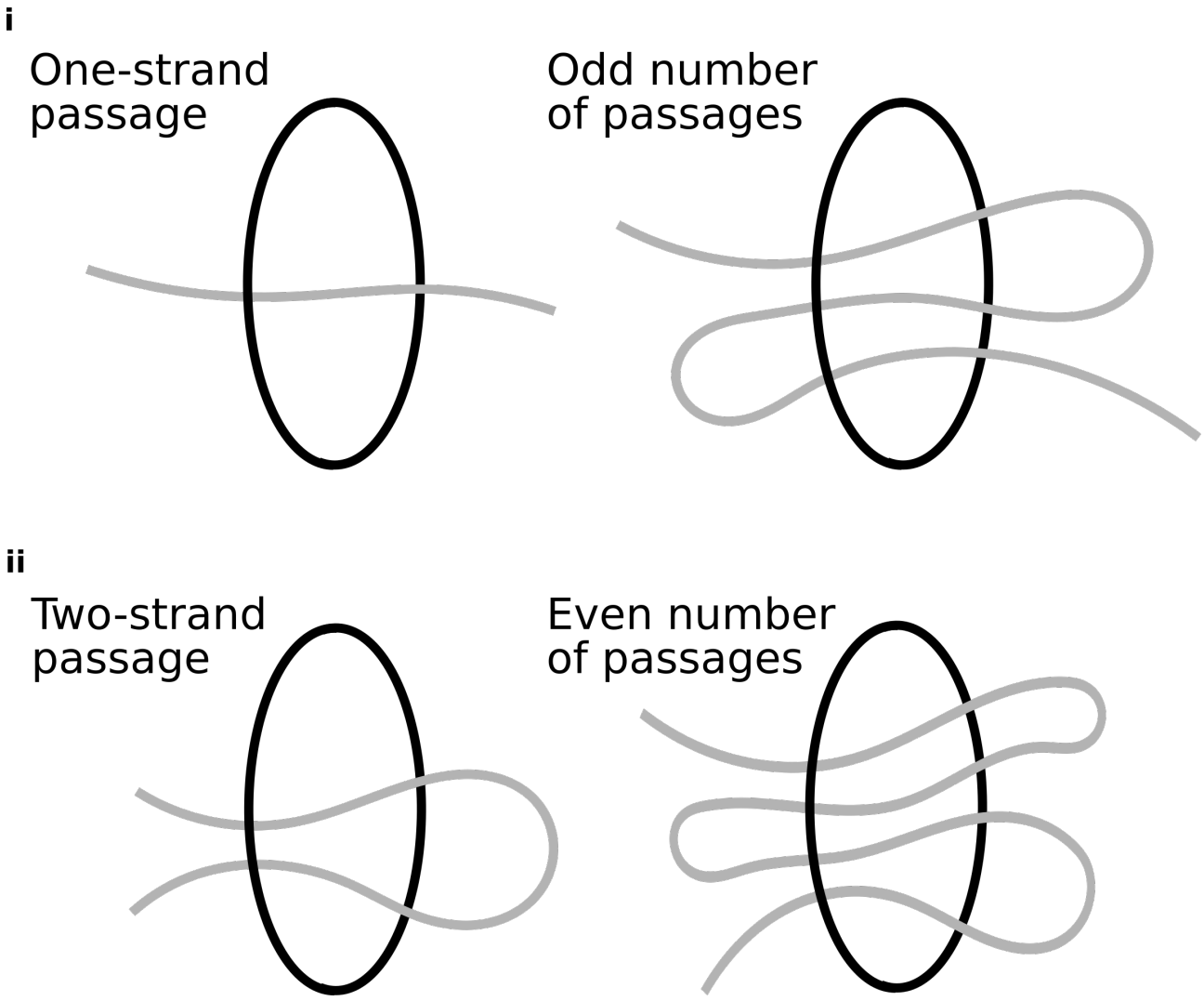


Figure 1-9. The topology of lines within rings.

i) Left-hand panel - One-strand passage topology between a line and a ring. Right-hand panel – Odd number of passages through a ring. Pulling these lines from either end away from a ring will convert any odd number of passages to a one-strand passage topological association. **ii**) Left-hand panel – Two-strand passage topology. Right-hand panel – Even number of passages through a ring. Pulling a line end away from the ring will always first convert an even-number of passages to a two-strand passage topological association (a loop), before destroying the topological association entirely by pulling the loop out from the ring.

7, etc), the circle must first be broken, and the line must pass through once. Functionally speaking, a one-strand passage mode of association is then topologically equivalent to any number of odd passages through the ring. This can be conceptualised if you image pulling on each end of the line (Figure 1-9i right panel). Eventually, you will pull out all of the loops trapped within the ring, but you will always be left with a one-strand passage mode of association (unless you break the ring again). When discussing S-K entrapment, it is a one-strand passage topology which is being referred to.

You can, however, topologically associate with rings without first breaking and passing through them by instead inserting loops (Figure 1-9ii left panel). Inserting a single loop into a ring can be considered a two-strand passage topology, and in cohesin literature has been referred to as pseudo-topological. A two-strand passage is functionally equivalent to any even number of passages through a ring (2, 4, 6, etc), as pulling on the ends of the lines away from the ring will always revert back to a two strand passage topology (before pulling the loop out completely). Importantly, to create a two-strand passage topology does not require breaking the ring at any point. A two-strand passage topology does not result in S-K entrapment, but could reflect entrapment of DNA loops.

Thesis Objectives

Further understanding of how cohesin is able to establish SCC during S phase and organise chromosomes into loops during interphase and mitosis will require a precise description of how cohesin interacts with DNA and the topological nature of these interactions. To address this, I set out to purify the *S. cerevisiae* cohesin complex and develop a protocol to measure S-K entrapment of DNA by cohesin in vitro. Studying entrapment in vitro allows one to ask very simple questions surrounding the mechanism of DNA entrapment without the many confounding variables present inside cells. In order to make unambiguous deductions on the nature of the topology between cohesin and DNA, entrapment must be measured directly, through covalent circularisation of cohesin on the DNA. This will be carried out using a protocol for cysteine-cysteine crosslinking like that employed in vivo (Gligoris et al., 2014). Once established, I will use this system to further elucidate the nature of cohesin's association with DNA and the mechanism through which DNA becomes entrapped.

Chapter 2 - Measuring S-K Entrapment of DNA by Cohesin in vitro

Most of the data described in the following chapters have been published in Collier et al., 2020.

Introduction

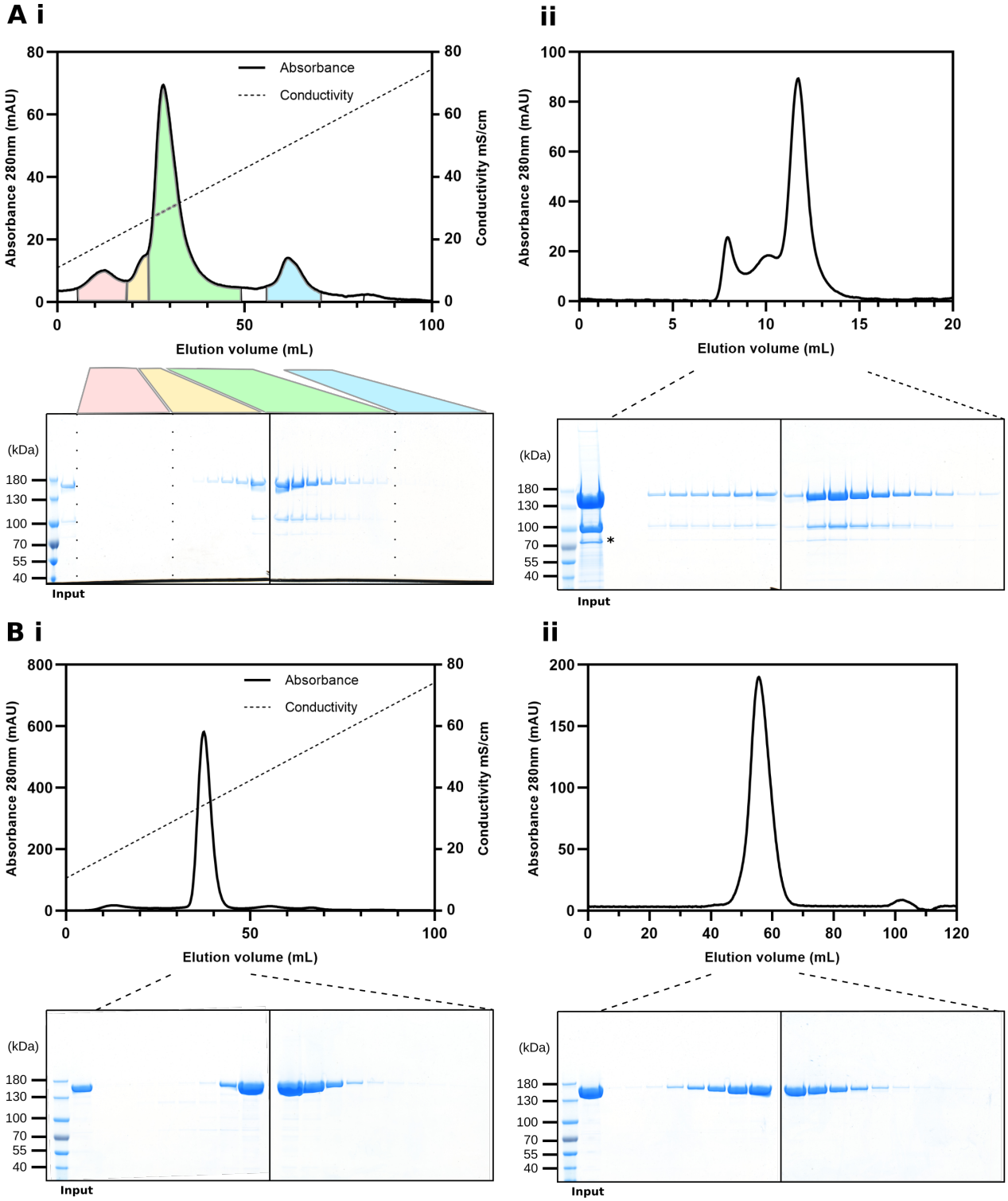
Previous attempts to demonstrate entrapment of DNA by S-K rings in vitro have used resistance to high ionic strength washes as their criteria (Murayama and Uhlmann, 2014; Onn and Koshland, 2011). This criteria was selected based on the observation that subjecting isolated chromosomes to high ionic strength washes caused the dissociation of most associated proteins (Paulson and Laemmli, 1977). A small fraction of proteins would resist these washes, and it has since been reasoned that this pool of proteins could not be associated via simple electrostatic association alone and that only association through a topological principle, namely a one-strand passage topology, could lead to such stability. Subsequent in vitro studies managed to reproduce this salt resistant association with cohesin, and found such association was dependent on a closed topology for both cohesin and DNA (Murayama and Uhlmann, 2014), with cleavage of either sufficient to disrupt this salt stable association. While this infers a topological mechanism is at play, it fails to demonstrate this directly. A direct measurement of topology must involve covalent entrapment of cohesin on DNA. Without directly measuring the topology of this association there is significant ambiguity in interpreting the nature of association. For example, is DNA being entrapped within the S-K ring? If so, is DNA entrapped in the S compartment or the K compartment? Is DNA entrapped in a manner distinct from S-K entrapment, such as by DNA passage between then heads into the S compartment, or is DNA instead somehow clamped between a HAWK and the cohesin ring?

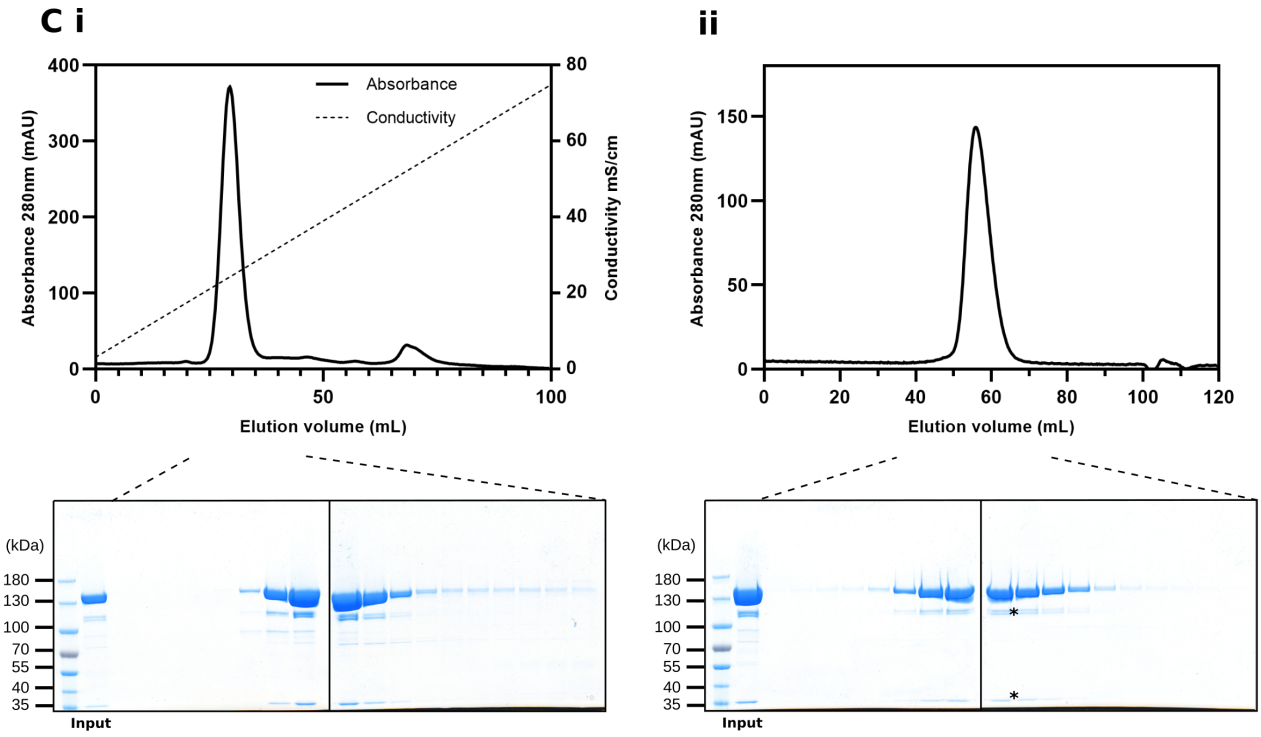
Expression and purification of the cohesin complex

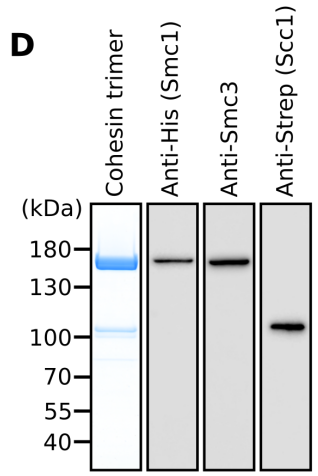
To address these questions, I set out to express and purify cohesin S-K rings. Despite Scc3 often being thought of as a constitutive member of the cohesin complex (Tóth et al., 1999), I decided to express cohesin trimers (Smc1, Smc3, Scc1), rather than

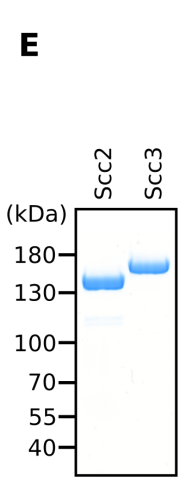
cohesin tetramers (Smc1, Smc3, Scc1, and Scc3) to allow me to identify Scc3 independent activities. Any reference to cohesin tetramers throughout this work refers to reconstituted cohesin tetramers created through addition of purified cohesin trimers to purified Scc3. First, the *S. cerevisiae* cohesin genes were synthesised and codon optimised for expression in *Spodoptera frugiperda*. The C-terminus of *SCC1* and *SCC2* were tagged with a StrepII tag, the N-terminus of *SCC3* tagged with a StrepII tag, and the C-terminus of *SMC1* tagged with a 6xHis tag. The N-terminus of *SCC2,* which binds Scc4, was then removed to generate $Scc2^{133\text{-}1493}$ as the C-terminal region of Scc2 has previously been shown to be sufficient to drive cohesin's ATPase (Petela et al., 2018, Murayama and Uhlmann, 2014) and facilitate stable association between cohesin and DNA (Minamino et al., 2018). *SMC1*-6xHIS*, SMC3,* $SCC2^{133\text{-}1493}$-StrepII*,* and StrepII-*SCC3* were then cloned into a pACEBac1 vector, and *SCC1*-StrepII was cloned into a pIDC vector. *SMC1*-6xHIS and *SMC3* were then cloned into the same vector. Vectors containing cohesin S-K rings were then generated by combining pIDC *SCC1*-StrepII with pACEBac1 *SMC1*-6xHis *SMC3* via a cre recombinase reaction. These expression vectors were then transformed into DH10Bac *Escherichia coli* cells which then insert into the bacterial artificial chromosome (bacmid) maintained in this strain. These bacmids were then isolated and transfected into Sf9 *S. frugiperda* cells to generate viral expression vectors which were then expressed in 500 ml Sf9 cultures.

Cells were harvested by centrifugation and lysed by sonication, following which cohesin was then purified from cell lysate via a three strep purification protocol: affinity chromatography followed by anion exchange chromatography (AEC) and then size exclusion chromatography (SEC). There were three peaks of absorbance at 280nm following AEC (Figure 2-1Ai – top panel), however, only the center peak contained protein (Figure 2-1Ai - bottom panel) and was isolated for further purification (bottom


A i
ii
Absorbance
Conductivity
Absorbance 280nm (mAU)
Conductivity mS/cm
Elution volume (mL)
(kDa)
180
130
100
70
55
40
Input
*
B i
ii


C i
ii
Absorbance
Conductivity
Absorbance 280nm (mAU)
Conductivity mS/cm
Elution volume (mL)
(kDa)
180
130
100
70
55
40
35
Input
*
*


D
Cohesin trimer
Anti-His (Smc1)
Anti-Smc3
Anti-Strep (Scc1)
(kDa)
180
130
100
70
55
40


E
Scc2
Scc3
(kDa)
180
130
100
70
55
40

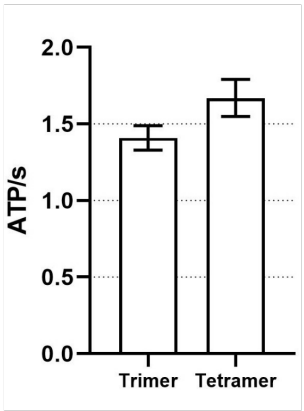

F
ATP/s
2.0
1.5
1.0
0.5
0.0
Trimer
Tetramer

Figure 2-1. Purification of the cohesin complex.

Cohesin trimers (Smc1-His, Smc3, and Scc1-StrepII), Scc2, and Scc3 were purified by a three-step purification protocol: Affinity pull-down followed by anion exchange chromatography (AEC) and then size exclusion chromatography (SEC). Top panels show absorbance profile at 280nm and the bottom panels the indicated fractions analysed by SDS-PAGE and Coomassie staining. **(Ai)** Cohesin trimers purified by AEC eluted across a gradient of 100mM to 1M NaCl at pH 7.5. Fractions appearing to contain both SMC proteins, and Scc1 (green region), were collected for further purification. (**Aii**) Cohesin trimers purified by SEC. Fractions between 11.5-13ml were collected. (* - identified as Hsp70 by mass spectrometry). (**Bii**) Scc3 purified by AEC under identical conditions to cohesin trimers. (**Bii**) Scc3 purified by SEC. Peak fractions were collected. (**Ci**) Scc2 purified by AEC across a gradient of 0mM to 1M NaCl at pH 8.0. (**Cii**) Scc2 purified by SEC. Peak fractions were collected (* - identified as degradation products of Scc2 by mass spectrometry). (**D**) Coomassie strain of cohesin trimers following the three-step purification protocol. Individual subunits were then probed for by western blotting. (**E**) Coomassie stain of Scc2 and Scc3 following the three-step purification protocol. (**F**) ATPase activity for purified cohesin trimers incubated with DNA, Scc2, and ATP in the presence of Scc3 (tetramer) or absence (trimer).

panel - shaded green). SEC also yielded three 280nm absorbance peaks for cohesin (Figure 2-1Aii – top panel), all of which were found to be of identical protein composition (Figure 2-Aii – bottom panel), the largest of which was selected for experimentation (elution volume 11.5ml - 13ml). The other two peaks could correspond to aggregation, or distinct structural conformations or oligomerization states. It has been suggested that ATP independent clustering by cohesin is indicative of phase separation and may play some functional role inside cells (Ryu et al., 2020), although this activity was dependent on the presence of DNA, which should be degraded during purification as the lysate is supplemented with super nuclease. This activity was not investigated further during this study.

Purified cohesin was analysed by SDS-PAGE and Coomassie staining, and the presence of Smc1-His, Smc3, and Scc1-StrepII was confirmed by western blotting (Figure 2-1D) and mass spectrometry. Coomassie staining revealed Scc1 to run as two bands, the lower identified as a degradation product by mass spectrometry. A faintly staining band running below Scc1, approximately 70 kDa (Figure 2-1Aii – * bottom panel), was analysed by mass spectrometry and identified to be Hsp70, a heat shock protein thought to aid in protein folding and possibly binds to the largely unstructured Scc1 subunit. $Scc2^{133-1493}$, and Scc3 were both expressed and purified by the same protocol ($Scc2^{133-1493}$ will be referred to as Scc2 throughout the remainder of this work). Both Scc3 and Scc2 ran as single peaks of absorbance at 280nm for both AEC and SEC (Figure 2-1Bi ii & Ci ii). Final purification products were then separated by SDS-PAGE and analysed by Coomassie staining (Figure 2-1E). Several smaller migration products were present in the Scc2 purified product (See Figure 2-1Cii - * bottom panel) and were all identified as degradation products of Scc2 by mass spectrometry.

To check whether the purified cohesin was functional, the ATPase activity of the complex was measured. Cohesin rings were incubated with Scc2 and Scc3, as well as a 40 bp dsDNA, following which ATP was added to the reaction mix. Rate of ATP hydrolysis was then measured by a coupled reaction, with Pi produced from the hydrolysis of ATP to ADP + Pi used as the substrate for conversion of 2-amino-6-mercapto-7-methylpurine riboside to ribose 1-phosphate and 2-amino-6-mercapto-7-methylpurine by purine nucleoside phosphorylase, which can be quantified by measuring the increase in absorbance at 360 nm. Cohesin was found to be active, with a rate of ATP hydrolysis of between 1.5 - 2.0 ATP s^{-1} (Figure 2-1F).

An assay to measure S-K entrapment of DNA by cohesin

I then set out to create an in vitro system to directly measure topological association between cohesin and DNA. This was based on an in vivo mini-chromosome entrapment assay (Gligoris et al., 2014), using cysteine pair substitutions in the protein interfaces of cohesin to facilitate their covalent linkage upon incubation with the homobifunctional crosslinking reagent bis-maleimidoethane (BMOE) (Figure 2-2A). Cohesin containing cysteine pairs to crosslink the Smc3 Scc1 (Smc3S1043C Scc1C56), hinge (Smc3E570C Smc1K639C), or Scc1 Smc1 interfaces (Scc1A547C Smc1G22C) were purified. These complexes were crosslinked by addition of BMOE and analysed by SDS-PAGE and Coomassie staining (Figure 2-2B). When all three interfaces were crosslinked simultaneously a unique crosslinking species was present, likely a covalent circularised cohesin S-K ring. Importantly, the presence of these cysteine substitutions had no measurable effect on cohesin's ATPase activity (Figure 2-2C).

To measure topological entrapment of DNA within S-K rings, cohesin containing all three cysteine pairs, Scc2, and Scc3 were incubated with a 2.7 kb circular dsDNA. Following

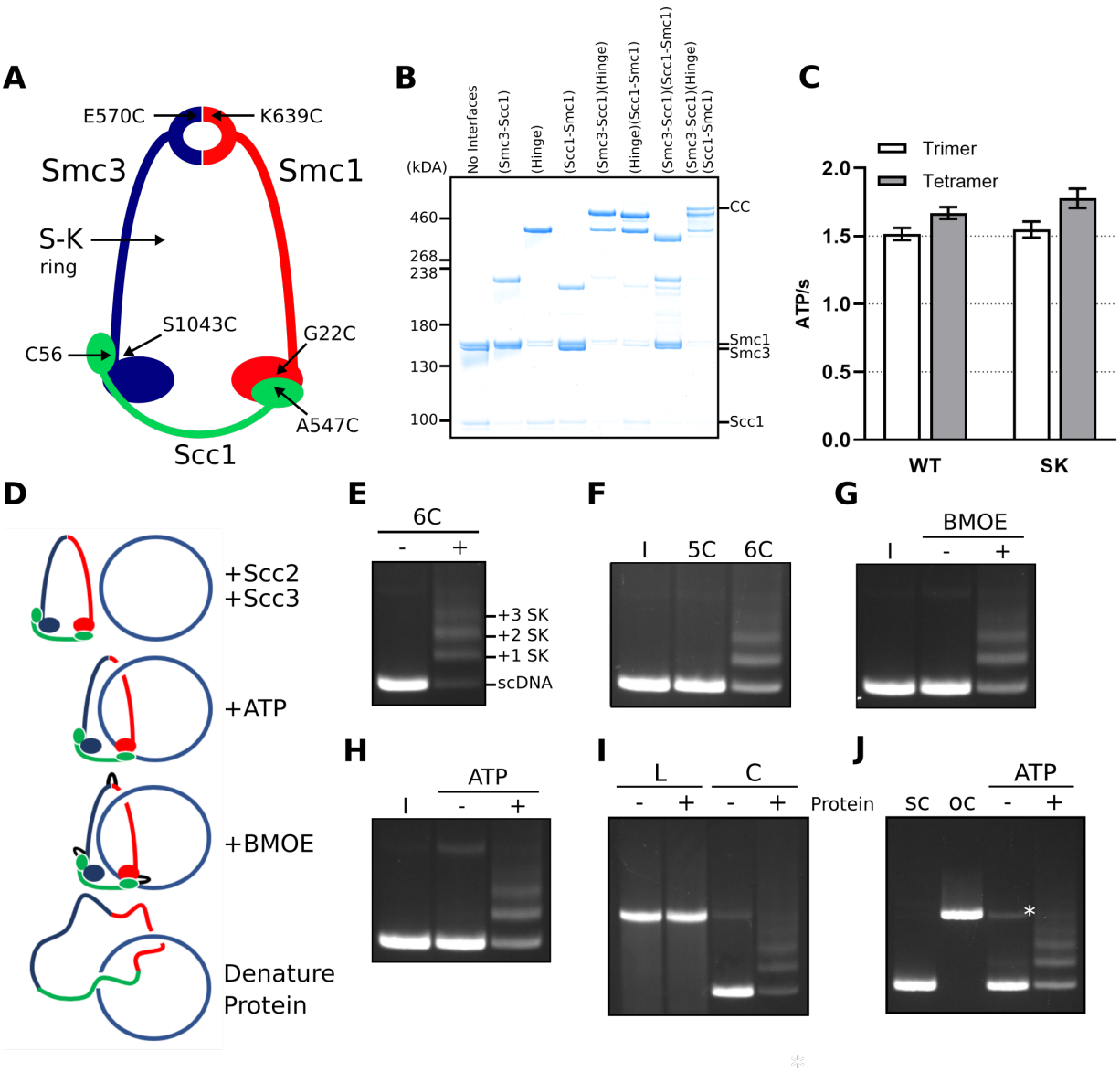


Figure 2-2. An assay to measure S-K entrapment of DNA by cohesin.

(A) Schematic of the cohesin S-K ring showing the position of the 6 cysteine residues used to covalently circularise it. (**B**) BMOE-induced crosslinking of S-K rings with cysteine pairs in the specified interfaces. CC = circular cohesin. (**C**) Rate of ATP hydrolysis per cohesin ring, either trimers or tetramers, incubated with DNA, Scc2, and ATP. Comparing WT cohesin against cohesin containing the cysteines to circularise the S-K ring. (**D**) The entrapment assay scheme. (**E**) Entrapment of DNA in S-K rings in the presence or absence of 6C cohesin, (**F**) in the presence of 5C cohesin lacking Scc1A547C, or of 6C cohesin, (**G**) in the presence or absence of BMOE, (**H**) in the presence or absence of ATP, or (**I**) comparing linear vs supercoiled circular DNA. (**J**) Entrapment assay in the presence or absence of ATP. DNA damaged in the absence of ATP (denoted by an *) runs identically to open circular DNA (OC). All entrapment assays were incubated for 40 min and carried out in the presence of Scc2 and Scc3. (I = input DNA).

this, ATP was added, and the reaction was incubated at 24 ˚C for 40 mins. BMOE was then added and the reaction incubated on ice for 6mins, before adding SDS to a final concentration of 1 % and incubating the reaction mix at 70 ˚C for 10 mins. Samples were then separated by agarose gel electrophoresis, run at 50 V for 17 hours at 4 ˚C and then visualised by EtBr staining and UV exposure (Figure 2-2D for schematic). This resulted in the retardation of the input DNA and formation of a DNA ladder (Figure 2-2E). In other words, through covalent circularisation of S-K rings it is possible to entrap single, or multiple, cohesin rings on circular DNA. As the efficiency of circularising the S-K ring by BMOE crosslinking is only ~20 % (this work; Gligoris et al., 2014), it is possible that each plasmid may be entrapped by anywhere up to 15 cohesin rings. Entrapment of this kind was dependent all six cysteines (Figure 2-2F), and a 5C cohesin lacking a single cysteine failed to shift any DNA. Importantly, this shift was dependent on the presence of both BMOE (Figure 2-2G) and ATP (Figure 2-2H), as well as DNA possessing a circular topology (Figure 2-2I). In the absence of ATP, and under conditions where cohesin does not efficiently entrap DNA, a faint higher molecular weight band was sometimes visible (denoted by an *) that runs identically to relaxed circular DNA and likely corresponds to DNA damaged by the protocol or some small contamination (Figure 2-2J).

S-K entrapment is dependent on Scc3 and ATP binding, and stimulated by Scc2 and ATP hydrolysis

I next looked at the requirement for Scc2 and Scc3 in stimulating S-K entrapment, observing these reactions over 40 min and taking time points every 10 min. Entrapment of DNA within S-K rings was strictly dependent on Scc3 and stimulated by the presence of Scc2 (Figure 2-3A & B). The low level of entrapment seen in the presence of Scc2 alone was comparable to entrapment in the absence of both Scc2 and Scc3 (Figure 2-3C), indicating that efficient S-K entrapment has a strict requirement for Scc3 and in its

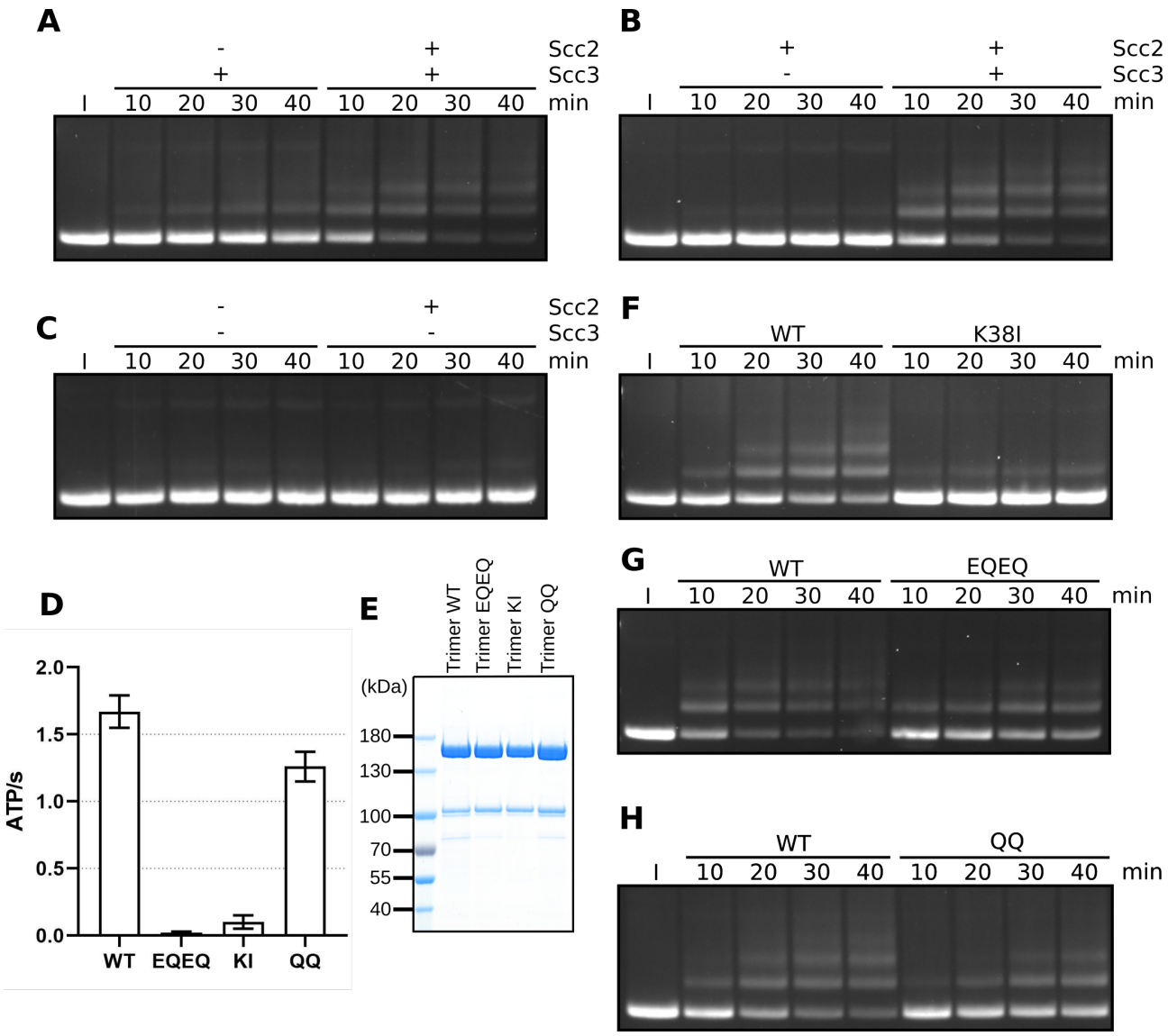


Figure 2-3. Entrapment of DNA in S-K rings depends on Scc3 and ATP binding, and is stimulated by Scc2 and ATP hydrolysis.

(**A**) Entrapment of DNA in S-K rings in the presence of Scc3, and the presence or absence of Scc2, or (**B**) the presence of Scc2, and the presence or absence of Scc3, or (**C**) comparing cohesin trimers against cohesin trimers in the presence of Scc2. (**D**) Rate of ATP hydrolysis per cohesin ring, Smc1E1158Q Smc3E1155Q (EQEQ), Smc3K38I (KI) or Smc3K112Q K113Q (QQ), all carried out in the presence of Scc2, Scc3, and DNA. (**E**) Coomassie stain of WT, EQEQ, KI, and QQ cohesin trimers. (**F**) DNA entrapment in S-K rings comparing WT cohesin to Smc3K38I (K38I), or (**G**) WT cohesin to Smc1E1158Q Smc3E1155Q (EQEQ), or (**H**) WT cohesin to Smc3K112Q K113Q (QQ), in the presence of both Scc2 and Scc3. Entrapment assays were carried out over 40 min with time points taken every 10 min. (I = input DNA).

absence only background levels on entrapment are seen. I next went on to investigate the role of cohesin's ATPase in promoting entrapment by S-K rings. Both ATP binding and its hydrolysis are required for cohesin's association with chromosomes in vivo (Arumugam et al., 2003; Hu et al., 2011) and so I made mutants defective in these activities (Figure 2-3E). Cohesin containing a mutation of Smc3's Walker A site (Smc3K38I), known to prevent ATP binding to Smc3, almost completely abolished ATP hydrolysis (Figure 2-3D), and mutation of both Walker B sites (Smc1E1158Q Smc3E1155Q - EQEQ) abolished it completely. Residual ATPase activity in the Smc3K38I mutant likely stems from the preservation of Smc1's Walker A site, which may be sufficient for some ATP binding and hydrolysis. These mutants were then tested for their ability to promote entrapment by S-K rings. Cohesin unable to bind ATP to Smc3 was also completely unable to entrap DNA (Figure 2-3F). Cohesin defective in ATP hydrolysis showed a significant reduction in entrapment, yet a relatively substantial amount of DNA was still shifted by 40 min (Figure 2-3G). The amount of DNA entrapped by 40 mins in the EQEQ mutant was comparable to that entrapped by WT cohesin by 10 min, demonstrating that in vitro DNA entrapment by S-K rings only partly depends on the ability of cohesin to hydrolyse ATP. A similar result has been reported for EQEQ cohesin's ability to stably associate with DNA in vitro (Murayama and Uhlmann, 2015). It is currently unclear why ATP hydrolysis is required for cohesin's association with chromosomes and S-K entrapment in vivo (Arumugam et al., 2003; Srinivasan et al., 2018), but not for S-K entrapment in vitro.

The Smc3 head domain has two highly conserved lysine residues, K112 K113, which are acetylated during cohesion establishment and whose mutation to glutamine, thought to somewhat mimic acetylation, is not viable in *S. cerevisiae*. This mutant shows only a minor defect in levels of ATP hydrolysis (Figure 2-3D). To ascertain whether this lethality

was due to problems entrapping DNA, I tested the ability of this mutant to entrap DNA in S-K rings (Figure 2-3H). Levels of S-K entrapment were reduced to a similar degree as to what was observed with EQEQ cohesin. Whether or not this reduction in S-K entrapment is sufficient to explain the lethality observed in vivo is unclear.

DNA binding to Scc3 facilitates entrapment by S-K rings

The mechanism through which Scc2 and Scc3 act in promoting DNA entrapment within S-K rings is unknown. Drawing inspiration from a recent structure of condensin's Ycg1 subunit, that was solved in complex with DNA (Kschonsak et al., 2017), we asked whether cohesin's Scc3 subunit might similarly bind to DNA. A 40 bp fluorescently labelled dsDNA was incubated with increasing concentrations of Scc3, and DNA binding was then analysed by means of an electromobility shift assay (EMSA). In the presence of Scc3 DNAs mobility was greatly retarded in the gel, confirming Scc3 indeed binds to DNA (Figure 2-4A). This activity was found to increase when Scc3 was first incubated with a fragment of Scc1 (residues 269-451) that binds Scc3. DNA binding to Ycg1 is mediated through a positively charged surface composed of several lysine and arginine residues. A similar positively charged surface is also present on Scc3 and so we investigated the impact that mutation of this surface had on DNA binding to Scc3. Scc3 containing mutation of two clusters of positively charged residues were mutated (Scc3K224E K225E R226E and Scc3K423 K513E K520E) on the groove within Scc3 equivalent to the DNA binding groove of Ycg1 (Figure 2-4B). These were then expressed and purified (Figure 2-4C) and their DNA binding activity assessed. Individually, each single triple mutant (3E) showed only minor defects in DNA binding (Figure 2-4D). Despite this, these mutations caused a substantial decrease in the ability of Scc3 to promote S-K entrapment (Figure 2-4E). Next, both triple mutants were combined to generate a

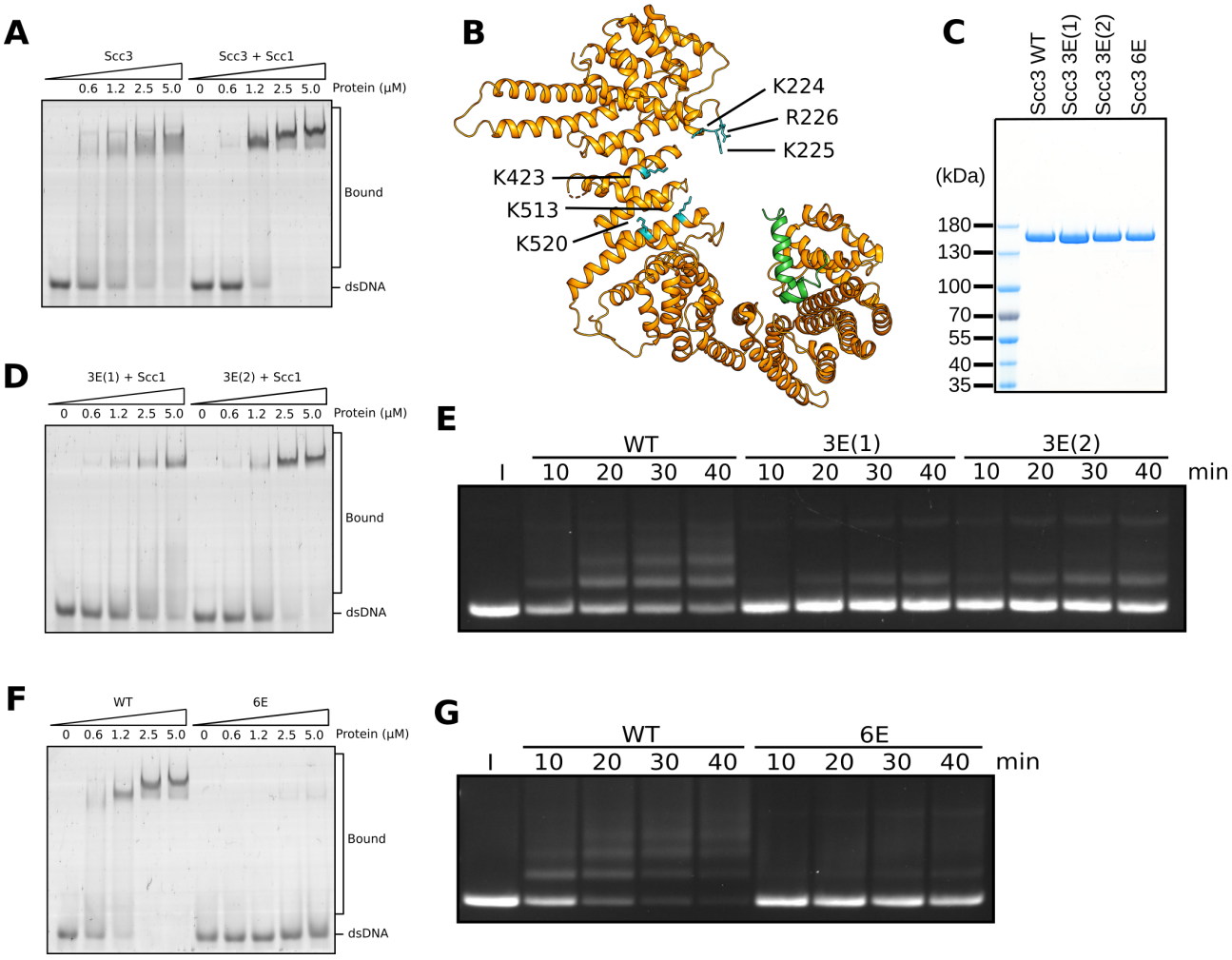


Figure 2-4. DNA binding to Scc3 is required for S-K entrapment.

(**A**) EMSA comparing the ability of Scc3 to bind dsDNA against Scc3-Scc1$^{269-451}$ complexes. (**B**) Structure of *S. cerevisiae* Scc3 (orange) in complex with a fragment of Scc1 (green) (PDB 6H8Q). Labelled are the six residues within the DNA binding groove of Scc3 that were mutated to glutamate (Scc3-6E). (**C**) Coomassie stain of WT, 3E(1), 3E(2), and 6E Scc3. (**D**) EMSA comparing the ability of Scc3-3E(1)-Scc1$^{269-451}$ (Scc3K224E K225E R226E) against Scc3-3E(2)-Scc1$^{269-451}$ (Scc3K423E K513E K520E) complexes to bind dsDNA. (**E**) DNA entrapment in S-K rings in the presence of Scc2, comparing WT Scc3, to Scc3-3E(1) and Scc3-3E(2). (**F**) EMSA comparing the ability of Scc3 to bind dsDNA against Scc3-6E-Scc1$^{269-451}$ complexes. (**G**) DNA entrapment in S-K rings in the presence of Scc2, comparing WT Scc3 to Scc3-6E. Entrapment assays incubated for 40 min with time points taken every 10 min. (I = input DNA).

sextuple mutant (6E), which resulted in the complete loss of both DNA binding activity (Figure 2-4F) and of the ability to promote entrapment within S-K rings (Figure 2-4G). During the course of this work a crystal structure was published of *S. cerevisiae* Scc3 bound to a fragment of Scc1 and dsDNA (PDB 6H8Q), revealing these residues to indeed make contact with DNA (Li et al., 2018).

DNA binding to Scc2 facilitates entrapment by S-K rings

The Scc2/Scc4 complex has previously been shown to bind to dsDNA (Chao et al., 2015; Murayama and Uhlmann, 2014), but the functional significance of this observation has never been determined. I found that the *S. cerevisiae* Scc2 complex also binds to DNA (Figure 2-5A). Unlike Scc3, whose DNA binding activity was increased when in complex with Scc1, DNA binding to Scc2 was inhibited when co-incubated with a fragment of Scc1 (residues 150-298) containing sequences necessary for Scc2's association with Scc1 (Petela et al., 2018) (Figure 2-5A). I then set out to identify whether Scc2 might be binding DNA in a similar manner to that of Scc3 and Ycg1. I mapped the *S. cerevisiae* Scc2 sequence onto an *Eremothecium gossypii* structure (PDB 5ME3) and aligned this against the Scc3-Scc1 structure bound to DNA. This revealed significant structural and sequence homology between Scc2 and Scc3 along the region of DNA binding. Four residues within this surface of Scc2 are particularly conserved (S717 K721 K788 H789; Figure 2-5B) and in *S. cerevisiae* both *scc2 S717L K721E* and *scc2 K788E K789E* double mutants are lethal and abolish the association of cohesin along most of the genome (Collier et al., 2020; Petela et al., 2018). Scc2 containing mutations in this putative DNA binding surface were expressed and purified (Figure 2-5C), and their DNA binding activity then assessed by EMSA. Each double mutant (2E) showed major defects in DNA binding (Figure 2-5D), however only minor reductions in levels of S-K entrapment

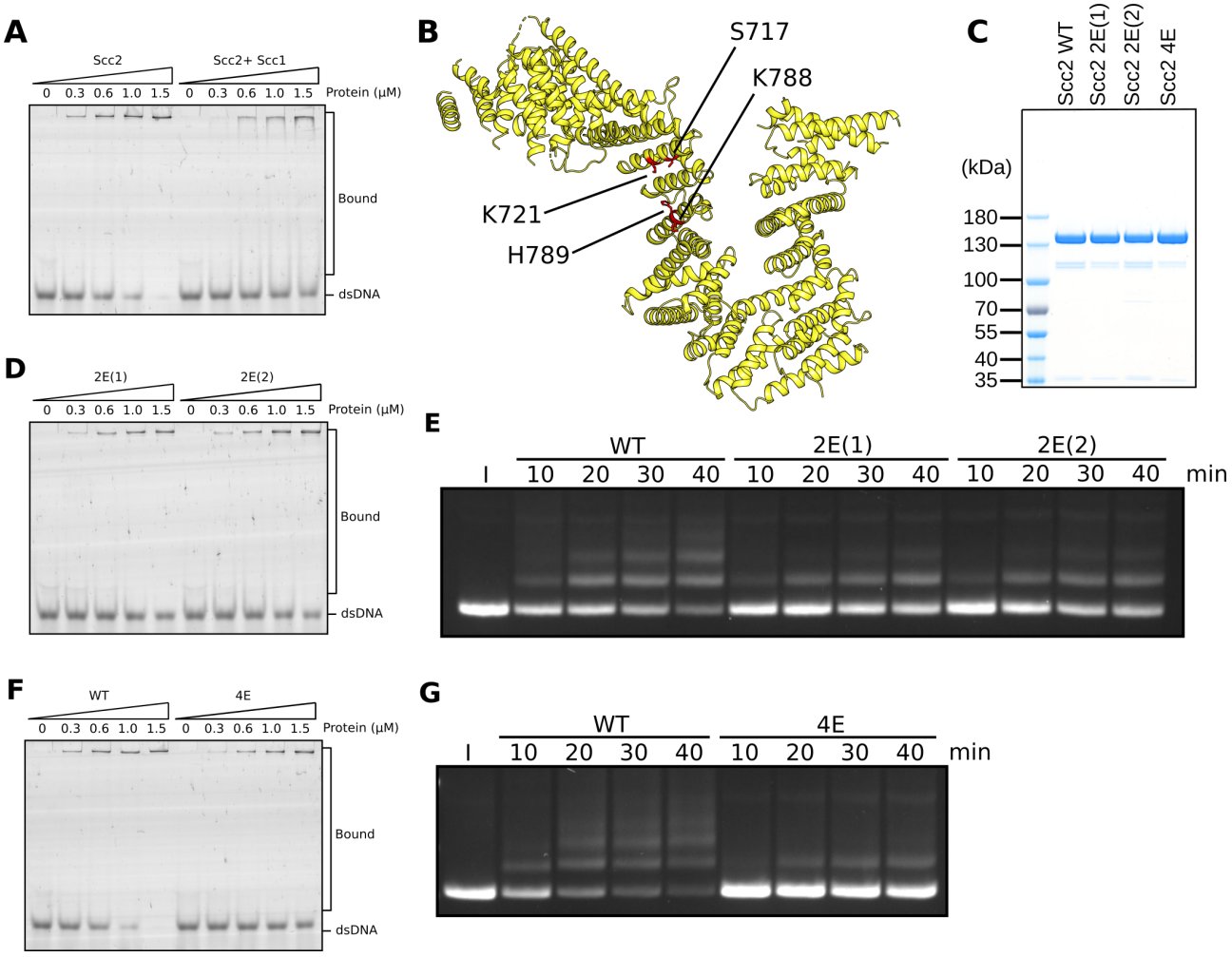


Figure 2-5. DNA binding to Scc2 is required for S-K entrapment.

(**A**) EMSA comparing the ability of Scc2 to bind dsDNA against Scc2-Scc1$^{150\text{-}298}$ complexes. (**B**) *S. cerevisiae* Scc2 (PDB 6ZZ6). Labelled are the four residues within the DNA binding groove of Scc2 that were mutated to glutamate (Scc2-4E). (**C**) Coomassie stain of WT, 2E(1), 2E(2), and 4E Scc2. (**D**) EMSA comparing Scc2-2E(1) (Scc2S717E K721E) and Scc2-2E(2) (Scc2K788E H789E) to bind dsDNA. (**E**) Entrapment of DNA in S-K rings in the presence of Scc3 and either Scc2, Scc2-2E(1), or Scc2-2E(2). (**F**) EMSA comparing the ability of Scc2 and Scc2-4E to bind dsDNA. (**F**) Entrapment of DNA in S-K rings in the presence of Scc3 and either Scc2 or Scc2-4E. Entrapment assays incubated for 40 min with time points taken every 10 min (I = input DNA).

(Figure 2-5E). Combining each mutation into a single quadruple mutant (4E) resulted in a similar reduction in DNA binding activity (Figure 2-5F), however, almost completely abolished levels of S-K entrapment (Figure 2-5G).

Chapter 3 – Does DNA reside in the S or K compartments?

Introduction

Very little evidence exists to support the notion that cohesin, or other SMC-kleisin complexes for that matter, ever structurally exists as an open ring. Cohesin contains a pair of ABC-like ATPase domains (Arumugam et al., 2003) and for stable association with chromosomes requires the ability to both bind and hydrolyse ATP (Hu et al., 2011). ATP binding would effectively partition the S-K ring into two by engaging the heads (E-state), resembling a figure of eight and creating two compartments: one between the SMC arms (S compartment), and the other “below” the SMC heads and between the kleisin (K compartment). Similarly, these compartments may exist in the absence of ATP as well (J-state), as the SMC heads are known to remain loosely associated with one another even in the absence of ATP (Chapard et al., 2019; Vazquez Nunez et al., 2019). This effectively creates two distinct compartments within which DNA can reside, either the S- or K-compartments with the heads either in the E- or J-states (refer to Figure 1-3). Identifying which of these compartments DNA resides in, and whether this is associated with an E or J head configuration, may help elucidate the mechanism through which DNA becomes entrapped in S-K rings, and more generally aid in linking our understanding of the ATP hydrolysis cycle to the transport of DNA inside SMC-kleisin complexes.

DNA is never entrapped in J-S compartments and only rarely in J-K compartments

I next set out to identify where in the S-K ring entrapped DNA resides, be that in the S compartment or the K compartment. By using a cysteine pair specific for J head association (Smc1S161C Smc3K160C) and combining this with the hinge cysteine pair, or with the Smc3-Scc1 and Smc1-Scc1 cysteine pairs, it is possible to covalently circularise both the J-S and J-K compartments (Figure 3-1A), respectively. By incubating cohesin containing cysteines necessary to circularise the J-S and J-K compartments

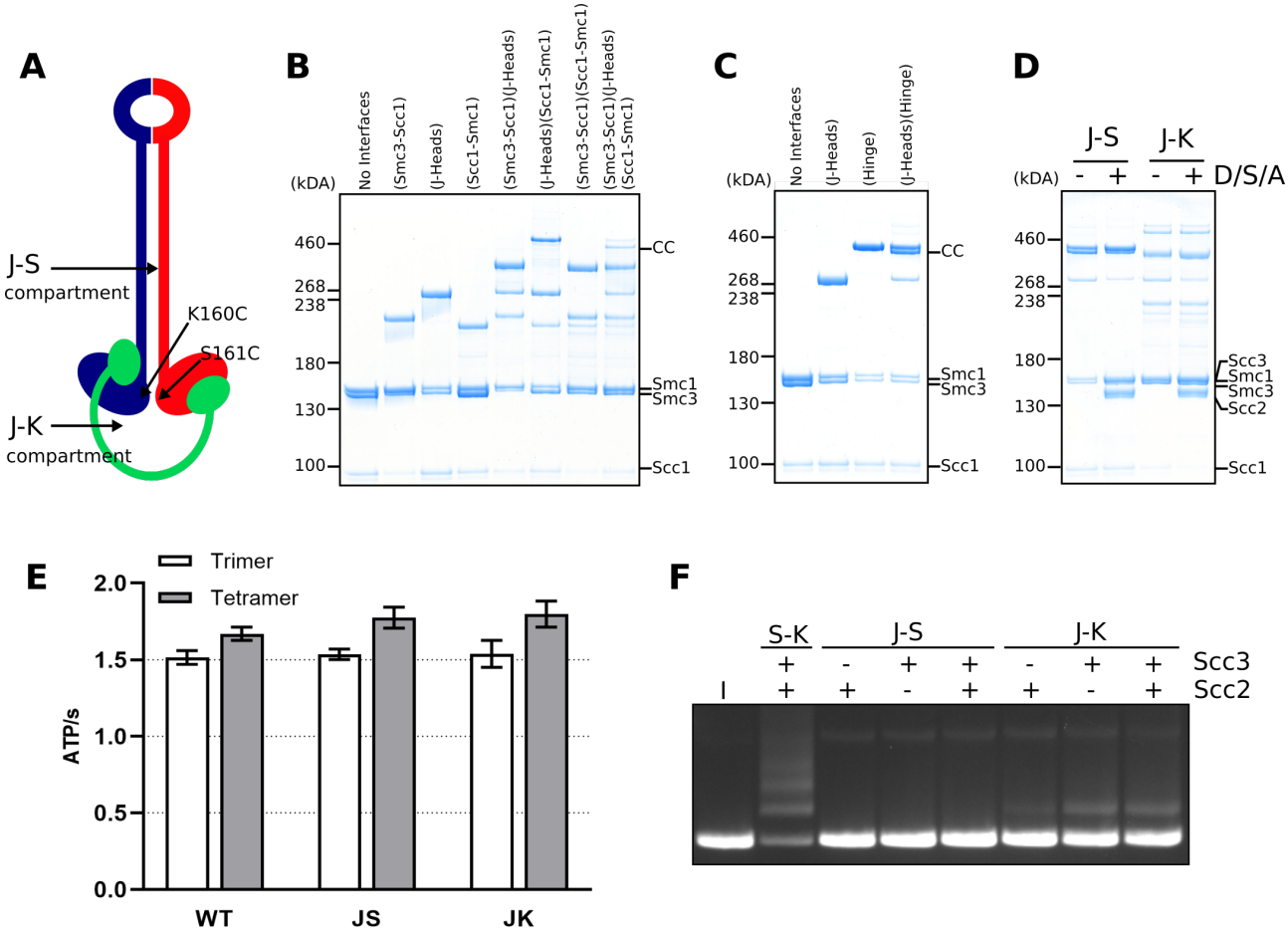


Figure 3-1. DNA is never entrapped in J-S compartments and only rarely in J-K compartments.

(**A**) Schematic of J-S and J-K compartments showing the position of the J-state specific cysteine residues. (**B**) BMOE-induced crosslinking of J-K compartments, or (**C**) of J-S compartments, with cysteine pairs in the specified interfaces. CC = circular cohesin. (**D**) BMOE-induced crosslinking of J-S or J-K compartments in the presence of ATP, Scc2, Scc3, and DNA, or the absence of all four. (**E**) Rate of ATP hydrolysis per cohesin ring, either trimers or tetramers, incubated with DNA, Scc2, and ATP. Comparing WT cohesin against cohesin containing the cysteines to circularise the J-S or J-K compartments. (**F**) Entrapment of DNA in either S-K rings, J-S, or J-K compartments, in the presence of Scc2, Scc3, or both Scc2 and Scc3. Incubated for 40min. (I = input DNA).

with BMOE and then separating the products by SDS-PAGE reveals migration products unique to these (Figure 3-1B & C), indicative of circularised J-S and J-K compartments. Importantly, cohesin's ATPase activity was unaffected by the presence of cysteine pairs needed to circularise either the J-S or J-K compartments (Figure 3-1E), suggesting these complexes remain fully functional. Circularisation of J-S and J-K compartments, and the efficiency of J-head crosslinking, changed very little on addition of Scc2, Scc3, DNA, and ATP (Figure 3-1D), conditions that give efficient S-K entrapment, although levels of J-S circularisation did appear to decrease slightly. Next, I tested whether under these conditions it is possible to entrap DNA in either the J-S or J-K compartment. This revealed almost no DNA entrapment in J-S compartments, and only low levels in J-K compartments (Figure 3-1F). This latter result was surprising considering that both CMs and CDs were found to be entrapped in J-K compartments in vivo (Chapard et al., 2019). Furthermore, low level J-K entrapment occurred entirely independently of Scc2. It is currently unclear why J-K entrapment was observed in vivo but not in vitro. It is possibly cell cycle related: J-S and J-K entrapment was only assessed in cycling cells and the observed levels of J-K entrapment could be from a population of G2 cells. Ascertaining whether J-K entrapment is equally efficient in G1 cells will be an important question for the future.

The rapid entrapment of DNA in E-S and E-K compartments

I next looked at combining a cysteine pair for E-state association (Smc1R1222C Smc3N1192C) with the hinge cysteine pair, or with the Smc3-Scc1 and Smc1-Scc1 cysteine pairs, to circularise the E-S and E-K compartments, respectively (Figure 3-2A). When crosslinking all three E-K interfaces and analysing the products by SDS-PAGE, a migration product unique to crosslinking all three interfaces was visible, indicative of circularised E-K compartments (Figure 3-2B). A similar product was not visible when

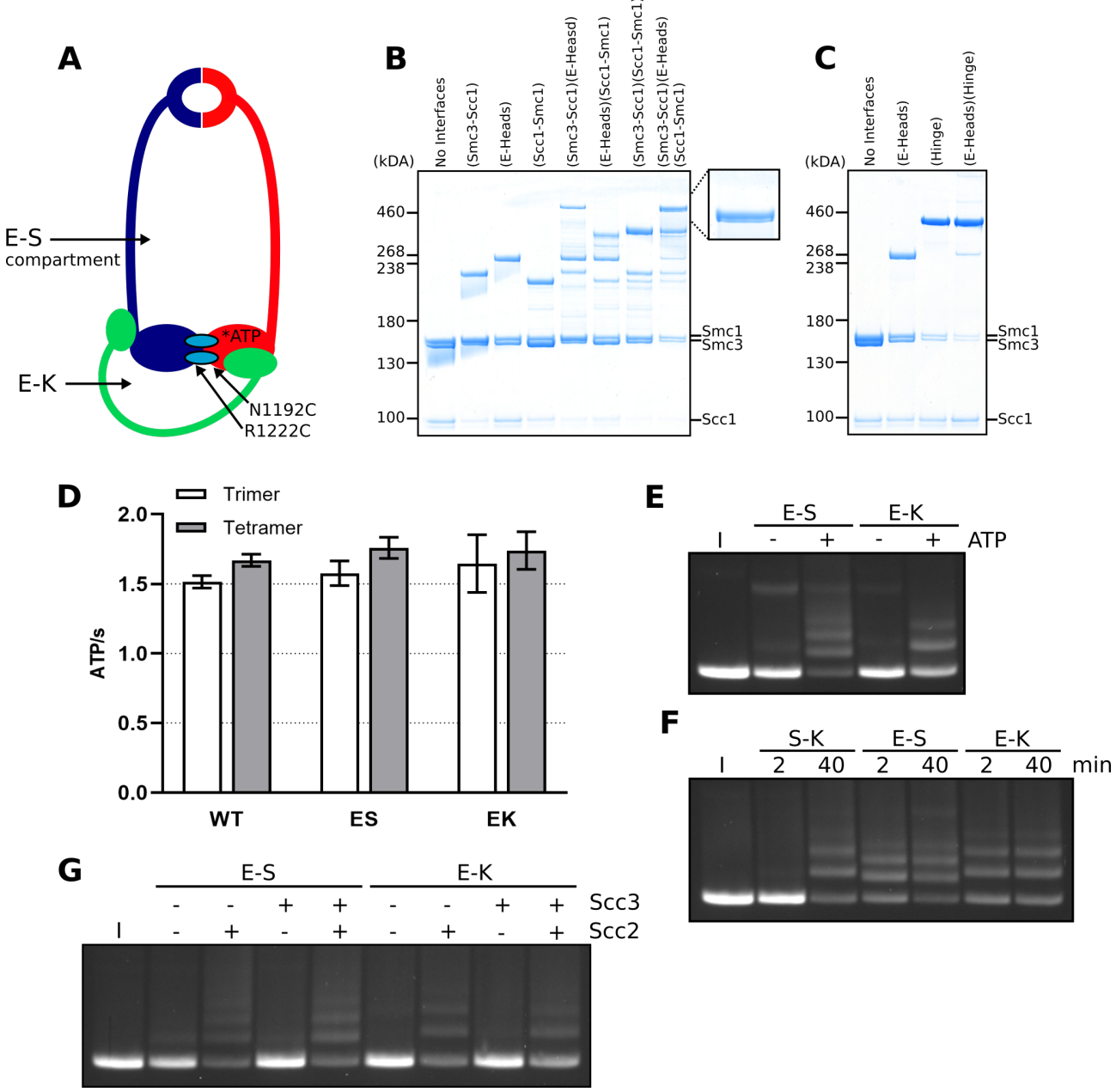


Figure 3-2. The rapid entrapment of DNA in E-S and E-K compartments.

(**A**) Schematic of E-S and E-K compartments showing the position of the E-state specific cysteine residues. (**B**) BMOE-induced crosslinking of E-K compartments, or (**C**) of E-S compartments, carried out in the presence of ATP, with cysteine pairs in the specified interfaces. (**D**) Rate of ATP hydrolysis per cohesin ring, either trimers or tetramers, incubated with DNA, Scc2, and ATP. Comparing WT cohesin against cohesin containing the cysteines to circularise the J-S or J-K compartments.(**E)** Entrapment of DNA in the E-S and E-K compartments in the presence of Scc2 and Scc3, and in the presence or absence of ATP. Incubated for 40min. (**F**) Entrapment of DNA in S-K rings, E-S, or E-K compartments, in the presence of Scc2, Scc3, and ATP. Incubated for either 2 min or 40 min. (Continued on next page).

(**G**) Entrapment of DNA in E-S or E-K compartments in the presence of Scc2, Scc3, Scc2 and Scc3, or absence of both. Entrapment assays were incubated for 40min unless otherwise specified. (I = input DNA).

crosslinking both E-S interfaces (Figure 3-2C), likely due to this species migrating at an identical rate to hinge crosslinked cohesin. Considering circularised E-S compartments have been described in vivo (Chapard et al., 2019), and DNA entrapment within E-S compartments is described later in this work, the covalent circularisation of E-S compartments must take place in vitro as well. However, unlike with J-state crosslinking, which occurred readily, the efficient crosslinking of the E-state, and thus circularisation of the E-S and E-K compartments, required both the presence of ATP and $MgCl_2$. Like with J-state cysteines, cohesin possessing the cysteine pairs required to circularise the E-S or E-K compartments had no effect on cohesin's ATPase activity (Figure 3-2D).

Next, I tested if under conditions that give efficient S-K entrapment cohesin can entrap DNA in the E-S and E-K compartments. Cohesin was incubated with Scc2, Scc3, DNA, and ATP and then crosslinked at both interfaces of the E-S compartment, or all three interfaces of the E-K compartment (Figure 3-2E). This revealed DNA to be entrapped in both the E-S and E-K compartments. Like entrapment within S-K rings, this was dependent on ATP. Furthermore, entrapment was much more rapid than was observed in S-K rings, with significant levels of DNA entrapped within just 2 min (Figure 3-2F). I next went on to investigate whether, like with entrapment within S-K rings, entrapment within both the E-S and E-K compartments required the presence of both Scc2 and Scc3. To my surprise, Scc2 alone was sufficient to drive entrapment within E-S and E-K compartments at both 2 min at 40 min time points (Figure 3-2G). While on the surface entrapment in E-S and E-K compartments without S-K entrapment seems paradoxical, effectively producing entrapment inside cohesin without entrapment in S-K rings, I propose a simple hypothesis that can explain how this takes place. In brief, entry either into the ring through either of the S-K rings three protein interfaces (the hinge, Smc1-Scc1, or Smc3-Scc1 interfaces) would result in S-K ring entrapment. As no S-K ring

entrapment occurs under conditions that give entrapment in the E-S and E-K compartments in the presence of Scc2, DNA must therefore be passing into the ring in a manner that does not involve passage through either of these three interfaces. As entrapment is occurring in both the E-S and E-K compartments in the presence of Scc2, any model must provide a mechanism to create both E-S and E-K entrapment through a single mechanism. I propose DNA passes “up” through the heads of Smc1 and Smc3, which subsequently engage in the presence of ATP. This entraps DNA in both E-S and E-K compartments without passing DNA through any of the three S-K interfaces. (see Discussion for more details).

The reaction driven by Scc2 was highly efficient, and reached near saturation levels within 2 min, but increased slightly for both E-S and E-K entrapment by 40 min (Figure 3-3A). Addition of Scc3 to these reactions had little effect on Scc2 driven E-S entrapment at either 2 or 40 min time points, which continued to show increased levels of entrapment at 40 min. However, the addition of Scc3 had a clear effect on entrapment in E-K compartments. Whilst in the absence of Scc3 levels of Scc2 stimulated E-K entrapment increased from 2 to 40 min, in the presence of Scc3 levels of E-K entrapment either did not change or decreased slightly. Strikingly, both E-S and E-K entrapment were completely unaffected by cohesin possessing both Walker B mutations (Smc3E1155Q Smc1E1158Q; Figure 3-3B), implying that neither form of entrapment requires ATP hydrolysis. The same was not true for cohesin possessing a Walker A mutation (Smc3K38I) that showed a decrease in levels of E-S entrapment (Figure 3-3C). This is in contrast to what is observed with S-K entrapment (Figure 2-3F), in which presence of Smc3K38I is sufficient to completely abolish entrapment. Cohesin possessing Smc3K38I was found to have a significant defect in head engagement (Figure 3-3E), as measured by crosslinking of the E-state. This defect could be partially

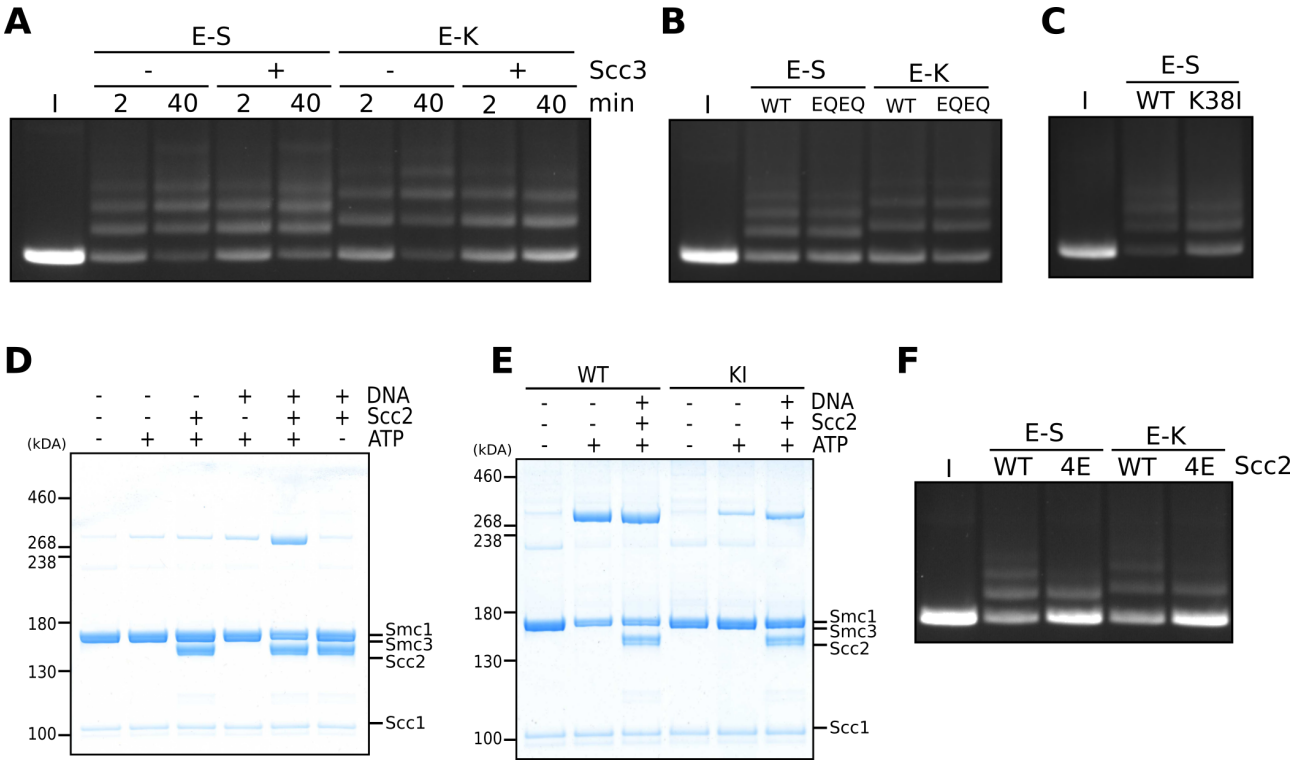


Figure 3-3. Further characterisation of E-S and E-K entrapment.

(**A**) Entrapment of DNA in E-S or E-K compartments in the presence of Scc2, and either the presence of absence of Scc3. Incubated for either 2 min or 40 min. (**B**) Entrapment of DNA in E-S or E-K compartments in the presence of Scc2, comparing WT cohesin to cohesin containing Smc1E1158Q Smc3E1155Q (EQEQ) mutations, or (**C**) comparing WT cohesin to cohesin containing the Smc3K38I (KI) mutation. (**D**) BMOE-induced crosslinking of the E-state cysteine pair in the absence of $MgCl_2$ and the presence of Scc2, DNA, and ATP in various combinations. (**E**) BMOE-induced crosslinking of the E-state cysteine pair in the presence or absence of ATP, and either the presence or absence of Scc2 and DNA, comparing WT cohesin to cohesin containing the Smc3K38I (KI) mutation. (**F**) Entrapment of DNA in E-S or E-K compartments in the presence of either WT Scc2 or Scc2-4E. Entrapment assays incubated for 2 min unless otherwise specified. (I = input DNA).

overcome by addition of both DNA and Scc2. Omission of $MgCl_2$ also caused a reduction in E-state crosslinking (Figure 3-3D), and this could similarly be partially rescued by addition of Scc2 and DNA. That levels of E-S entrapment of Smc3K38I cohesin mutants decreases by roughly the same degree as levels of E-state crosslinking is unsurprising considering E-S circularisation depends on the formation of E-state head association. Entrapment within E-S and E-K compartments was reduced by Scc2-4E (Figure 3-3F), suggesting this reaction at least partially depends on Scc2's ability to bind to DNA.

Chapter 4 – How does DNA become entrapped in the E-S and E-K compartments?

Introduction

The path that DNA takes into the S-K ring is a long unanswered question. Studies have implicated both the Smc3-Scc1 (Higashi et al., 2020; Murayama and Uhlmann, 2015) and hinge interfaces (Gruber et al., 2006) as entry gates, however neither study was conclusive. The findings of this study, namely that DNA enters the ring in a manner that does result in S-K entrapment, further complicates the matter. Is entrapment in E-S and E-K compartments a pre-requisite to S-K entrapment? Or are they produced through independent mechanisms? To shed light on these questions, I set out to investigate the mechanism through which DNA becomes entrapped in both the E-S and E-K compartments.

E-S entrapment disrupts coiled coil interactions proximal to the heads

Understanding how the Smc1/Smc3 coiled coils associate in the presence and absence of ATP, and/or DNA, may help elucidate how DNA enters the E-S and E-K compartments. For example, if the coiled coils are usually associated close to the heads in the absence of DNA, but dissociate in its presence, this may suggest that DNA entrapment leads to coiled coil dissociation close to the heads and that DNA may occupy this region of the E-S compartment. To investigate the dynamics of the coiled coils, I combined the E-specific cysteine pair with one specific for the coiled coils (Smc1K201C Smc3K198C), in close proximity to the joint (Figure 4-1A). This revealed that double crosslinking can indeed occur in the presence of ATP (Figure 4-1B). Double crosslinking also occurred efficiently when the coiled coil pair was combined with one to crosslink the hinge. These cysteine pair combinations enabled me to test for DNA entrapment within two sub-compartments of the E-S compartment (Figure 4-1Ai): one created by simultaneous crosslinking engaged heads and coiled coils (E-C compartment; Figure 4-1Aii) and another by the simultaneous crosslinking of the coiled

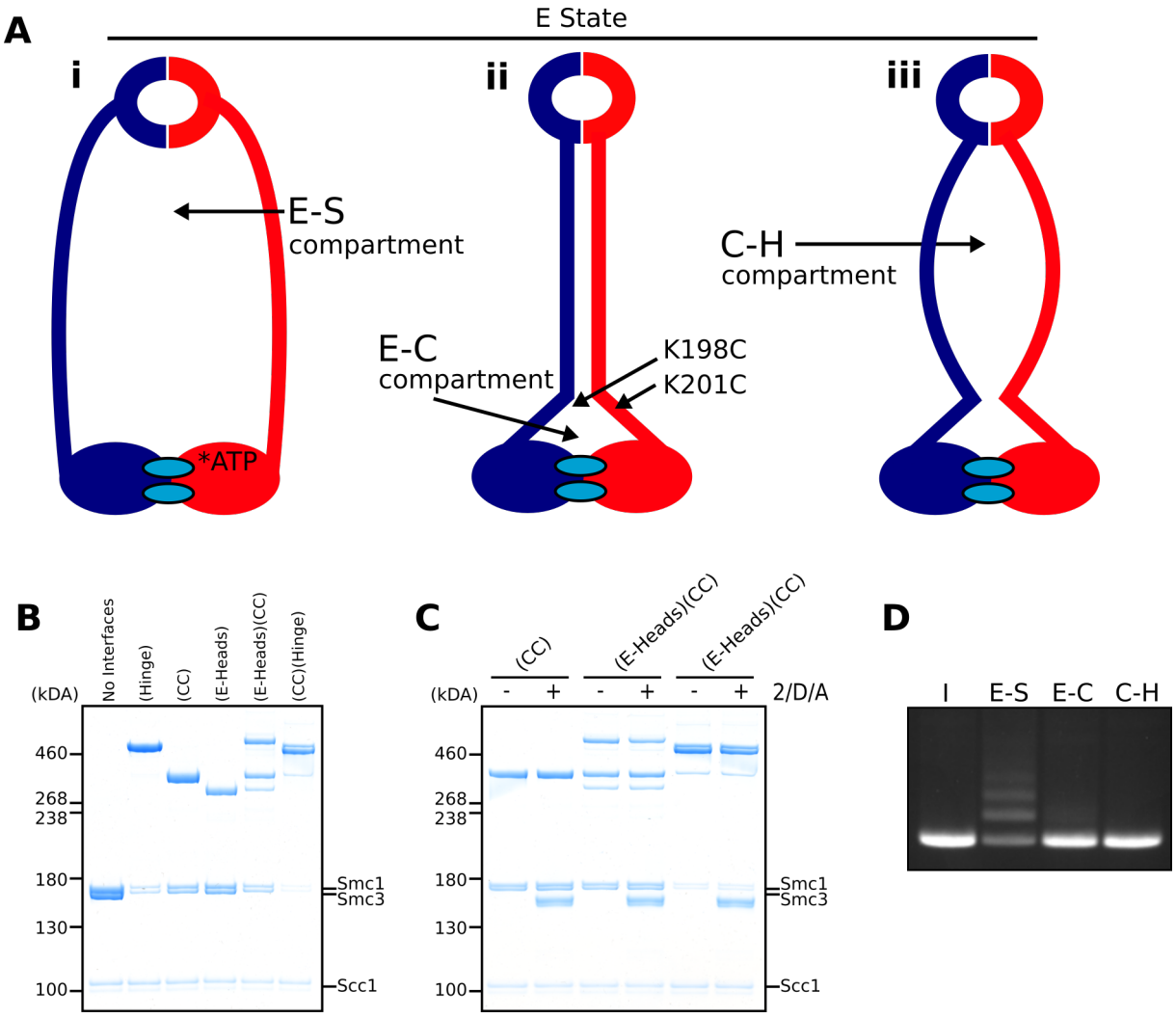


Figure 4-1. E-S entrapment disrupts coiled coil interactions proximal to the heads.
(**A**) Schematic of the Smc1 Smc3 dimer with heads engaged in the presence of ATP and showing the position of the cysteine pair used to crosslink the coiled coils proximal to the heads. Head engagement may disrupt coiled coil association leading to different conformations for the E-S compartment. **i)** Head engagement completely disrupts all coiled coil interactions. **ii)** Head engagement disrupts coiled coil interactions proximal to the heads, forming an engaged heads and coiled coil (E-C) sub-compartment. **iii)** Head engagement disrupts coiled coil interactions proximal to the hinge, forming a coiled coil and hinge (C-H) sub-compartment. (**B**) BMOE-induced crosslinking of the E-C and C-H sub-compartments in the presence of ATP, or (**C**) of the coiled coil cysteine pair, and E-C and C-H sub-compartments, in either the presence of Scc2, DNA, and ATP (2/D/A), or their absence. (**D**) Entrapment of DNA in E-S compartments, or E-C and C-H sub-compartments, in the presence of Scc2. Incubated for 2min. (I = input DNA).

coils and the hinge (E-C compartment; Figure 4Aiii). If DNAs entrapped in E-S compartments are in molecules whose coiled coils are associated, at least in the vicinity of their joint regions, then they must be entrapped either in the E-C or the C-H sub-compartments. On the other hand, if the entrapment of DNAs within E-S compartments is accompanied by (or indeed causes), dissociation of the coiled coils in the vicinity of the Smc1K201C Smc3K198C cysteine pair, then DNA should not be trapped in either of these sub-compartments.

Despite efficient crosslinking at both cysteine pairs (Figure 4-1B), few if any DNAs were entrapped by cohesin trimers containing hinge and coiled coil cysteine pairs in the presence of Scc2 and ATP (Figure 4-1D). Likewise, few if any DNAs were entrapped by cohesin trimers containing both E-state and coiled coil cysteine pairs. I deduce from this result that entrapment of DNAs within E-S compartments in the presence of Scc2 is accompanied by dissociation of their coiled coils in a manner that precludes crosslinking between Smc1K201C and Smc3K198C. It is important to point out that this feature was not apparent when analysing the crosslinking efficiency between Smc1K201C and Smc3K198C under the same conditions (Figure 4-1C), namely in the presence of Scc2, ATP, and DNA. To explain this, I suggest that despite the addition of DNA, complexes exist, at least transiently, that have engaged their heads and have zipped up their coiled coils but have not in fact trapped DNA within their E-S compartments. Consistent with this notion is my finding that simultaneous crosslinking of coiled coils and engaged heads occurs efficiently even in the absence of DNA (Figure 4-1B).

Scc2 and DNA disrupt the J-state in the absence of ATP

One mechanism through which DNA can become entrapped in the E-S and E-K compartments, without giving rise to S-K ring entrapment, would be to pass DNA “up”

through the Smc1 Smc3 head domains (see Discussion). For this to take place, the head domains would need to be opened up sufficiently to enable DNA to pass between them. Such a state would be formed at the expense of the J-state and would not be associated with E-state formation (although the E-state may subsequently form). I therefore set out to identify conditions that caused a disruption in the J-state as measured by crosslinking of the J-state cysteine pair. It was found that conditions that promote E-state crosslinking, namely the addition of Scc2, DNA, and ATP caused a modest ~ 20 % reduction in J-state crosslinking (Figure 4-2A), confirming that the E-state is formed at the expense of the J-state. Other combinations of these three factors had much less effect, bar one. Surprisingly, addition of Scc2 and DNA in the absence of ATP had the greatest effect, causing a ~ 50 % reduction in J-state crosslinking. Importantly, this does not correspond to E-state formation as almost no crosslinking takes place between Smc1N1192C and Smc3R1222C under these conditions (Figure 4-2B). One possible explanation for this is that in the absence of ATP, both Scc2 and DNA disrupt the J-state by driving the ATPase heads apart, a process that could facilitate the passage of DNA between them and thereby facilitate its entrapment in E-S compartments when heads subsequently engage in the presence of ATP.

Rapamycin induced head dimerization does not prevent chromosome association

If DNA passage between the heads were responsible for forming E-S and E-K entrapment, then by tethering the heads together it should be possible to block DNA entry through the heads. To test this, cohesin expressing Fkbp12 and Frb proteins fused to Smc1 and Smc3 head domains respectively was expressed in yeast. Upon addition of rapamycin, Fkbp12 and Frb will dimerize and seal this interface. Cells expressing either *SMC1*-Fkbp12 or *SMC3*-Frb proteins were viable, even in the presence of rapamycin (Figure 4-3A). Cells expressing both *SMC1*-Fkbp12 and *SMC3*-Frb were viable in the

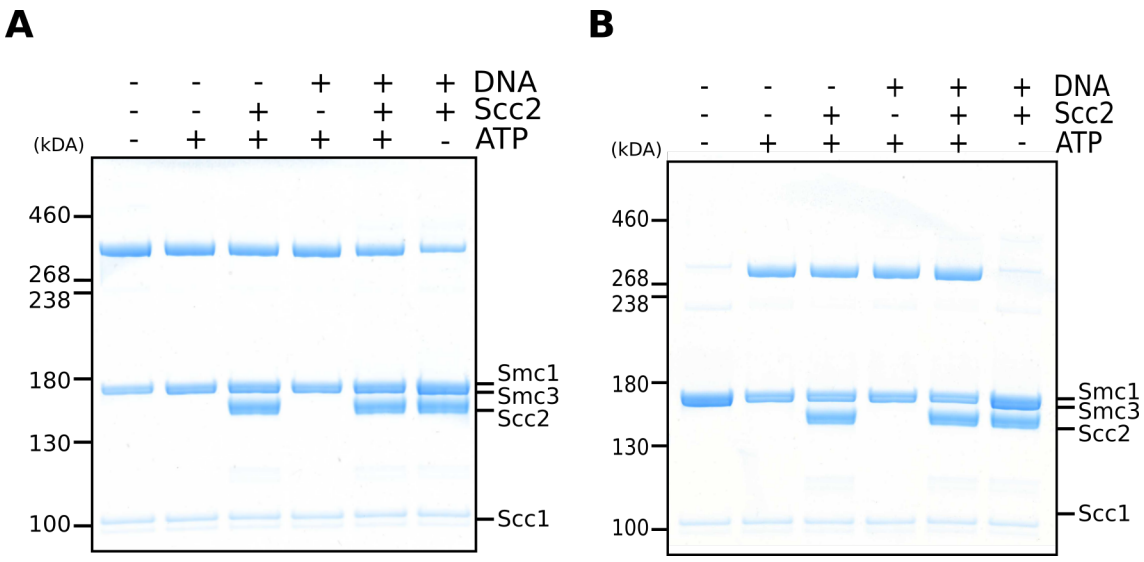


Figure 4-2. Scc2 and DNA disrupt the J-state in the absence of ATP.

(**A**) BMOE-induced crosslinking of the J-state cysteine pair, in the presence of Scc2, DNA, and ATP in various combinations, or (**B**) of the E-state cysteine pair, in the presence of Scc2, DNA, and ATP in various combinations.

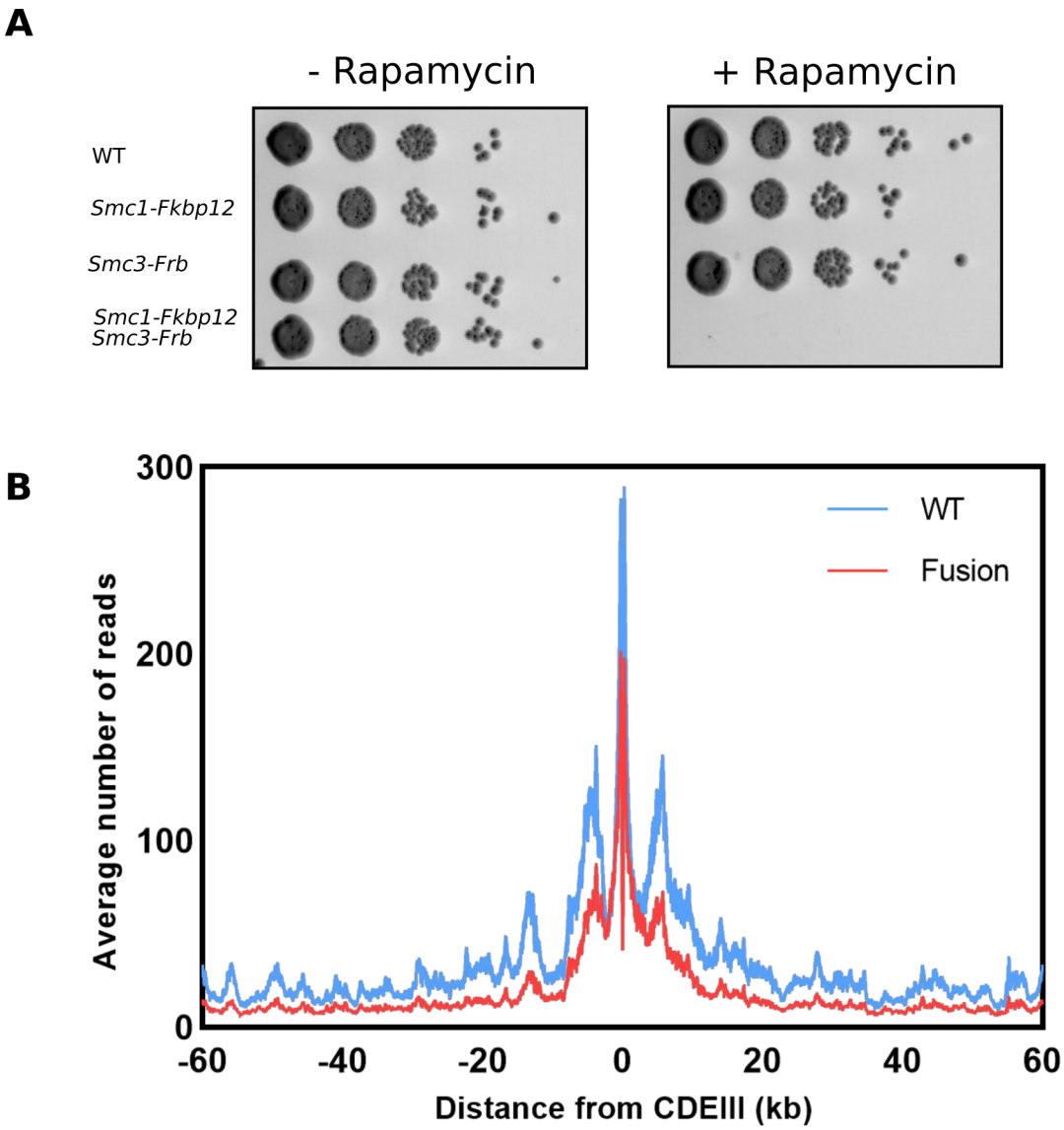


Figure 4-3. Rapamycin induced head dimerization does not prevent chromosome association.

(**A**) Viability assay showing yeast expressing either WT cohesin (KN 10599), or Smc1-Fkbp12 (KN28238), Smc3-Frb (KN28239), or both Smc1-Fkbp12 and Smc3-Frb (KN28237) grown on YPD in the presence or absence of rapamycin. Cells spotted at a density of $1x10^7$ cells ml^{-1} and then in 10 fold serial dilution from left to right. (**B**) Average calibrated ChIP-seq profiles 60 kb either side of *CENs* for cells expressing either WT Smc1 Smc3 (KN10599) or Smc1-Fkbp12 Smc3-Frb (fusion; KN28237). Cells were arrested in G1 with α-factor at 25°C before being released into media supplemented with nocodazole and rapamycin.

absence of rapamycin but failed to support viability in its presence. We next looked at whether lack of viability was due to an inability to associate normally with chromosomes, and so measured this activity by ChIP. Despite causing lethality, addition of rapamycin caused only a minor defect in chromosome association (Figure 4-3B). It is possible that rapamycin induced head engagement does not prevent DNA passage through the heads entirely, and the DNA binding surface on top of the heads can still be bound in these constructs which may be sufficient to associate with chromosomes in the manner observed by ChIP. The next step will be to combine this system with the crosslinking assay described in this study to ascertain whether E-S/E-K entrapment is truly abolished or if lethality is due to defects in other activities.

Chapter 5 - Discussion

Entrapment of DNA molecules within S-K rings has been demonstrated in vivo and this study now provides a demonstration of this activity in vitro. I show S-K ring entrapment directly, through the formation of covalent catenations between cohesin and DNA that are able to resist protein denaturation. Entrapment within S-K rings has a requirement for Scc3 and ATP binding, and is stimulated by the presence of Scc2 and ATP hydrolysis. This is similar to what has been reported in assays measuring salt resist association (Murayama and Uhlmann, 2014; Onn and Koshland, 2011). However, by measuring the nature of the topological association directly I am able to overcome the limitations of this approach and make unambiguous deductions about the precise topology between DNA and cohesin. Due to the efficiency of BMOE-induced circularisation of cohesin being ~ 20 % (this study; Gligoris et al., 2014), it is possible that the true rate of entrapment is 5-fold higher that what is observed in our gels, with anywhere up to 15 molecules of cohesin entrapping any one individual molecule of DNA.

Entrapment of DNA by S-K rings in vitro reflects cohesin's behaviour in vivo: it depends on Scc2 and Scc3, on ATP binding and is affected by mutation of Smc3K112 K113 to glutamine. However, unlike what I observe in vitro, CM formation in vivo is never associated with a ladder formation, with only one band visible in these southern stains compared to the 3+ seen in my gels. Furthermore, CM formation in vivo requires not just ATP binding but also its hydrolysis. While the ability to hydrolyse ATP does stimulate entrapment in vitro, significant levels of DNA is still entrapped by cohesin possessing the Walker B mutations Smc3E1155Q Smc1E1158Q, mutations which in vivo cause the complete loss of CM formation (Srinivasan et al., 2018). The cause of this discrepancy is unclear.

An important outstanding question is how DNA is entering S-K rings. DNA must pass through either the Scc1-Smc1, Smc3-Scc1, or hinge interfaces. It has been suggested that at least one route DNA takes is through the Scc1-Smc3 interface, due to the ability of Pds5/Wpl1 to promote salt stable association with cohesin in vitro (Murayama and Uhlmann, 2015). As Pds5/Wpl1 are thought to promote cohesin dissociation through the Smc3-Scc1 interface this is a plausible site for entry (Beckouët et al., 2016). In vivo studies involving fusing the N- and C-terminal of Scc1 to Smc3 and Smc1, respectively, have conversely found these interfaces do not need to open for S-K entrapment (Srinivasan et al., 2018), which suggests that DNA can either enter through either Scc1 interface, or instead must come through the hinge. Further progress here will depend on a similar method to covalently close interfaces that is orthogonal to BMOE induced cysteine-cysteine crosslinking, combined with the in vitro assay described in this study to measure S-K entrapment.

Two further questions pertaining to S-K entrapment include where DNA is positioned when entrapped; be that in the S or K compartments, and whether this was associated with the heads adopting an E- or J-state. For obvious reasons I was unable to address whether S-K entrapment was associated with dissociation of the heads. Under conditions where I observed efficient S-K entrapment, namely in the presence of Scc2, Scc3, and ATP, DNA is efficiently entrapped in both the E-S and E-K compartments and only inefficiently in the J-K compartment. This observation was surprising considering that in vivo both CMs and CDs are entrapped in J-K compartments (Chapard et al., 2019). However, these experiments were carried out in cycling cells and whether CM formation occurs efficiently during G1 has yet to be established. In vitro, J-K entrapment was solely dependent on Scc3 and levels of entrapment were similar to those observed in E-K and S-K compartments in the presence of Scc3. This suggests that the low levels

of S-K entrapment driven by Scc3 corresponds to DNA entrapped in the K-compartment, and both J-K and E-K entrapment are being driven by a similar, if not identical, mechanism.

I was surprised to find that unlike with S-K entrapment, that requires Scc3, entrapment in the E-S and E-K compartments was driven by Scc2 alone. While on the surface this observation is puzzling, it can easily be explained if you envisage DNA entering the E-S compartment via its passage through disengaged head domains and their subsequent engagement upon binding ATP (Figure 5-1A). This would create a one-strand passage topology with respect to the E-S compartment. Similarly, a one-strand passage topology with respect to the E-K compartment arises naturally from this process, and thus a single type of DNA passage could be responsible for entrapment within both the E-S and E-K compartments. That the kinetics of E-S and E-K entrapment appear identical suggests a mechanism such as this may well be taking place. Importantly, entrapment of this nature does not involve DNA passage through the hinge, or either Scc1 interface, and so would not result in entrapment within S-K rings.

Alternative mechanisms could also give rise to E-S/E-K entrapment. For example, if a loop of DNA were inserted into an open S-K ring when the head domains were apart, with one segment of DNA being above the heads, and the other below (Figure 5-1B), head engagement would then simultaneously give rise to E-S and E-K entrapment. Topological association of this kind is a result of two-strand passage through the ring and would not initially result in covalent catenation between cohesin and DNA. However, head engagement and subsequent crosslinking splits the ring into a figure of eight, and one segment of the loop becomes trapped "north" of the heads, and another "south". This would convert a two-strand passage association with respect to the S-K ring into

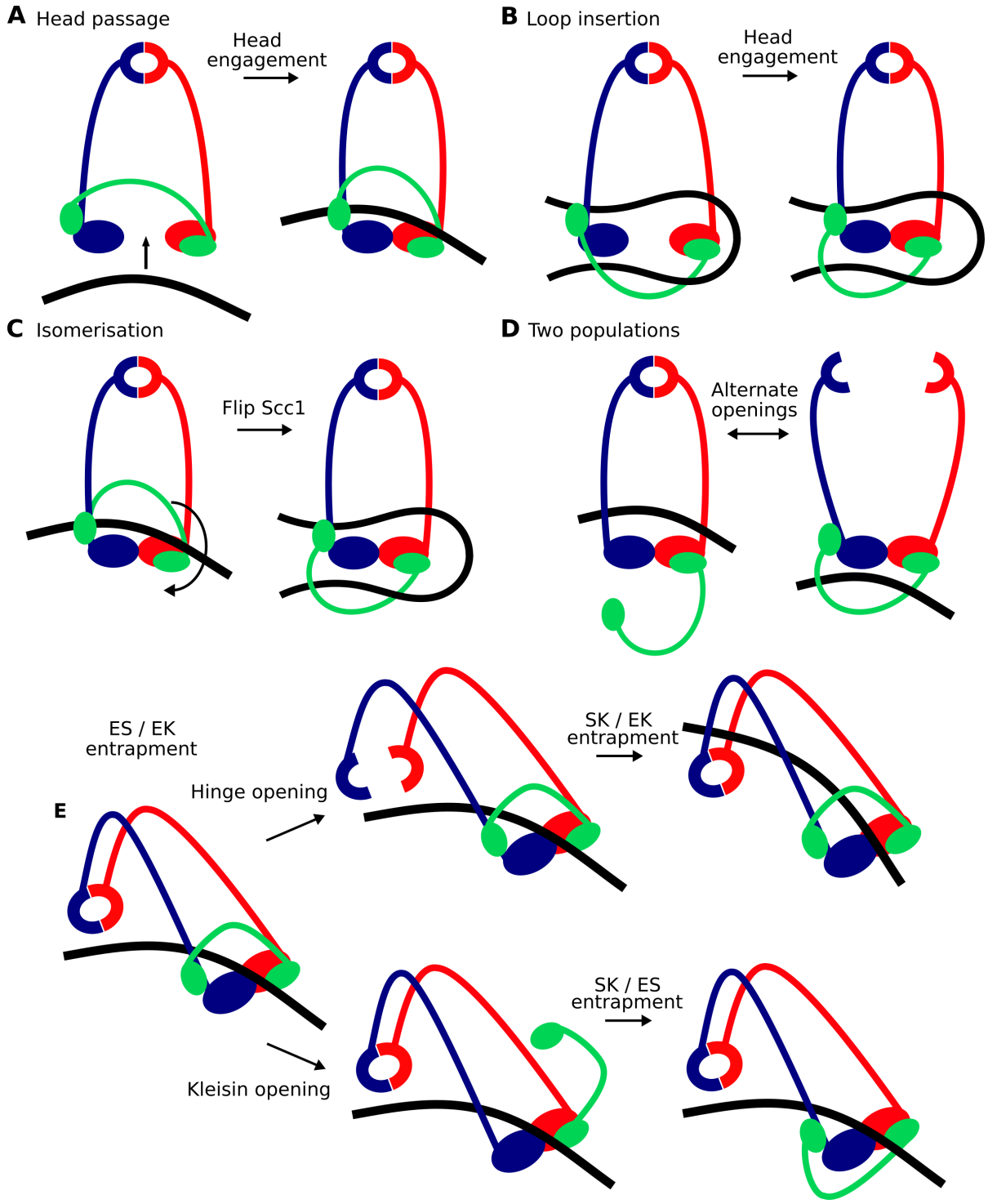


Figure 5-1. Potential mechanisms for Scc2-driven E-S/E-K entrapment and subsequent S-K ring entrapment.

(**A**) E-S and E-K entrapment through passing DNA between open heads, or (**B**) through inserting a loop. (**C**) Topological isomerism between A and B. (**D**) E-S and E-K entrapment resulting from two different populations of cohesin. Both populations have broken S-K rings and thus would not show S-K ring entrapment. (**E**) Models for converting E-S/E-K entrapment to S-K ring entrapment.

one-strand passage associations with respect to both the E-S and E-K compartments; one strand passage with respect to either the S-K ring or any of its constitutive compartments is necessary to create covalent catenations that can be detected by this assay. It is interesting to note that the state created by a single piece of DNA passing through the heads (Figure 5-1A) would be a topological isomer to that created through loop insertion and subsequent engagement of the head domains (Figure 5-1B). Conversion from the former state to the latter can be achieved by rotating the central region of Scc1 “down” through 180° (Figure 5-1C). Whether cohesin ever undergoes such a transition is wildly speculative, although would provide one route through which to introduce a loop into DNA that may be necessary for any LE activity by cohesin.

There is one caveat to the models for creating E-S and E-K entrapment thus far proposed. While E-S and E-K entrapment show similar kinetics and appear to occur simultaneously, as I am measuring entrapment via two different combinations of cysteine pairs I am unable to say with certainty that this is indeed the case. It is possible that E-S and E-K entrapment is not a reflection of a single population of cohesin associated with DNA, but instead two populations (Figure 5-1D). One of these populations would have DNA entrapped in the E-S compartment and have either one or both kleisin interfaces open. The second population would conversely have DNA entrapped in the E-K compartment and simultaneously have the hinge open. The existence of two populations of this nature could explain the observation of E-S and E-K entrapment in the absence of S-K entrapment, as the S-K ring would be "broken" in both instances. It is however difficult to envisage how Scc2 would simultaneously promote two entirely different modes of association and as such renders this model unlikely.

A key prediction of the head-passage model is that DNA entrapment in the E-S and E-K compartments should be driven primarily by head engagement, and that ATP hydrolysis is unnecessary for this process. This is exactly what has been observed, with cohesin possessing both Walker B mutations (Smc1E1158Q Smc3E1155Q) showing almost no defect in levels of E-S or E-K entrapment. In contrast, cohesin possessing the Smc3 Walker A mutation (Smc3K38I), which greatly impairs levels of E-state crosslinking, shows a corresponding defect in levels of E-S entrapment, as predicted. That conditions which cause defects in ATP driven head engagement, such as possession of Smc3K38I or omission of $MgCl_2$, can be partially rescued by addition of both Scc2 and DNA, and as it is Scc2 that drives entrapment of DNA in E-S and E-K compartments, suggests that the mechanism through which Scc2 and DNA promote head engagement may be identical to that of how Scc2 promotes entrapment of DNA within E-S and E-K compartments.

In yeast, Walker B mutations cause a massive reduction of cohesin association across the genome (Hu et al., 2011), with the exception of *CEN* sequences, which show substantial enrichment compared to WT. It has been suggested that this enrichment is due to Scc4 recruiting cohesin to the *CEN* through interactions with the *CEN* specific histone protein Ctf19 (Chao et al., 2015; Hinshaw et al., 2017). Interestingly, cohesin possessing Walker A mutations do not show this same enrichment and instead fail to associate with the genome entirely, despite presumably still being able to associate with Scc2/4 and Ctf19. This suggests that the inability of Walker A mutants to associate at *CEN* sequences stems instead from an activity which they have lost yet Walker B mutants still possess. This activity most likely corresponds to ATP-driven head engagement, which is significantly impaired in Smc3K38I mutants but largely unaffected in Smc1E1158Q Smc3E1155Q mutants. The enrichment of Walker B mutants at *CEN*

sequences might then not be due to Ctf19 recruitment alone, but also from E-S and E-K entrapment driven by head engagement that stabilises cohesin at these sites. Similarly, cohesin containing hinge mutations that fail to entrap DNA within S-K rings, but nonetheless associate with the genome at levels similar to that of WT cohesin (Srinivasan et al., 2018), may also show entrapment within E-S and E-K compartments. Entrapment within E-S compartments has yet to be observed in yeast, however, has been found to take place in *B. subtilus* SMC complexes containing Walker B mutations (Vazquez Nunez et al., 2019). Similar experiments will need to be done in yeast as it is possible Walker B mutants help stabilise head engagement and thus may help stabilise E-S entrapment.

During the course of this work, several cryo-EM structures were published with cohesin's head domains engaged in the presence of Scc2 and DNA (Figure 5-2). Remarkably, each of these structures showed an identical mode of binding to DNA (Collier et al., 2020; Higashi et al., 2020; Shi et al., 2020b), with DNA bound to a positive groove on the top of the Smc1 and Smc3 head domains that is formed by their engagement, like that observed in a Rad50 structure (Liu et al., 2016). Scc2 is bound in these structures and makes contacts with both head domains as well as with the Smc3 coiled coil just north of the N-terminal Scc1 binding site. Association of Scc2 with the head and coiled coils of Smc3 creates a compartment between Scc2 and Smc3, through which DNA bound on top of the head passes through. This clamps DNA between Scc2 and Smc3 close to the N-terminal Scc1 Smc3 interface. Importantly, a lower resolution structure of cohesin bound to a relaxed, circular plasmid shows cohesin associated with an extended, linear section of DNA (Collier et al., 2020), informing us that this state has not formed through loop entrapment (Figure 5-1B) but has instead formed by entrapping a linear section of DNA (Figure 5-1A). The curvature of DNA and the path it takes over the

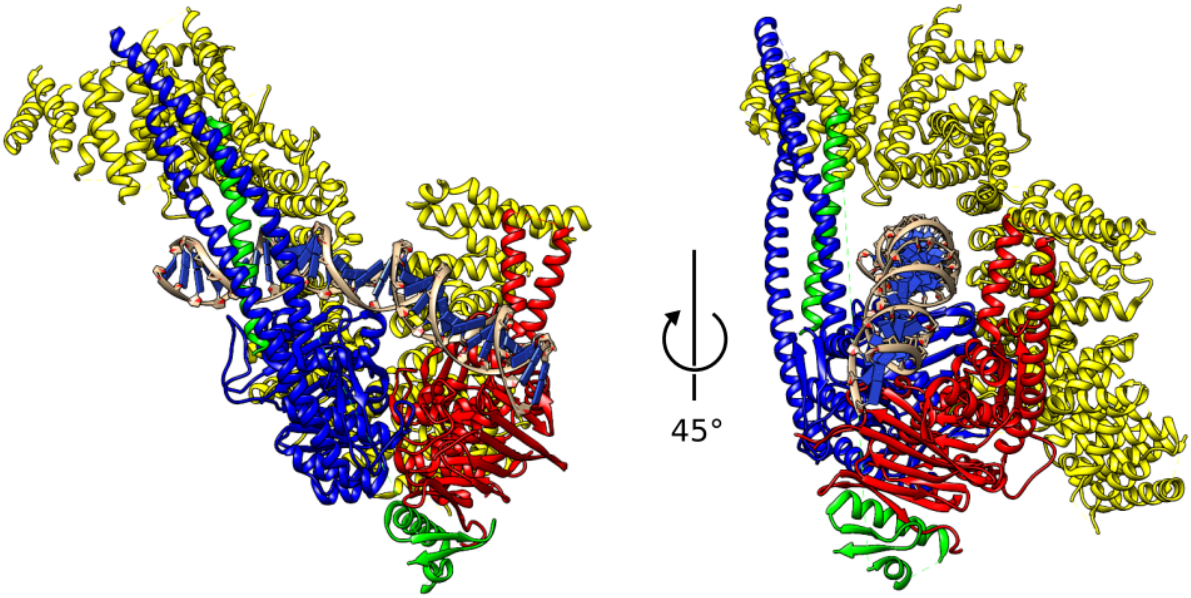


Figure 5-2. DNA is clamped between Scc2 and on top of engaged heads.

DNA is clamped between engaged heads and Scc2 (PDB 6ZZ6). Smc3 head domain in blue, Smc1 head domain in red, Scc1 N- and C-terminal domains in green, and Scc2 in yellow.

heads suggests that DNA passes underneath the hinge in these structures, which has important implications for the topological state between cohesin and DNA. As DNA appears to pass under the hinge, and above the heads, DNA must be entrapped in the E-S compartment in these structures. If DNA had instead passed above the hinge, DNA would not be entrapped in the E-S compartment, however, would have to be clamped between the coiled coils.

It is tempting to speculate as to whether cohesin engaged with DNA in this clamped state might reflect cohesin engaged in LE. As it has been reported that entrapment by S-K rings is entirely unnecessary for LE, any attempt to explain the mechanism of LE must consider this fact. The observation that entry into the E-S and E-K compartments can occur entirely independently of S-K entrapment, through passing DNA up through the heads, provides one such route for cohesin to engage with DNA that is consisted with this data. However, low resolution images of cohesin engaged with larger DNA molecules have shown an absence of any loops of DNA (Collier et al., 2020). As these structures were built in the absence of Scc3, a subunit shown to be required for LE in vitro, it will be interesting to see if loop structures emerge in its presence. Alternatively, individual cohesin rings may possess no LE activity per se and may instead only function as DNA translocators. Dimerization between two cohesin rings, with them both translocating in opposite directions, may be required for LE activities to emerge. Interestingly, Scc3 has been shown to dimerize in vitro and structures of Scc3 dimers have been reported (Li et al., 2018), although it is possible these structures are crystal packing artefacts. Obtaining similar structures of cohesin engaged with large DNA molecules, but this time in the presence of Scc3, will be important moving forward.

A positively charged loop at the extreme N-terminal of Scc1 appears to make several contacts with DNA in both the human and *S. pombe* structures (Higashi et al., 2020; Shi et al., 2020b), however, this positive loop is largely absent in *S. cerevisiae* and so the significance of this interaction is not clear. What is clear from all three structures is that K112 K113 of Smc3 are right at the heart of a composite interface between Scc2, Smc3, and DNA, and despite being in close proximity to the DNA backbone appear to instead be orientated towards, and interact with, a highly conserved negatively charged patch of Scc2. This suggests a function for acetylation during cohesion establishment is to disrupt this interaction and could be the molecular basis for Pds5 replacing Scc2 (Petela et al., 2018), thought to be important for both cohesion establishment as well as its maintenance. That Scc2 is bound to Smc3 is such close proximity to the N-terminal Scc1-Smc3 interface could also explain the requirement of Scc2 in preventing cohesin's dissociation from DNA during G1 (Srinivasan et al., 2019), as the Scc2 Smc3 interaction may somehow stabilise Smc3’s interaction with the N-terminus of Scc1.

The precise path the kleisin takes as it bridges Smc1 and Smc3 is not clear from these structures, probably due to the majority of the protein being unstructured. Despite clear density for Scc1's N- and C-terminus, structural information for the intervening peptide chain is almost entirely absent. A consequence of this is that it is unclear as to whether Scc1 is passing above, or below, DNA bound on top of the heads. In both scenarios DNA is entrapped in the E-S compartment, however, Scc1 passing below the heads is also associated with S-K entrapment, while it passing above them is not. Fortunately, it is possible to instead deduce the path of the kleisin based on the *S. cerevisiae* structure. While both the human and *S. pombe* structures were solved in complex with Scc3 (Higashi et al., 2020; Shi et al., 2020b), the *S. cerevisiae* structure was solved in its absence (Collier et al., 2020). Importantly, this tells us that these structures are capable

of forming in the presence of just Scc2, DNA, and cohesin in the complete absence of Scc3. The conditions under which the *S. cerevisiae* structure has formed thus involves identical conditions to those for entrapping DNA within the E-S and E-K compartments, and so suggests that cohesin I am crosslinking in vitro under these conditions are in fact associated with DNA in a manner identical to that observed in this structure. As Scc2 alone drives entrapment in both the E-S and E-K compartments, but not the S-K ring, the kleisin must pass over the DNA in the *S. cerevisiae* structure. That the kleisin passes over the DNA was also the conclusion drawn by Higashi et al., 2020 based on their biochemical crosslinking experiments.

If the *S. cerevisiae* structure does indeed represent cohesin with DNA entrapped in the E-S/E-K compartments, and if E-S/E-K entrapment is a pre-requisite for S-K entrapment, then E-S/E-K entrapment can be converted into S-K entrapment through two possible mechanisms (Figure 5-1E). One, by passing DNA out of the E-S compartment through the hinge, resulting in E-K/S-K entrapment (Figure 5-1E – top pathway). The second, through disengaging one, or both, Scc1 interfaces and subsequently re-engaging as to release DNA from the E-K compartment, resulting in E-S/S-K entrapment (Figure 5-1E – bottom pathway). A clue as to which of these is taking place has coming from studying the dynamics of entrapment in each of these compartments. If S-K entrapment were occurring at the expense of either E-S or E-K then it would be expected that, as S-K entrapment increased over 40 min, entrapment in either the E-S or E-K compartment would show a corresponding decrease. Interestingly, something similar to this does indeed take place. In the absence of Scc3, levels of both E-S and E-K entrapment increase over 40 min. Under conditions that promote S-K entrapment, namely in the presence of Scc2 and Scc3, levels of E-S shows a similar pattern, increasing over 40 min. However, this is not the case for levels of E-K entrapment, which no longer

increases over 40 min and instead shows a slight decrease. This suggests that S-K entrapment is forming at the expense of E-K entrapment and that a mechanism similar to the bottom pathway may be taking place.

As the *S. cerevisiae* structure has formed in the absence of Scc3, and as it is Scc3 that promotes S-K entrapment, it is unclear as to whether the human and *S. pombe* structures are showing E-S/E-K entrapment, or instead some form of S-K entrapment. As the path of the kleisin is not visible in any of these structures, it is possible that Scc3 has modified Scc1's path in the *S. pombe* and human structures and released DNA from the E-K compartment to create E-S/S-K entrapment. Scc3 was able to be positioned in both the human and *S. pombe* structures and found to be located behind Scc2 and in close proximity to the hinge (Higashi et al., 2020; Shi et al., 2020b). Whether or not the state observed in the *S. pombe* and human structures corresponds to S-K entrapment, that Scc3 is positioned so close to the hinge was a curious finding, considering it is the hinge that was initially implicated as the entry gate (Gruber et al., 2006). With such conflicting evidence to date, solving the mystery of what path DNA takes into S-K rings is still very much there for the taking.

These structures provide a clear explanation for how the mutations in Scc2 described in this study (Scc2S717E K721E K788E H789E) abolish DNA binding, as these residues appear to be in direct contact with the DNA backbone. This mode of interaction is similar to that observed for both Scc3 and Ycg1 (Kschonsak et al., 2017; Li et al., 2018). DNA binding to Scc2 in this manner appears to “clamp” DNA against Smc3, and that mutation of the DNA binding surface strongly inhibits E-S/E-K entrapment suggests that this activity is required for either the formation of the clamped state or its stability once formed. It is however unclear why Scc1 binding might promote DNA binding to Scc3 yet

inhibit its binding to Scc2. One possibility is that Scc1 and DNA compete for the same binding site on Scc2, and the binding of DNA to Scc2 may depend on Scc2 first binding to other regions of the complex. As Scc1 is known to make contacts with DNA close to Scc3's DNA binding site (Li et al., 2018) it is not beyond the realms of possibility that Scc1's binding site on Scc2 is located in a similar position, but rather than promoting DNA binding as it appears to do with Scc3, it instead occupies this DNA binding site on Scc2 and thus inhibits DNA binding. However, as Scc1 is clearly not bound across the DNA binding surface of Scc2 in the clamped structure, when, and why, binding to this surface might take place is unclear.

How DNA might enter the E-S and E-K entrapment is an outstanding question. The simplest scenario has the Smc1 Smc3 head domains transiently dissociate and have DNA pass through, following which ATP binding would cause head engagement and trap DNA inside (Figure 5-1A). This state should be formed at the expense of the J-state yet be independent of the E-state formation. Interestingly, such a state may have been captured when crosslinking the J-state in the presence of Scc2 and DNA and in the absence of ATP. Under these conditions, there is a significant decrease in J-state crosslinking without a corresponding increase in E-state crosslinking, suggestive that a state distinct from both is forming. Something similar has been observed in condensin, which in the presence of Ycs4 was found to be able to bridge the Smc2 Smc4 head domains sufficiently far enough apart for DNA to comfortably pass through (Lee et al., 2020). If a similar structure were forming between cohesin and Scc2, the DNA binding surface of Scc2 would be exposed, facing "down" and away from of the E-S compartment, and suggests a simple mechanism for how Scc2 is able to recruit DNA into the E-S compartment (Figure 5-3). DNA would need only to bind to this surface

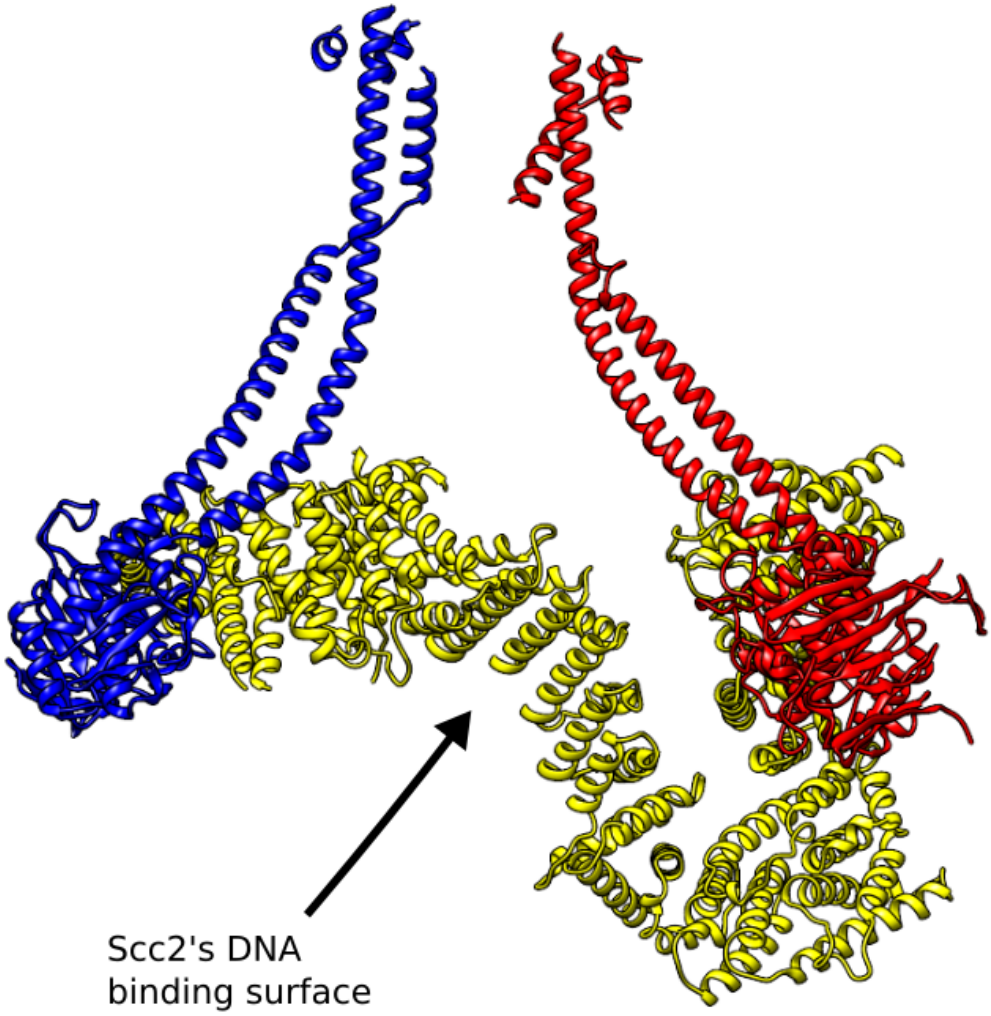


Figure 5-3. Model for how head dissociation and DNA binding to Scc2 may recruit DNA into the E-S compartment.

Model of a putative bridged conformation between Scc2 (yellow) and the Smc1 (red) and Smc3 (blue) heads. Scc2 would hold open the heads in the same way Ycs4 does with condensin, as described in Lee et al., 2020. This positions Scc2's DNA binding surface "down" facing away from the E-S compartment. DNA binding to this surface, followed by closing the SMC heads upon ATP binding would lead to entrapment in the E-S compartment.

when Scc2 was bridging the Smc1 Smc3 head domains for ATP binding and head engagement to then trap DNA inside the E-S/E-K compartments.

Alternatively, it has been suggested that DNA association on top of the heads is not a product of DNA passing “up” through the heads, followed by the subsequent engagement, but is instead a result of DNA passing “down” between the Smc1 and Smc3 coiled coils onto the DNA binding surface formed by head engagement (Figure 5-4). This is supported by DNA-protein mass spectrometry data (Higashi et al., 2020), that suggests in the absence of ATP, DNA associates with the coiled coils above the heads, and only in the presence of ATP then binds to the DNA binding surface on top of engaged heads. Furthermore, closure of the head gate seems to have little effect on DNA association as measured by their assay. Direct measure of the topological nature of cohesin in the *S. pombe* gripped state suggested that DNA is not entrapped in the E-S compartment but is entrapped in the E-K compartment. This state was proposed to be reached by DNA passing down through the coiled coils towards the DNA binding site created by ATP driven head engagement. During head engagement, they propose the N-terminal Scc1 interface opens and guides DNA through this interface and down to bind on top of the heads. Re-engagement of the N-terminus of Scc1 with the Smc3 neck, coupled with conformational changes in Scc2 then grips DNA in place. DNA is then suggested to pass down through the heads to complete the entrapment process.

Passing DNA "down" between the coiled coils and through an open Scc1-Smc3 interface would produce E-K as well as S-K entrapment, as one of the S-K ring interfaces would have been opened and passed through. Head opening through ATP hydrolysis was then suggested to complete the entrapment process, which would destroy E-K entrapment, leaving only S-K entrapment in its wake. While there is evidence for the Scc1 Smc3

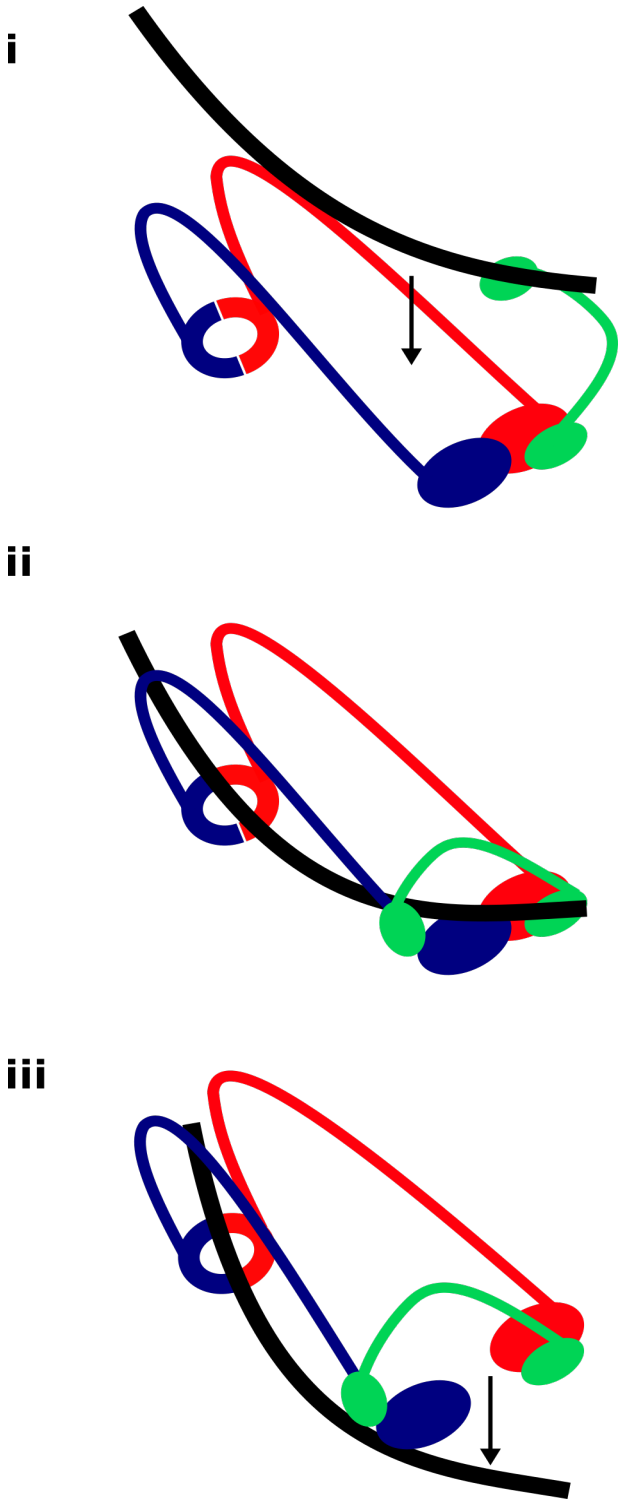


Figure 5-4. Model proposed by Higashi et al., 2020 for how DNA is recruited to the DNA binding surface on top of engaged heads.

i) DNA first passes “down” between the coiled coils. The Scc1 N-terminal domain may be disengaged and act to guide DNA. **ii)** DNA passes through an open Scc1-Smc3 interface and binds on top of engaged heads. **iii)** ATP hydrolysis opens the heads domains and completes the entrapment process.

interface as being a point of entry into the S-K ring (Murayama and Uhlmann, 2015) it cannot be the only one, as cohesin containing a fusion of the N-Scc1 to Smc3 is viable and still able to carry out S-K entrapment (Gruber et al., 2006; Srinivasan et al., 2018). Even if the long linker used in these studies allowed DNA to pass through this interface and trap DNA in a sub-compartment between the linker and the Smc3-Scc1 interface, there is no cysteine pair between N-Scc1 and Smc3. Following denaturation, the sub-compartment created between the inside of the N-Scc1, Smc3, and linker would be destroyed and release any entrapped DNA. For DNA to be entrapped in S-K rings by cohesin containing this Smc3-Scc1 fusion, there must at least be one further point of entry into S-K rings.

One important discrepancy between the results reported in this study and those reported in Higashi et al., 2020 is whether or not DNA is entrapped in the E-S compartment. Whereas they see no entrapment of DNA within E-S compartments, I see very efficient E-S entrapment in the presence of Scc2, as well as in the presence of Scc2 and Scc3. I also see entrapment in the E-S/E-K compartments in the absence of Scc3, and thus the absence of S-K entrapment. The formation of the gripped state as proposed in their model (Figure 5-4ii) would result in S-K entrapment, and so offers no mechanism to create E-S entrapment as I observe. Passing DNA down through the heads (Figure 5-4iii) would be one mechanism to create E-S entrapment, provided the heads were to re-engage after DNA passes through, but this would also lead to S-K entrapment, a finding inconsistent with this study. Furthermore, to reach E-S entrapment through this model would require ATP hydrolysis which I show is unnecessary for both E-S and E-K entrapment. As the protocols for circularising the E-S compartments differed between this study and Higashi et al., 2020, it is possible that this is where the source of the discrepancy lies. It would be interesting to see if by using a more direct crosslinking

protocol, such as cysteine-cysteine crosslinking, *S. pombe* cohesin might also be able to entrap DNA in E-S compartments.

Concluding remarks

The assay described in this study is a powerful new in vitro tool to aid in understanding how cohesin interacts with DNA, and thus how SMC complexes in general are capable of organising giant molecules of DNA. This approach measures the topology between DNA and cohesin directly, through covalent circularisation of the cohesin ring on circular DNA molecules. Through this approach, I have identified a novel mode of interaction between cohesin and DNA, one that does not involve entrapment of DNA in the S-K ring, but one in which cohesin has nonetheless entrapped DNA in its E-S and E-K compartments. This state has yet to be described in vivo, revealing the power of in vitro systems in detecting what may be transient or fragile conformational states. The structural conformation I deduce must exist from my biochemistry data for cohesin that has entrapped DNA in the E-S/E-K compartments shows many of the same features as present in recently published cryo-EM structures, and I suggest these structures may indeed reflect the conformation I have described. Moving forward, combining this system with a second crosslinking method, orthogonal to cysteine-cysteine crosslinking, will be necessary to address how DNA enters the S-K ring, as well as the E-S and E-K compartments. By understanding how DNA enters cohesin and is subsequently transported around the complex, we may finally understand how SMC complexes carry out such phenomenal organisational activities.

Chapter 6 – Bibliography

Anderson, D.E., Losada, A., Erickson, H.P., and Hirano, T. (2002). Condensin and cohesin display different arm conformations with characteristic hinge angles. J. Cell Biol. *156*, 419–424.

Arumugam, P., Gruber, S., Tanaka, K., Haering, C.H., Mechtler, K., and Nasmyth, K. (2003). ATP Hydrolysis Is Required for Cohesin's Association with Chromosomes. Curr. Biol. *13*, 1941–1953.

Banigan, E.J., and Mirny, L.A. (2020a). Loop extrusion: theory meets single-molecule experiments. Curr. Opin. Cell Biol. *64*, 124–138.

Banigan, E.J., and Mirny, L.A. (2020b). The interplay between asymmetric and symmetric DNA loop extrusion. eLife 9, e63528

Beckouët, F., Srinivasan, M., Roig, M.B., Chan, K.L., Scheinost, J.C., Batty, P., Hu, B., Petela, N., Gligoris, T., Smith, A.C., et al. (2016). Releasing Activity Disengages Cohesin's Smc3/Scc1 Interface in a Process Blocked by Acetylation. Mol. Cell *61*, 563–574.

Bürmann, F., Shin, H.C., Basquin, J., Soh, Y.M., Giménez-Oya, V., Kim, Y.G., Oh, B.H., and Gruber, S. (2013). An asymmetric SMC-kleisin bridge in prokaryotic condensin. Nat. Struct. Mol. Biol. *20*, 371–379.

Bürmann, F., Lee, B.G., Than, T., Sinn, L., O'Reilly, F.J., Yatskevich, S., Rappsilber, J., Hu, B., Nasmyth, K., and Löwe, J. (2019). A folded conformation of MukBEF and cohesin. Nat. Struct. Mol. Biol. *26*, 227–236.

Çamdere, G.O., Carlborg, K.K., and Koshland, D. (2018). Intermediate step of cohesin's ATPase cycle allows cohesin to entrap DNA. Proc. Natl. Acad. Sci. U. S. A. *115*, 9732–9737.

Castilho, P.V., Williams, B.C., Mochida, S., Zhao, Y., and Goldberg, M.L. (2009). The M phase kinase greatwall (Gwl) promotes inactivation of PP2A/B55delta, a phosphatase directed against CDK phosphosites. Mol. Biol. Cell. *20*, 4777-4789.

Chan, K.L., Roig, M.B., Hu, B., Beckouët, F., Metson, J., and Nasmyth, K. (2012). Cohesin's DNA exit gate is distinct from its entrance gate and is regulated by acetylation. Cell *150*, 961–974.

Chan, K.L., Gligoris, T., Upcher, W., Kato, Y., Shirahige, K., Nasmyth, K., and Beckouët, F. (2013). Pds5 promotes and protects cohesin acetylation. Proc. Natl. Acad. Sci. U. S. A. *110*, 13020–13025.

Chao, W.C.H., Murayama, Y., Muñoz, S., Costa, A., Uhlmann, F., and Singleton, M.R. (2015). Structural Studies Reveal the Functional Modularity of the Scc2-Scc4 Cohesin Loader. Cell Rep. *12*, 719–725.

Chapard, C., Jones, R., van Oepen, T., Scheinost, J.C., and Nasmyth, K. (2019). Sister DNA Entrapment between Juxtaposed Smc Heads and Kleisin of the Cohesin Complex. Mol. Cell *75*, 224-237.e5.

Cheng, T.M.K., Heeger, S., Chaleil, R.A.G., Matthews, N., Stewart, A., Wright, J., Lim, C., Bates, P.A., and Uhlmann, F. (2015). A simple biophysical model emulates budding yeast chromosome condensation. eLife *4*, e05565.

Chiu, A., Revenkova, E., and Jessberger, R. (2004). DNA interaction and dimerization of eukaryotic SMC hinge domains. J. Biol. Chem. *279*, 26233–26242.

Ciosk, R., Zachariae, W., Michaelis, C., Shevchenko, A., Mann, M., and Nasmyth, K. (1998). An ESP1/PDS1 complex regulates loss of sister chromatid cohesion at the metaphase to anaphase transition in yeast. Cell *93*, 1067–1076.

Collier, J.E., Lee, B.-G., Roig, M.B., Yatskevich, S., Petela, N.J., Metson, J., Voulgaris, M., Gonzalez Llamazares, A., Löwe, J., and Nasmyth, K.A. (2020). Transport of DNA within cohesin involves clamping on top of engaged heads by Scc2 and entrapment within the ring by Scc3. eLife *9*, e59560.

Cundell, M.J., Hutter, L.H., Nunes Bastos, R., Poser, E., Holder, J., Mohammed, S., Novak, B., and Barr, F.A. (2016). A PP2A-B55 recognition signal controls substrate dephosphorylation kinetics during mitotic exit. J. Cell. Biol. *214*, 539-554.

Davidson, I.F., Goetz, D., Zaczek, M.P., Molodtsov, M.I., Huis in ’t Veld, P.J., Weissmann, F., Litos, G., Cisneros, D.A., Ocampo-Hafalla, M., Ladurner, R., et al. (2016). Rapid movement and transcriptional re-localization of human cohesin on DNA. EMBO J. *35*, 2671–2685.

Davidson, I.F., Bauer, B., Goetz, D., Tang, W., Wutz, G., and Peters, J.-M. (2019). DNA loop extrusion by human cohesin. Science *366*, 1338–1345.

Diebold-Durand, M.L., Lee, H., Ruiz Avila, L.B., Noh, H., Shin, H.C., Im, H., Bock, F.P., Bürmann, F., Durand, A., Basfeld, A., et al. (2017). Structure of Full-Length SMC and Rearrangements Required for Chromosome Organization. Mol. Cell *67*, 334-347.e5.

Dixon, J.R., Selvaraj, S., Yue, F., Kim, A., Li, Y., Shen, Y., Hu, M., Liu, J.S., and Ren, B. (2012). Topological domains in mammalian genomes identified by analysis of chromatin interactions. Nature *485*, 376–380.

Dohadwala, M., da Cruz e Silva, E.F., Hall, F.L., Williams, R.T., Carbonaro-Hall, D.A., Nairn, A.C., Greengard, P., and Berndt, N. Phosphorylation and inactivation of protein phosphatase 1 by cyclin-dependent kinases. Proc. Natl. Acad. Sci. U. S. A. *91*, 6408-6412.

Earnshaw, W.C., and Laemmli, U.K. (1983). Architecture of metaphase chromosomes and chromosome scaffolds. J. Cell Biol. *96*, 84–93.

Eng, T., Guacci, V., and Koshland, D. (2015). Interallelic complementation provides functional evidence for cohesin-cohesin interactions on DNA. Mol. Biol. Cell *26*, 4224–4235.

Fudenberg, G., Imakaev, M., Lu, C., Goloborodko, A., Abdennur, N., and Mirny, L.A. (2016). Formation of Chromosomal Domains by Loop Extrusion. Cell Rep. *15*, 2038–2049.

Gandhi, R., Gillespie, P.J., and Hirano, T. (2006). Human Wapl Is a Cohesin-Binding Protein that Promotes Sister-Chromatid Resolution in Mitotic Prophase. Curr. Biol. *16*, 2406–2417.

Ganji, M., Shaltiel, I.A., Bisht, S., Kim, E., Kalichava, A., Haering, C.H., and Dekker, C. (2018). Real-time imaging of DNA loop extrusion by condensin. Science *360*, 102–105.

Gerguri, T., Fu, X., Kakui, Y., and Khatri, B.S. (2020). Computational and experimental analyses of mitotic chromosome formation pathways in fission yeast. https://doi.org/10.1101/2020.10.15.341305

Gerlich, D., Koch, B., Dupeux, F., Peters, J.M., and Ellenberg, J. (2006). Live-Cell Imaging Reveals a Stable Cohesin-Chromatin Interaction after but Not before DNA Replication. Curr. Biol. *16*, 1571–1578.

Gligoris, T.G., Scheinost, J.C., Bürmann, F., Petela, N., Chan, K.L., Uluocak, P., Beckouët, F., Gruber, S., Nasmyth, K., and Löwe, J. (2014). Closing the cohesin ring: Structure and function of its Smc3-kleisin interface. Science *346*, 963–967.

Gorr, I.H., Boos, G., and Stemmann, O. (2005). Mutual Inhibition of Separase and Cdk1 by Two-Step Complex Formation. Mol. Cell *19*, 135-141.

Griese, J.J., Witte, G., and Hopfner, K.P. (2010). Structure and DNA binding activity of the mouse condensin hinge domain highlight common and diverse features of SMC proteins. Nucleic Acids Res. *38*, 3454–3465.

Gruber, S., Haering, C.H., and Nasmyth, K. (2003). Chromosomal cohesin forms a ring. Cell *112*, 765–777.

Gruber, S., Arumugam, P., Katou, Y., Kuglitsch, D., Helmhart, W., Shirahige, K., and Nasmyth, K. (2006). Evidence that Loading of Cohesin Onto Chromosomes Involves Opening of Its SMC Hinge. Cell *127*, 523–537.

Guacci, V., Koshland, D., and Strunnikov, A. (1997). A direct link between sister chromatid cohesion and chromosome condensation revealed through the analysis of MCD1 in S. cerevisiae. Cell *91*, 47–57.

Haering, C.H., Löwe, J., Hochwagen, A., and Nasmyth, K. (2002). Molecular architecture of SMC proteins and the yeast cohesin complex. Mol. Cell *9*, 773–788.

Haering, C.H., Schoffnegger, D., Nishino, T., Helmhart, W., Nasmyth, K., and Löwe, J. (2004). Structure and stability of cohesin's Smc1-kleisin interaction. Mol. Cell *15*, 951–964.

Haering, C.H., Farcas, A.M., Arumugam, P., Metson, J., and Nasmyth, K. (2008). The cohesin ring concatenates sister DNA molecules. Nature *454*, 297–301.

Hanna, J.S., Kroll, E.S., Lundblad, V., and Spencer, F.A. (2001). Saccharomyces cerevisiae CTF18 and CTF4 Are Required for Sister Chromatid Cohesion. Mol. Cell. Biol. *21*, 3144–3158.

Higashi, T.L., Eickhoff, P., Sousa, J.S., Locke, J., Nans, A., Flynn, H.R., Snijders, A.P., Papageorgiou, G., O'Reilly, N., Chen, Z.A., et al. (2020). A Structure-Based Mechanism for DNA Entry into the Cohesin Ring. Mol. Cell. *79*, 917-933.

Hinshaw, S.M., Makrantoni, V., Harrison, S.C., and Marston, A.L. (2017). The Kinetochore Receptor for the Cohesin Loading Complex. Cell *171*, 72-84.e13.

Hirano, T., and Mitchison, T.J. (1994). A heterodimeric coiled-coil protein required for mitotic chromosome condensation in vitro. Cell *79*, 449–458.

Hirano, T., Kobayashi, R., and Hirano, M. (1997). Condensins, Chromosome Condensation Protein Complexes Containing XCAP-C, XCAP-E and a Xenopus Homolog of the Drosophila Barren Protein. Cell *89*, 511–521.

Holland, I.B., and A. Blight, M. (1999). ABC-ATPases, adaptable energy generators fuelling transmembrane movement of a variety of molecules in organisms from bacteria to humans. J. Mol. Biol. *293*, 381–399.

Hu, B., Itoh, T., Mishra, A., Katoh, Y., Chan, K.L., Upcher, W., Godlee, C., Roig, M.B., Shirahige, K., and Nasmyth, K. (2011). ATP hydrolysis is required for relocating cohesin from sites occupied by its Scc2/4 loading complex. Curr. Biol. *21*, 12–24.

Huang, C.E., Milutinovich, M., and Koshland, D. (2005). Rings, bracelet or snaps: Fashionable alternatives for Smc complexes. Philos. Trans. R. Soc. B Biol. Sci. *360*, 537–542.

Ivanov, D., Schleiffer, A., Eisenhaber, F., Mechtler, K., Haering, C.H., and Nasmyth, K. (2002). Eco1 is a novel acetyltransferase that can acetylate proteins involved in cohesion. Curr. Biol. *12*, 323–328.

Kim, Y., Shi, Z., Zhang, H., Finkelstein, I.J., and Yu, H. (2019). Human cohesin compacts DNA by loop extrusion. Science (80-.). *366*, 1345–1349.

Kschonsak, M., Merkel, F., Bisht, S., Metz, J., Rybin, V., Hassler, M., and Haering, C.H. (2017). Structural Basis for a Safety-Belt Mechanism That Anchors Condensin to Chromosomes. Cell *171*, 588-600.e24.

Kueng, S., Hegemann, B., Peters, B.H., Lipp, J.J., Schleiffer, A., Mechtler, K., and Peters, J.M. (2006). Wapl Controls the Dynamic Association of Cohesin with Chromatin. Cell *127*, 955–967.

Kurze, A., Michie, K.A., Dixon, S.E., Mishra, A., Itoh, T., Khalid, S., Strmecki, L., Shirahige, K., Haering, C.H., Löwe, J., et al. (2011). A positively charged channel within the Smc1/Smc3 hinge required for sister chromatid cohesion. EMBO J. *30*, 374–378.

Lammens, A., Schele, A., and Hopfner, K.-P. (2004). Structural Biochemistry of ATP-Driven Dimerization and DNA-Stimulated Activation of SMC ATPases. Curr. Biol. *14*, 1778–1782.

Larionov, V.L., Karpova, T.S., Kouprina, N.Y., and Jouravleva, G.A. (1985). A mutant of Saccharomyces cerevisiae with impaired maintenance of centromeric plasmids. Curr. Genet. *10*, 15–20.

Lee, B., Merkel, F., Allegretti, M., Hassler, M., Cawood, C., Lecomte, L., Reilly, F.J.O., Sinn, L., Gutierrez-escribano, P., Bravo, S., et al. (2020). Cryo-EM structures of holo condensin reveal a subunit flip-flop mechanism. Nat. Struct. Mol. Biol. *27*, 743-751.

Li, Y., Muir, K.W., Bowler, M.W., Metz, J., Haering, C.H., and Panne, D. (2018). Structural basis for Scc3-dependent cohesin recruitment to chromatin. eLife *7*, e38356.

Liu, Y., Sung, S., Kim, Y., Li, F., Gwon, G., Jo, A., Kim, A., Kim, T., Song, O., Lee, S.E., et al. (2016). ATP -dependent DNA binding, unwinding, and resection by the Mre11/Rad50 complex . EMBO J. *35*, 743–758.

Marcos-Alcalde, Í., Mendieta-Moreno, J.I., Puisac, B., Gil-Rodríguez, M.C., Hernández-Marcos, M., Soler-Polo, Di., Ramos, F.J., Ortega, J., Pié, J., Mendieta, J., et al. (2017). Two-step ATP-driven opening of cohesin head. Sci. Rep. *7*, 1–14.

Mayer, M.L., Gygi, S.P., Aebersold, R., and Hieter, P. (2001). Identification of RFC(Ctf18p, Ctf8p, Dcc1p): An alternative RFC complex required for sister chromatid cohesion in S. cerevisiae. Mol. Cell *7*, 959–970.

Mayer, M.L., Pot, I., Chang, M., Xu, H., Aneliunas, V., Kwok, T., Newitt, R., Aebersold, R., Boone, C., Brown, G.W., et al. (2004). Identification of Protein Complexes Required for Efficient Sister Chromatid Cohesion. Mol. Biol. Cell *15*, 1736–1745.

Michaelis, C., Ciosk, R., and Nasmyth, K. (1997). Cohesins: Chromosomal proteins that prevent premature separation of sister chromatids. Cell *91*, 35–45.

Minamino, M., Higashi, T.L., Bouchoux, C., and Uhlmann, F. (2018). Topological in vitro loading of the budding yeast cohesin ring onto DNA. Life Sci. Alliance DOI: 10.26508/lsa.201800143

Murayama, Y., and Uhlmann, F. (2014). Biochemical reconstitution of topological DNA binding by the cohesin ring. Nature *505*, 367–371.

Murayama, Y., and Uhlmann, F. (2015). DNA Entry into and Exit out of the Cohesin Ring by an Interlocking Gate Mechanism. Cell *163*, 1628–1640.

Murayama, Y., Samora, C.P., Kurokawa, Y., Iwasaki, H., and Uhlmann, F. (2018). Establishment of DNA-DNA Interactions by the Cohesin Ring. Cell *172*, 465-477.e15.

Musacchio, A., and Salmon, E.D. (2007). The spindle-assembly checkpoint in space and time. Nat. Rev. Mol. Cell Biol. *8*, 379–393.

Nasmyth, K. (2001). Disseminating the Genome: Joining, Resolving, and Separating Sister Chromatids During Mitosis and Meiosis. Annu. Rev. Genet. *35*, 673–745.

Nasmyth, K. (2005). How might cohesin hold sister chromatids together? Philos. Trans. R. Soc. B Biol. Sci. *360*, 483–496.

Nora, E.P., Lajoie, B.R., Schulz, E.G., Giorgetti, L., Okamoto, I., Servant, N., Piolot, T., Van Berkum, N.L., Meisig, J., Sedat, J., et al. (2012). Spatial partitioning of the regulatory landscape of the X-inactivation centre. Nature *485*, 381–385.

Oldham, M.L., and Chen, J. (2011). Snapshots of the maltose transporter during ATP hydrolysis. Proc. Natl. Acad. Sci. U. S. A. *108*, 15152–15156.

Oliveira, R.A., Hamilton, R.S., Pauli, A., Davis, I., and Nasmyth, K. (2010). Cohesin cleavage and Cdk inhibition trigger formation of daughter nuclei. Nat. Cell Biol. *12*, 185–192.

Onn, I., and Koshland, D. (2011). In vitro assembly of physiological cohesin/DNA complexes. Proc. Natl. Acad. Sci. U. S. A. *108*, 12198–12205.

Onn, I., Aono, N., Hirano, M., and Hirano, T. (2007). Reconstitution and subunit geometry of human condensin complexes. EMBO J. *26*, 1024–1034.

Paulson, J.R., and Laemmli, U.K. (1977). The structure of histone-depleted metaphase chromosomes. Cell *12*, 817–828.

Petela, N.J., Gligoris, T.G., Metson, J., Lee, B.G., Voulgaris, M., Hu, B., Kikuchi, S., Chapard, C., Chen, W., Rajendra, E., et al. (2018). Scc2 Is a Potent Activator of Cohesin's ATPase that Promotes Loading by Binding Scc1 without Pds5. Mol. Cell *70*, 1134-1148.e7.

Petronczki, M., Chwalla, B., Siomos, M.F., Yokobayashi, S., Helmhart, W., Deutschbauer, A.M., Davis, R.W., Watanabe, Y., and Nasmyth, K. (2004). Sister-chromatid cohesion mediated by the alternative RF-CCtf18/Dcc1/Ctf8, the helicase Chl1 and the polymerase-α-associated protein Ctf4 is essential for chromatid disjunction during meiosis II. J. Cell Sci. *117*, 3547–3559.

Rao, S.S.P., Huang, S.C., Glenn St Hilaire, B., Engreitz, J.M., Perez, E.M., Kieffer-Kwon, K.R., Sanborn, A.L., Johnstone, S.E., Bascom, G.D., Bochkov, I.D., et al. (2017). Cohesin Loss Eliminates All Loop Domains. Cell *171*, 305-320.e24.

Rhodes, J.D.P., Haarhuis, J.H.I., Grimm, J.B., Rowland, B.D., Lavis, L.D., and Nasmyth, K.A. (2017). Cohesin Can Remain Associated with Chromosomes during DNA Replication. Cell Rep. *20*, 2749–2755.

Rolef Ben-Shahar, T., Heeger, S., Lehane, C., East, P., Flynn, H., Skehel, M., and Uhlmann, F. (2008). Eco1-dependent cohesin acetylation during establishment of sister chromatid cohesion. Science *321*, 563-566.

Ryu, J.-K., Bouchoux, C., Liu, H.W., Kim, E., Minamino, M., Groot, R. de, Katan, A.J., Bonato, A., Marenduzzo, D., Michieletto, D., et al. (2020). Phase separation induced by cohesin SMC protein complexes. DOI: https://doi.org/10.1101/2020.06.13.149716

Sanborn, A.L., Rao, S.S.P., Huang, S.C., Durand, N.C., Huntley, M.H., Jewett, A.I., Bochkov, I.D., Chinnappan, D., Cutkosky, A., Li, J., et al. (2015). Chromatin extrusion explains key features of loop and domain formation in wild-type and engineered genomes. Proc. Natl. Acad. Sci. U. S. A. *112*, E6456–E6465.

Shi, D., Zhao, S., Zuo, M.Q., Zhang, J., Hou, W., Dong, M.Q., Cao, Q., and Lou, H. (2020a). The acetyltransferase Eco1 elicits cohesin dimerization during S phase. J. Biol. Chem. *295*, 7554–7565.

Shi, Z., Gao, H., Bai, X., and Yu, H. (2020b). Cryo-EM structure of the human cohesin-NIPBL-DNA complex. Science *368*, 1454–1459.

Shimogawa, M.M., Widlund, P.O., Riffle, M., Ess, M., and Davis, T.N. (2009). Bir1 Is Required for the Tension Checkpoint. Mol. Biol. Cell *20*, 915–923.

Soh, Y.M., Bürmann, F., Shin, H.C., Oda, T., Jin, K.S., Toseland, C.P., Kim, C., Lee, H., Kim, S.J., Kong, M.S., et al. (2015). Molecular basis for SMC rod formation and its dissolution upon DNA binding. Mol. Cell *57*, 290–303.

Srinivasan, M., Scheinost, J.C., Petela, N.J., Gligoris, T.G., Wissler, M., Ogushi, S., Collier, J.E., Voulgaris, M., Kurze, A., Chan, K.L., et al. (2018). The Cohesin Ring Uses Its Hinge to Organize DNA Using Non-topological as well as Topological Mechanisms. Cell *173*, 1508-1519.e18.

Srinivasan, M., Petela, N.J., Scheinost, J.C., Collier, J., Voulgaris, M., Roig, M.B., Beckouët, F., Hu, B., and Nasmyth, K.A. (2019). Scc2 counteracts a wapl-independent mechanism that releases cohesin from chromosomes during G1. eLife *8*, 1–34.

Srinivasan, M., Fumasoni, M., Petela, N.J., Murray, A., and Nasmyth, K.A. (2020). Cohesion is established during dna replication utilising chromosome associated cohesin rings as well as those loaded de novo onto nascent dnas. eLife *9*, 1–27.

Stemmann, O., Zou, H., Gerber, S.A., Gygi, S.P., and Kirschner, M.W. (2001). Dual Inhibition of Sister Chromatid Separation at Metaphase. Cell *107*, 715-726.

Strunnikov, A. V., Larionov, V.L., and Koshland, D. (1993). SMC1: An essential yeast gene encoding a putative head-rod-tail protein is required for nuclear division and defines a new ubiquitous protein family. J. Cell Biol. *123*, 1635–1648.

Sumara, I., Vorlaufer, E., Gieffers, C., Peters, B.H., and Peters, J.M. (2000). Characterization of vertebrate cohesin complexes and their regulation in prophase. J. Cell Biol. *151*, 749–761.

Tanaka, T.U. (2010). Kinetochore-microtubule interactions: Steps towards bi-orientation. EMBO J. *29*, 4070–4082.

Tanaka, T.U., Rachidi, N., Janke, C., Pereira, G., Galova, M., Schiebel, E., Stark, M.J.R., and Nasmyth, K. (2002). Evidence that the Ipl1-Sli15 (Aurora Kinase-INCENP) complex promotes chromosome bi-orientation by altering kinetochore-spindle pole connections. Cell *108*, 317–329.

Tóth, A., Ciosk, R., Uhlmann, F., Galova, M., Schleiffer, A., and Nasmyth, K. (1999). Yeast cohesin complex requires a conserved protein, Eco1p(Ctf7), to establish cohesin between sister chromatids during DNA replication. Genes & Dev *13*, 320-333.

Uhlmann, F., and Nasmyth, K. (1998). Cohesion between sister chromatids must be established during DNA replication. Curr. Biol. *8*, 1095–1102.

Uhlmann, F., Lottspelch, F., and Nasmyth, K. (1999). Sister-chromatid separation at anaphase onset is promoted by cleavage of the cohesin subunit Scc1. Nature *400*, 37–42.

Uhlmann, F., Wernic, D., Poupart, M.-A., Koonin, E. V, and Nasmyth, K. (2000). Cleavage of Cohesin by the CD Clan Protease Separin Triggers Anaphase in Yeast. Cell *103*, 375–386.

Unal, E., Heidinger-Pauli, J.M., Kim, W., Guacci, V., Onn, I., Gygi, S.P., and Koshland, D.E. (2008). A Molecular Determinant for the Establishment of Sister Chromatid Cohesion. Science *321*, 566–569.

Vazquez Nunez, R., Ruiz Avila, L.B., and Gruber, S. (2019). Transient DNA Occupancy of the SMC Interarm Space in Prokaryotic Condensin. Mol. Cell *75*, 209-223.e6.

Weitzer, S., Lehane, C., and Uhlmann, F. (2003). A Model for ATP Hydrolysis-Dependent Binding of Cohesin to DNA. Curr. Biol. *13*, 1930-1940.

Wells, J.N., Gligoris, T.G., Nasmyth, K.A., and Marsh, J.A. (2017). Evolution of condensin and cohesin complexes driven by replacement of Kite by Hawk proteins. Curr. Biol. *27*, R17–R18.

Wutz, G., Várnai, C., Nagasaka, K., Cisneros, D.A., Stocsits, R.R., Tang, W., Schoenfelder, S., Jessberger, G., Muhar, M., Hossain, M.J., et al. (2017). Topologically associating domains and chromatin loops depend on cohesin and are regulated by CTCF, WAPL, and PDS5 proteins. EMBO J. *36*, 3573–3599.

Xu, H., Boone, C., and Klein, H.L. (2004). Mrc1 Is Required for Sister Chromatid Cohesion To Aid in Recombination Repair of Spontaneous Damage. Mol. Cell. Biol. *24*, 7082–7090.

Xu, H., Boone, C., and Brown, G.W. (2007). Genetic dissection of parallel sister-chromatid cohesion pathways. Genetics *176*, 1417-1429.

Xu, X., Kanai, R., Nakazawa, N., Wang, L., Toyoshima, C., and Yanagida, M. (2018). Suppressor mutation analysis combined with 3d modeling explains cohesin's capacity to hold and release DNA. Proc. Natl. Acad. Sci. U. S. A. *115*, E4833–E4842.

Yamano, H., Ishii, K., and Yanagida, M. (1994). Phosphorylation of dis2 protein phosphatase at the C-terminal cdc2 consensus and its potential role in cell cycle regulation. EMBO J. *13*, 5310-5318.

Zachariae, W. and Nasmyth, K. (1999). Whose end is destruction: cell division and the anaphase-promoting complex. Genes & Dev. *13*, 2039-2058.

Zhang, N., Kuznetsov, S.G., Sharan, S.K., Li, K., Rao, P.H., and Pati, D. (2008). A handcuff model for the cohesin complex. J. Cell Biol. *183*, 1019–1031.

Chapter 7 – Materials and methods

ATPase assay

ATPase activity was measured by using the EnzChek phosphate assay kit and following the protocol as provided. Cohesin and its subunits were added to a final concentration of 50 nM and 40 bp dsDNA added to a concentration of 700 nM. NaCl concentration was adjusted to 50 mM and the reaction initiated by addition of ATP to a final concentration of 1 mM. ATP hydrolysis was then measured by observing an increase in absorbance at 360 nm over 1 hour. The number of ATP molecules hydrolysed per cohesin complex was then calculated and plotted.

Calibrated ChIP-sequencing

Calibrated ChIP-sequencing experiments were carried out as described in Petela et al., 2018.

DNA entrapment assay

For DNA entrapment assays, 13 µl reactions were prepared containing 165 nM protein and 9.3 nM supercoiled pUC19 (buffered with 50 mM HEPES pH 7.5, 20 mM NaCl, 1 mM $MgCl_2$, 5% glycerol). Scc2 was added to a concentration of 50 nM. These were incubated on ice for 5 min before reactions were initiated by addition ATP to a final concentration of 5 mM (1 µl ATP added to 12 µl protein DNA mix). Typically, reactions were then incubated at 24^{o}C for either 40 min or 2 min depending on the compartment being assessed. To these, 1.5 µl BMOE was added to a final concentration of 0.64 mM and samples were incubated on ice for 6 min. Samples were then denatured by addition of 1.5 µl 10% SDS and heated at 70^{o}C for 20 min. DNA loading dye was added and mixtures separated in a 0.8% agarose gel, run at 50 V for 17 hours at 4^{o}C. The gel was stained with EtBr and visualised by UV light. Images shown are representative of 2 independent experiments.

Electromobility shift assay (EMSA)

A FAM-labelled 39 base pair HPLC purified DNA oligo (GAATTCGGTGCGCATAATGTATATATTATGTTAAATAAGCTT) was annealed to a complementary DNA oligo to form dsDNA by heating to 95^{o}C for 5 min and then decreasing the temperature to 4^{o}C in 0.1^{o}C increments (buffered in 100 mM potassium acetate, 50 mM HEPES pH 7.5) to a final concentration of 45 µM. The reactions were then prepared by adding 0.3 µM FAM-dsDNA to increasing

concentrations of protein (buffered in 50 mM HEPES pH 7.5, 75 mM NaCl, 1 mM TCEP, 10% glycerol) in a final volume of 10 µL. The reaction mix was then incubated on ice for 30 min in the dark. These were then separated in 5% acrylamide gels prepared with 0.5% TAE (40 mM Tris, 20 mM acetic acid, 1 mM EDTA) run at 100 V for 1 hour at 4°C in the dark. FAM-labelled DNA was visualised directly on a Fujifilm FLA7000 scanner with the LD473/Y[520] filter.

Protein crosslinking assay

For protein crosslinking assays, 10 µl reactions were prepared containing 570 nM protein (buffered with 50 mM HEPES pH 7.5, 50 mM NaCl, 5 mM $MgCl_2$, 1 mM TCEP, 5% glycerol). If added, ATP and pUC19 were added to a concentration of 5 mM and 60 nM respectively. Reactions mixes were first incubated on ice for 5 min before adding 1 µl BMOE to a final concentration of 0.64 mM. Reactions were then incubated on ice for 6 min. Samples were denatured by adding 4xLDS buffer and heating at 70°C for 10 min before being separated in 3-8% Tris-acetate gels run at 100 V for 4.5 hours. Gels were stained with Quick Coomassie stain.

S. cerevisiae cell viability spot assay

10 ml YPD liquid media was inoculated with *S. cerevisiae* and incubated overnight at 25°C with shaking at 100 rpm. Cell cultures were then diluted to OD_{600} = 1. Four 10-fold serial dilutions were then made for each strain. Of each dilution, 2 µl was then spotted onto a YPD agar plate (or YPD + 100nM rapamycin agar plate).

Recombinant yeast cohesin complex cloning

The *S. cerevisiae* genes *SMC1, SMC3, SCC3, SCC2, SCC1, and SCC4* were codon optimised for expression in *S. frugiperda* cells and synthesised using the Genescript Thermo Fisher service. These were then cloned into MultiBac vectors. Tag introduction and mutagenesis was achieved through Gibson assembly to generate *SMC1*-His, 2xStrepII-*SCC3*, *SCC1*-2xStrepII, *SCC2*-2xStrepII, $SCC2^{133-1493}$-2xStrepII, and His-*SCC4*. *SMC3 SMC1*-His, 2xStrepII-*SCC3, SCC2*-2xStrepII, and $SCC2^{133-1493}$-2xStrepII were cloned into pACEBac1 vectors, and *SCC1*-2xStrepII cloned into a pIDC vector. pIDC vectors must be maintained in PIR+ cells. *SMC1*-His and *SMC3* were then combined into the same vector via cloning to create a pACEBac1 *SMC1*-His *SMC3*. Vectors containing cohesin trimers were generated by

combining pACEBac1 *SMC1*-His *SMC3* with pIDC *SCC1*-2xStrepII by a Cre recombinase reaction.

Virus generation and protein expression

DNAs were first transformed into DH10Bac cells and bacmids containing the expression vector screened for by blue-white selection. DNA was then extracted and 2 µg of bacmid DNA was transfected into 2 ml *S. frugiperda* Sf9 cells at a cell density of $1x10^6$ cells ml^{-1} using FuGENE HD reagent, grown in Sf900 II SFM media. These were then incubated at 27°C for 5 days to create P1 virus. P2 virus was then amplified by infecting 50 ml Sf9 cells at a density of $2x10^6$ cells ml^{-1} with 500µl P1 virus and incubating in the dark at 27°C for 3 days with shaking at 100 rpm. P2 virus was then harvested by pelleting cells by centrifugation at 4000g and decanting into 5% FBS, and then stored in the dark at 4°C. Typically, proteins were then expressed by adding 5 ml P2 virus to 500 ml Sf900 cells at a density of $2x10^6$ cells ml^{-1} and incubating in the dark at 27°C for 2 days with shaking at 100 rpm. Cells were then harvested by centrifugation at 1000g, washed with PBS, and then frozen in liquid nitrogen and stored at -80°C.

Protein purification

Cell pellets were thawed in Buffer A (50 mM HEPES pH 7.5, 150 mM NaCl, 1 mM TCEP, 5% glycerol) supplemented with 1 Complete Protease Inhibitor (EDTA-free) tablet, 70 µg RNAse A, and 100 U ml^{-1} Supernuclease and then lysed by sonication on ice for 1 min using a Vibra Cell sonicator (model VCX130PB-1) at 80% amplitude, with 5 s bursts. Following sonication, cell lysate was supplemented with 1 mM PMSF. Proteins were then purified via a three strep purification protocol. First, proteins were purified via affinity pulldown of their StrepII tags using a StrepTrap HP column and eluted into Buffer A supplemented with 2.5mM desthiobiotin. Scc2 constructs were eluted into 50 mM Tris pH 8.0 rather than 50 mM HEPES pH 7.5. Proteins were then further purified by anion exchange chromatography using a 5 ml HiTrap Q HP column across a gradient of 100 mM to 1M NaCl. Scc2 constructs were eluted across a gradient of 0 mM to 1 M NaCl. Finally, proteins were purified via size exclusion chromatography using a Superose 6 increase 10/300 GL column for cohesin trimers and a HiLoad 16/600 Superdex 200 column for Scc3 and the Scc2 constructs.

Protein gel electrophoresis and western blotting

Samples were mixed with 4xLDS sample buffer, loaded onto a 3-8% Tris-acetate gel and separated at 150 V for 50 min. Gels were then either stained with Quick Coomassie stain or transferred onto a 0.2 µm nitrocellulose membrane using a Trans-blot Turbo transfer pack (Bio-Rad). The antibodies used for western blotting were anti-His (1:2000 dilution), anti-Strep HRP (1:4000 dilution) and anti-Smc3 (1:500 dilution). Primary antibodies were probed with anti-mouse HRP (1:5000 dilution) antibody.

Purification of DNA

pUC19 plasmid was transformed into TOP10 cells and grown overnight at 37°C. The next day a single colony was inoculated into 250 ml SOB++ media and grown at 37°C overnight for 16 hours. DNA was then purified via MaxiPrep using precooled reagents and equipment and eluted into 50 mM HEPES pH 7.5. To generate linear and open-circular DNA, this was then either incubated with HindIII-HF or Nt.BspQI respectively. DNA was further purified by $CsCl_2$ density gradient centrifugation in the presence of EtBr. The DNA was then extracted and the EtBr removed by washing several times with butanol saturated with 50 mM HEPES pH 7.5 and then the butanol phase discarded. The $CsCl_2$ was then removed by dialysis against 2 L 50 mM HEPES pH 7.5 buffer over 24 hours at 4°C, with two buffer changes. The DNA was then collected and stored at -20°C.

Yeast strains

KN 10599	Mat A, fpr1::NatMX, ade2-1, trp1-1, can1-100, leu2-3,112, his3-11,15, ura3, GAL, psi+
KN 28237	Mat A, fpr1::NatMX, Scc1-PK9::TRP1, Smc3-GL-mFrb::HIS3, Smc1-GL-FKBP12::KanMx, ade2-1, trp1-1, can1-100, leu2-3,112, his3-11,15, ura3, GAL, psi+
KN 28238	Mat A, fpr1::NatMX, Scc1-PK9::TRP1, Smc1-GL-FKBP12::KanMx, ade2-1, trp1-1, can1-100, leu2-3,112, his3-11,15, ura3, GAL, psi+
KN 28239	Mat A, fpr1::NatMX, Scc1-PK9::TRP1, Smc3-GL-mFrb::HIS3, ade2-1, trp1-1, can1-100, leu2-3,112, his3-11,15, ura3, GAL, psi+

E. coli Strains

DH10Bac	F⁻*mcr*A Δ(*mrr*-hsdRMS-*mcr*BC) Φ80*lac*ZΔM15 Δ*lac*X74 *rec*A1 *end*A1 *ara*D139 Δ(*ara*, *leu*)7697 *gal*U *gal*K λ⁻*rps*L *nup*G/pMON14272/pMON7124
PIR+	F-Δlac169 rpoS(Am) robA1 creC510 hsdR514 endA recA1 uidA(ΔMluI)::pir-116
TOP10	F- *mcrA*Δ(*mrr-hsd*RMS-*mcr*BC) Φ80*lac*ZΔM15 Δ*lac*X74 *rec*A1 *ara*D139 Δ(*araleu*)7697 *gal*U *gal*K *rps*L (StrR) *end*A1 *nup*G

Other Strains

Sf9	ThermoFisher Cat# 11496015

Plasmid List

pACEBac1 Smc1-His
pACEBac1 Smc3
pACEBac1 Smc1-His Smc3
pACEBac1 Scc2-StrepII
pACEBac1 Scc2$^{133-1493}$-StrepII
pACEBac1 StrepII-Scc3
pIDC Scc1-StrepII

Reagents

Name	Company	Identifier
Antibodies		
Anti-His (mouse)	Sigma	Cat# SAB1305538- 400UL
Anti-mouse HRP	ThermoFisher	Cat# 62–6520
Anti-Smc3	Bethyl Laboratories	Cat# A300-060A
Anti-Strep HRP	iba	Cat# 2-1502-001
Enzymes		
Cre Recombinase	NEB	Cat# M0298S
HindIII-HF	NEB	Cat# R3104T
Nt.BspQI	NEB	Cat# R0644S
RNase A	Roche	Cat# 10109169001
Supernuclease	SinoBiological	Cat# SSNP01
Kits and Equipment		
Enzcheck phophatase assay kit	Invitrogen	Cat# E6646
Gibson Assembly Mix	NEB	Cat# E2611L
HiTrap Q HP	GE Healthcare Fisher	Cat# GE29-0513-25
HiSpeed Plasmid Maxi Kit	Qiagen	Cat# 12663
StrepTrap HP	Fisher Scientific	Cat# 11540654
Superose 6 increase 10/300 GL	VWR	Cat# 29-0915-96
Superdex 200 Hiload 16/60	GE Healthcare	Cat# GE28-9893-35
Reagents		
Acetic Acid	Sigma	A6283-100ML
Agarose	Sigma	A9539-500G
ATP	Sigma	Cat# 11140965001
BMOE	ThermoFisher	Cat# 22323
Butanol	Sigma	Cat# B7906-500ML
EDTA-free Protease Inhibitor	Roche	Cat# 4693132001

Cocktail		
CsCl	Sigma	Cat# 289329-100G
Desthiobiotin	Fisher Scientific	Cat# 12753064
EDTA	ThermoFisher	Cat# 17892
EtBr	ThermoFisher	Cat# 15585011
FBS	Sigma	Cat# 12303C
FuGENE HD	Promega	Cat# E2311
Glycerol	ThermoFisher	Cat# 17904
HEPES	ThermoFisher	Cat# 11344041
Immobilon Western ECL	Millipore	Cat# WBLKS0500
K-Acetate	Fisher Scientific	Cat# 127-08-2
4xLDS	ThermoFisher	Cat# NP0007
$MgCl_2$	Fisher Scientific	Cat# M/0600/53
NaCl	Fisher Scientific	Cat# S/3160/60
NuPAGE 3–8% Tris-Acetate Protein Gels	ThermoFisher	Cat# EA0378BOX
PMSF	Fisher Scientific	Cat# 36978
Quick Coomassie stain	Generon	Cat# GEN-QC-STAIN
Sf900 SFM	ThermoFisher	Cat# 10902104
TCEP	ThermoFisher	Cat# 20490
Tris base	Fisher Scientific	Cat# BP152-500